NSF Grant ATM- 320959
NSF Grant ATM - 0132190
National Science Foundation

NORTH ATLANTIC OCEAN-ATMOSPHERE INTERACTION ON INTRASEASONAL TIME SCALES

by Laura M. Ciasto

Colorado State University

DEPARTMENT OF ATMOSPHERIC SCIENCE

PAPER NO. 773

NORTH ATLANTIC OCEAN-ATMOSPHERE INTERACTION ON INTRASEASONAL TIME SCALES

Submitted by

Laura M. Ciasto

Department of Atmospheric Science

In partial fulfillment of the requirements

For the Degree of Master of Science

Colorado State University

Fort Collins, Colorado

Summer 2004

ABSTRACT

NORTH ATLANTIC OCEAN-ATMOSPHERE INTERACTION ON INTRASEASONAL TIME SCALES

A substantial fraction of midlatitude sea surface temperature (SST) variability on time scales ranging from months to years can be interpreted as the passive thermodynamic response of the ocean mixed layer to stochastic atmospheric forcing. Subsequently, the dominant structures of monthly and seasonal mean Northern Hemisphere SST variability owe their existence to variations in the extratropical atmosphere. To what extent midlatitude SST variability, in turn, gives rise to anomalies in the dominant structures of extratropical atmospheric variability remains unclear. Presumably, if the extratropical atmosphere exhibits a deep and statistically significant response to midlatitude SST anomalies, the dynamics of the response should occur on time scales shorter than the monthly and seasonal mean data used in most observational analyses of midlatitude atmosphere-ocean interaction. The motivation of the thesis is to investigate the interaction between North Atlantic SST variability and the extratropical atmospheric circulation on intraseasonal time scales.

First, the climatology of the North Atlantic SST field and the overlying atmospheric circulation is described. The largest variance in intraseasonal and seasonal mean SST anomalies is located within a zone of enhanced SST gradients in the Gulf Stream

extension. The region of maximum SST variance also underlies a region of marked wintertime cyclogenesis over the western edge of the North Atlantic storm track. Patterns of North Atlantic weekly SST variability are further investigated using Empirical Orthogonal Function (EOF) analysis. EOFs of both weekly summertime and wintertime SST anomalies reflect a mix of two patterns, variability in the Gulf Stream extension region and a meridionally banded structure of SST anomalies commonly referred to as the tripole. These patterns are most clearly evident in EOFs based on intraseasonal wintertime SST anomalies.

Wintertime atmosphere-ocean interaction on intraseasonal time scales is then examined using lagged correlation/regression analysis. The results show that the tripole and variability in the Gulf Stream extension region emerge not only as the leading EOFs of intraseasonal wintertime SST variability but also in association with the leading pattern of Northern Hemisphere atmospheric variability, referred to as the Northern Annular Mode (NAM). Consistent with previous results, the strongest correlations between midlatitude SSTs and the NAM occur when variations in the NAM lead the tripole by ~2 weeks. However, the present results also show a coherent and statistically significant pattern of SST anomalies over the Gulf Stream extension region that precedes changes in the NAM by ~ 2 weeks.

Laura M. Ciasto
Department of Atmospheric Science
Colorado State University
Fort Collins, CO 80523
Summer 2004

TABLE OF CONTENTS

CHAPTER ONE

Introduction

Understanding the nature of ocean-atmosphere interactions has become an increasingly popular area of research over the past fifty years. The ocean covers roughly 74% of the Earth's surface and stores more heat in 2.5 m of water than in the entire overlying atmospheric column (Hurrell et al. 2003). The vast source of thermal inertia in the ocean gives rise to considerable persistence in sea surface temperature (SST) anomalies, much more than that observed in association with tropospheric variability. Thus, there is the potential to use relatively low frequency variability in the ocean as a climate predictor.

The most obvious example of ocean-atmosphere interaction is the El Niño Southern Oscillation (ENSO). In the warm phase of ENSO, the easterly trade winds relax throughout the tropical Pacific Ocean, allowing warm water pooled in the western tropical Pacific to spread eastward and reducing the amount of cold upwelling in the central and eastern Pacific (Philander 1990). The warmer water in the central and eastern Pacific is associated with increased atmospheric convection and precipitation in these regions. On the basis of the persistence in tropical SSTs alone, the opposing phases of ENSO can be predicted out to several months in advance.

ENSO is the only widely accepted mode of coupled ocean-atmosphere variability in the climate system, and the nature of coupled ocean-atmosphere interactions in the mid-

latitudes remains particularly unclear. Specifically, it is well-established that midlatitude SSTs respond to variability in the extratropical atmosphere, but to what extent the extratropical atmosphere responds to anomalous midlatitude SSTs has not been well-determined.

This chapter reviews the literature concerning ocean-atmosphere interactions in the midlatitudes, with an emphasis on the North Atlantic basin. First, we review the processes whereby the midlatitude ocean responds to atmospheric variability. Second, we discuss the mechanisms through which the atmosphere might respond to variations in midlatitude SSTs, and offer a synthesis of the modelling and observational work that has sought evidence in support of these mechanisms. Finally, we review recent observational research that explores midlatitude ocean-atmosphere interaction in submonthly data and outline the motivation for this thesis.

1.1 Response of the Midlatitude SSTs to Atmospheric Variability

This section focuses on the response of the midlatitude ocean to atmospheric variability. We start with a review of stochastic climate models. We then focus on relevance of these models to observations by exploring the relationships between the dominant patterns of North Atlantic SST variability and the dominant patterns of the Northern Hemisphere extratropical atmospheric variability.

1.1.1 Stochastic climate models

Through the application of a simple stochastic climate model, Frankignoul and Hasselman (1977; hereafter referred to as FH77) examined the response of the midlatitude

SST field to atmosphere forcing. The model is stochastic in the sense that variability in SSTs is determined by the random forcing by the white noise atmosphere. In the model, the upper ocean is represented by a mixed layer of fixed depth H. Changes in the SST T' are forced by stochastic atmospheric noise F' determined by surface heat fluxes and are damped back to space by a constant feed back factor λ which is a function of mean wind speed and is represented by the following equation:

$$(\rho c_p H)\frac{d}{dt}T' = F' - \lambda T', \tag{1.1}$$

where ρ is the density of seawater, c_p is the heat capacity of the ocean. Because the effective heat capacity $\rho c_p H$ of the ocean is large, the SST field responds slowly to variability in the atmospheric forcing. Thus, the SST field integrates the white noise atmospheric forcing producing a red response in the SST spectrum.

FH77 demonstrates that the observed persistence of midlatitude SST variability on time scales up to six months is consistent with the passive thermodynamic response of the mixed layer ocean to stochastic atmospheric variability. The results of the model showed strong agreement with observed SST anomalies in midlatitudes. Because the model in equation (1.1) describes the basic response of the midlatitude ocean to stochastic atmospheric forcing, it can be viewed as a null hypothesis for interpreting low-frequency variability in the ocean.

Note that the model in equation (1.1) is simplified and ignores key aspects of the climate system. For example, the model is designed for regions of the ocean away from intense currents and thermal boundaries (e.g., the Gulf Stream). Additionally, the influence of mixed layer processes on the variability of midlatitude SSTs is absent in equation

(1.1). Such mixed layer processes include mesoscale eddies, advection by mean currents and re-emergence of SST anomalies. Deser et al. (2003; hereafter referred to as DAT03) extended FH77 to explicitly include the re-emergence mechanism.

The re-emergence mechanism contributes to the observed persistence of midlatitude SST anomalies from one winter to the next (Namias and Born 1970, 1974; Wallace and Jiang 1987). As described by Alexander and Deser 1995 and Alexander et al. 1999, the mechanism is envisioned to operate as follows: in the spring, the mixed layer shoals and midlatitude SST anomalies induced during the previous winter are sequestered beneath the mixed layer throughout the summer (Figure 1.1 right). During the fall and winter, the mixed layer deepens due to increased storm activity and entrains sequestered SST anomalies back into the mixed layer. Hence, midlatitude winter SST anomalies are strongly correlated with those of the previous winter but weakly correlated with those of the previous summer.

To investigate the role of re-emergence in the persistence of midlatitude winter SST anomalies, DAT03 modified the stochastic model of FH77 to explicitly account for entrainment (Figure 1.1). The entrainment model is given as:

$$(\rho C_p)\frac{d}{dt}(HT)' = F' - \lambda T' + (\rho C_p W_e)(T' - T'_b), \qquad (1.2)$$

where ρ is the density of seawater; C_p the heat capacity of the ocean; H the seasonally varying depth of the mixed layer; T the mixed layer temperature anomaly; λ the linear damping coefficient similar to FH77; F' the stochastic white noise forcing; W_e=dH/dt the entrainment velocity and T_b' the temperature anomaly formed at an earlier time t_e below the mixed layer. During the spring and summer months, the mixed layer is steady or

shoaling and W_e=0. Thus the last term in equation (1.2) is eliminated and the equation reduces to the form similar in equation (1.1). During the fall and winter months, the mixed layer deepens ($W_e \neq 0$) and the change in T is a function of the stochastic atmospheric forcing as well as the difference in T' due to entrainment from below the mixed layer.

Figure 1.2 shows select results from DAT03. The top panel compares the observed seasonal cycle of the mixed layer with that of the simulated mixed layer from DAT03. The modeled values of the mixed layer agree well with the observed values, demonstrating that the model can account for the deepening of the mixed layer during the fall and winter and its subsequent shoaling in the spring. In the bottom panel, the results of equation (1.2) are plotted as monthly lag autocorrelations from a starting month of March in year 0. The observed and modeled SST in the North Atlantic generally show good agreement; however, the model tends to over (under) predict the observed autocorrelations in the winter (summer). In the winter, the simulated SSTs are highly correlated with those of March of year 0 with weak correlation in the summers due to the sequestration of SSTs below the mixed layer. The autocorrelations of heat content, defined as the vertically integrated SST anomaly from surface to H_{eff} in all months, and SSTs are similar during the winter months, consistent with the fact that winter SST anomalies extend to H_{eff}.

Because FH77 did not consider the re-emergence mechanism, their model only accounts for the persistence of midlatitude SST anomalies out to six months. The autocorrelations of SST anomalies from the model outlined DAT03 are virtually identical to those from FH77 during the spring and summer months because the mixed layer is either shoaling or steady and little entrainment is observed. However, the model outlined in FH77 grossly underestimates the autocorrelation of winter midlatitude SST anomalies when the

mixed layer deepens, entraining SST anomalies from the previous winter. Thus, inclusion of re-emergence in DAT03 provides a better estimate of the persistence of SST anomalies expected solely due to thermodynamic coupling with variations in the overlying atmosphere.

1.1.2 Dominant patterns of North Atlantic SST variability

In the previous section, we used the results of two stochastic climate models to demonstrate that a large fraction of midlatitude SST variability can be explained as the passive thermodynamic response to stochastic atmospheric forcing. This section applies the results from FH77 and DAT03 to the interpretation of the large-scale variability in the extratropical atmosphere and its influence on variability in the North Atlantic SST field.

Observations suggest that the extratropical atmospheric circulation organizes itself into large-scale patterns of variability. Walker and Bliss (1932) noted that wintertime variability of the North Atlantic extratropical atmosphere is characterized by the fluctuation of mass between low pressure centered over Iceland and high pressure centered over the Azores Islands. This pattern is widely established as the dominant pattern of North Atlantic atmospheric variability and is commonly referred to as the North Atlantic Oscillation (NAO; Wallace and Gutzler 1981; Marshall et al. 2001a; Hurrell et al. 2003). In the positive phase of the NAO, the Azores high and Icelandic low are enhanced and the attendant westerlies ~45° – 55° N intensify. As a result, the winter storm track strengthens and shifts northward, leading to warm wet winters in northern Europe and cold dry winters in Canada and Greenland (van Loon and Rogers 1978). The opposite is true in the negative phase of the NAO.

The time series of the NAO can be characterized as red noise with an e-folding time scale of ~10 days (Feldstein 2000). Thus, the NAO exhibits temporal variability within each winter season, from one winter to the next, and on decadal time scales. During the 1960s, the NAO was characterized by predominantly negative values but over the past 30 years has favored its positive phase. The trend in the NAO has contributed substantially to recent Northern Hemisphere temperature trends especially over Northern Europe and Canada (Hurrell 1995; Thompson et al. 2000).

Recently, it has been argued that the NAO is a regional expression of a hemispheric mode of variability referred to as the Northern Annular Mode (NAM, also known as the Arctic Oscillation; Thompson and Wallace 1998, 2000). In contrast to the NAO, the NAM is characterized by a redistribution of atmospheric mass not only between the Arctic and the subtropical North Atlantic, but between the Arctic and the North Pacific, as well as evidenced by the leading EOF of wintertime SLP anomalies (Figure 1.3; Kutzbach 1970; Wallace and Gutzler 1981; Thompson and Wallace 1998, 2000). In the Southern Hemisphere a similar pattern of variability called the Southern Annular Mode (SAM) is observed. These patterns arise as the result of a positive feedback between anomalies in the fluxes of eddy momentum and in the zonal mean zonal flow at midlatitudes (Lorenz and Hartmann 2001, 2003). In the Northern Hemisphere, anomalous baroclinic wave activity arises in the same latitude as the midlatitude jet. As the waves propagate away from the jet, momentum is pumped into the jet, creating positive zonal wind anomalies. Subsequently, a meridional circulation is induced which enhances the temperature gradient and the baroclinic eddies.

The interpretation of the NAM as a preferred mode of Northern Hemisphere atmospheric variability is still debated. Deser (2000) demonstrated that the Arctic and North Atlantic centers of action are significantly correlated, but that the relationship between the Arctic and Pacific is relatively weak. Deser (2000) also showed that the North Pacific and North Atlantic centers of action are weakly correlated (i.e., they do not vary in phase). Thompson and Wallace (2002) counter that the weak teleconnectivity between the two centers may arise from the presence of another mode of variability that prefers an out of phase relationship between the Atlantic and Pacific such as the Pacific North American (PNA) pattern. For the purpose of this thesis, we will assume the NAM and NAO reflect the same phenomenon.

The relationship between the NAO and the North Atlantic ocean was first documented by Bjerknes (1959, 1962, 1964) using SST and sea level pressure (SLP) data from the first half of the century. Bjerknes demonstrated that, on interannual timescales, changes in North Atlantic SSTs are negatively correlated with the strength of the westerlies along 45° – 55°N. Composite differences in SLP and SST fields between years of strong and weak westerlies indicate that warmer SSTs in the Sargasso Sea and cooler SSTs in the subpolar region are associated with a deepening of the low (high) pressure centers over Iceland (Azores). Bjerknes also observed that variability in North Atlantic SSTs is not consistent with atmospheric forcing of the ocean on interdecadal time scales.

More recent studies correlating anomalous SSTs with the NAO index confirm the relationship between the extratropical atmospheric circulation and midlatitude SST variability (e.g., Kushnir, 1994; Seager et al. 2000; Marshall et al. 2001b). Similar to Bjerknes (1964), warmer than normal SSTs in the Sargasso Sea and cooler than normal SSTs in the

subpolar North Atlantic emerge in association with the positive phase of the NAO. Additionally, cooler than normal SSTs in the subtropical North Atlantic appear to be related to the NAO (Kaplan 1997, 1998).This meridionally banded structure of SST anomalies is commonly referred to as the tripole and is considered the dominant pattern of North Atlantic SST variability during the winter (Marshall et al. 2001a; Czaja et al. 2003; Visbeck et al. 2003). It is interesting to note that only the tripole has been widely identified as an reproducible pattern of North Atlantic SST variability.

Cayan (1992a,b) demonstrated how the NAO gives rise to the tripole through anomalous turbulent heat fluxes at the surface. In the positive phase of the NAO, northerly winds along $45° - 55°N$ strengthen due to the deepening of the Icelandic low and advect cold air towards the southwest region of Greenland and the Labrador Sea (Dickson 2000). As a result, the net heat flux is out of the ocean (Figure 1.4b) and SSTs in this region cool (Figure 1.4a). Similarly, the strengthening of the Azores high sends relatively warm air from the Bermuda region towards the eastern coast of the United States and weakens the climatological westerlies. As a result, the net flux is into the ocean, creating warmer than normal SSTs in the Sargasso Sea. The enhanced anticyclonic flow also gives rise to stronger easterlies at ~20°N that cool the coastal region of North Africa and SSTs throughout the subtropical North Atlantic (Kaplan et al. 1997, 1998).

Variability in the tripole is also driven by Ekman transport, which is the volume of water transported at right angles to the direction of the surface wind (Brown et al. 1998; Visbeck et al. 2003). Figure 1.5a shows that the positive phase of the NAO is characterized by westerlies along ~50°N, which create southward transport of water. As a result, cold SSTs are advected in the subpolar North Atlantic and give rise to cooler than normal

SSTs south of Greenland (Fig. 1.5b). Similarly, the region of easterlies in the along 35°N lead to northward transport of warm SSTs into the Sargasso Sea.

1.2 Response of the Extratropical Atmosphere to Midlatitude SST Anomalies

The previous section shows that the dominant pattern of North Atlantic SST variability owes its existence to the dominant patterns of Northern Hemisphere atmospheric variability. To what extent midlatitude SSTs, in turn, give rise to variability in the extratropical atmosphere remains unclear. This section first reviews both simple and complex mechanisms that describe how the extratropical atmosphere might respond to midlatitude SSTs. We then offer a synthesis of the modelling and observational research seeking evidence of an atmospheric response to variations in midlatitude SSTs.

1.2.1 Mechanisms in which the extratropical atmosphere responds to midlatitude SSTs

a) The steady, linear response to thermal forcing

The steady, linear atmospheric response to both tropical and midlatitude thermal forcings was examined in Hoskins and Karoly (1981). In their study, the atmospheric response to thermal forcing at or near the surface was explained through the balance of the steady- state, linear, inviscid vorticity and thermodynamic equations given by:

$$\bar{u}\xi_x' + \beta v' = f w_z' \tag{1.3}$$

$$f\bar{u}v_z' - f\bar{u}_z v' + w'N^2 = Q, \tag{1.4}$$

where $\bar{u}$ is the zonal mean wind; ξ_x' is the change beta-plane vorticity in the zonal direction, β the meridional change of planetary vorticity, v' the meridional wind anomaly, f the

planetary vorticity, w' the change in vertical velocity; and Q the heat source. The subscripts denotes a derivative of the variable with respect to the subscript.

In the tropics, the horizontal temperature gradient is small and by the thermal wind relation, so are v'_z and $\bar{u}_z$ (the first and second terms in equation (1.4)). Therefore, positive heating ($Q>0$) in equation (1.4) must be balanced by upward motion ($w'>0$). The increase in vertical velocity gives rise to stretching of the air column where the heating occurred ($w'_z>0$). To maintain balance in (1.3), this vortex stretching must be compensated through poleward advection of planetary vorticity ($v'>0$ in the Northern Hemisphere). As a result, a trough will develop to the west of the heating source (Figure 1.6a).

In contrast, in the midlatitudes, horizontal temperature gradients are large and positive heating is balanced by horizontal temperature advection (the first and second terms in equation (1.4)). For example, if $Q>0$, cooler air from the polar regions will be advected equatorward ($v'<0$ in the Northern Hemisphere) to balance the anomalous change in temperature created by Q. Hence, a trough will develop to the east of the heating source (Figure 1.6b). To maintain balance in equation (1.3), $v'<0$ is compensated by vortex shrinking and downward motion in the region of Q or zonal advection of anomalous relative vorticity.

b) Damped Thermal Coupling

The effect of damped thermal coupling on the extratropical atmospheric response to midlatitude SSTs was explored by Barsugli and Battisti (1998; hereafter referred to as BB98). BB98 extended the stochastic climate model of FH77 to examine the basic effects

of ocean-atmosphere coupling in the midlatitudes. The physics of FH77 are still represented in BB98 but the model also considers the feedback from SSTs and surface fluxes onto the atmosphere. BB98 modeled the atmosphere-ocean as a coupled system using the following equations:

$$\gamma_a \frac{d\tilde{T}_a}{dt} = -\lambda_{sa}(\tilde{T}_s - \tilde{T}_o) - \lambda_a \tilde{T}_a + \tilde{F}, \tag{1.5}$$

$$\gamma_o \frac{d\tilde{T}_o}{dt} = \lambda_{so}(\tilde{T}_s - \tilde{T}_o) - \lambda_o \tilde{T}_o, \tag{1.6}$$

where subscripts a and o refer to the atmosphere and ocean, respectively; T is the anomalous temperature; T_s the surface air temperature; γ the heat capacity; λ the linearized coefficient of the sum of longwave, sensible and latent heat fluxes; and λ_a, λ_o are the radiative damping of each component. F represents stochastic atmospheric forcing. The surface air temperature T_s is linearly related to the free atmosphere temperature T_a (i.e., $T_s = cT_a$ where c is a constant). The left side of (1.5) and (1.6) represent the changes in ocean and atmosphere temperature and are controlled by: 1) the balance between surface and atmospheric temperatures through surface and radiative heat fluxes and 2) radiative damping.

Through the application of equations (1.5,1.6) in both coupled and uncoupled modes, BB98 argue that the basic effects of midlatitude ocean-atmosphere interactions are to enhance the low frequency variability of both media. For example, if a cold temperature anomaly is advected into a region over relatively warm SSTs, then the net heat flux will be out of the ocean into the atmosphere ($(\tilde{T}_s - \tilde{T}_o) < 0$). As a result, the ocean will cool

$\left(\frac{d\tilde{T}_o}{dt} < 0\right)$, the atmosphere will warm $\left(\frac{d\tilde{T}_a}{dt} > 0\right)$, and the fluxes between the two mediums will damp to zero as thermal equilibrium is attained. This is in contrast to previous atmospheric models where $\tilde{T}_o$ is prescribed and does not respond to $\tilde{T}_a$. In the absence of thermal coupling, when a cold temperature anomaly is advected into a region over warm SSTs, $\tilde{T}_o$ does not change and the net flux out of the ocean $(\tilde{T}_s - \tilde{T}_o)$ is enhanced relative to the example mentioned above. Thus, the ability of SSTs to respond to anomalous surface fluxes reduces the net heat flux and enhances low frequency variability in both media.

c) Non-linear mechanisms

The mechanisms explored by Hoskins and Karoly (1981) and BB98 reveal the simple atmospheric response to midlatitude surface heating. These mechanisms act to maintain thermodynamic balance between the atmosphere and ocean, but they do not necessarily produce a deep equivalent barotropic, large-scale atmospheric response to midlatitude SST anomalies. In the midlatitudes, the changes in horizontal temperature advection required to balance changes in SST are modest compared to background variability. It has been argued that in order to evoke a deep response more complex, non-linear mechanisms are necessary. One example involving the anomalous eddy feedback onto the midlatitude storm tracks is described below.

Several studies have argued that the position of SST gradients affect the position of the storm track (e.g., see Kushnir et al. 2002). In regions of strong baroclinicity, cyclogenesis is enhanced. As atmospheric perturbations grow, baroclinic eddies propagate vertically and then equatorward. Consequently, eddy momentum flux converges aloft (Figure

1.7). The resulting westerlies which strengthen the midlatitude jet are deflected equatorward, creating a meridional circulation characterized by equatorward flow aloft and poleward flow at the surface. The associated rising air poleward of the jet cools and the sinking air equatorward of the jet warms. As a result of this secondary circulation, the atmospheric perturbation and subsequently the SST anomaly are reinforced. Peng and Whitaker (1999) hypothesized that anomalous SSTs induced by an atmospheric perturbation would shift the position of the SST gradient, altering the location of the storm track and the midlatitude jet.

1.2.2 Modeling the atmospheric response to midlatitude SST anomalies

In this section, we review the attempts to model the atmospheric response to midlatitude SST anomalies. We start with a series of models forced with prescribed SST anomalies and then review results from models forced by more realistic, time-varying SST anomalies.

Palmer and Sun (1985) forced an AGCM with SST anomalies of 3K in the Gulf Stream. The resulting atmospheric pattern was dominated by an equivalent barotropic high located over the central North Atlantic, downstream of the SST anomalies. Ferranti et al. (1994) forced an AGCM with positive SST anomalies of 2K in a similar region and found an atmospheric response similar to that of Palmer and Sun (1985).When a negative SST anomaly of the same amplitude was used to force the AGCM, the atmospheric response was similar in structure and amplitude but of opposite sign (i.e. the response is linear).

The results of Palmer and Sun (1985) are not highly reproducible in other model experiments also forced with prescribed SST anomalies in the region of the Gulf Stream

extension. For example, Peng et al. (1995) forced an AGCM with 3K SST anomalies but found that the atmospheric response differed greatly between November and January. In November, the extratropical atmospheric response is dominated by an anomalous ridge located over the North Atlantic and a northward shift of the storm track. The response in January, however, exhibits a weak anomalous trough over the North Atlantic and a southward shift of the storm. It was also observed in Peng et al. (1995) that the atmospheric response to negative SST anomalies is not the opposite of that to positive SST anomalies. Ting and Peng (1995) and Peng and Fyfe (1995) reached similar conclusions.

Model experiments forced with prescribed SST anomalies in other regions of the North Atlantic and North Pacific basins also obtain varying atmospheric responses. Several studies found equivalent barotropic lows downstream of the SST anomalies regardless of the sign of the prescribed SST anomalies (Pitcher et al. 1988; Kushnir and Lau 1992) and other studies obtained weak baroclinic responses with surface lows and upper level highs downstream of the SST anomalies (Kushnir and Held 1996). In several cases, no atmospheric responses to midlatitude SSTs was observed (Lau and Nath 1994).

Another series of model studies investigated the atmospheric response to more realistic, time-varying midlatitude SST anomalies. Rodwell et al. (1999) forced an AGCM with observed historical wintertime SSTs of the last half of the 20th century and then calculated a simulated NAO index. The modeled index is only significantly correlated to the observed NAO index if a low-pass filter retaining periods greater than 6.5 years was applied to the data and at least six ensembles were averaged together. But based on this result, Rodwell et al. (1999) concluded that fluctuations in SSTs influence the strength of the NAO on dec-

adal time scales and therefore, argued that European winter climate could be predicted up to several years in advance. Mehta et al. (2000) reached a similar conclusion.

Bretherton and Battisti (2000) applied the stochastic climate model constructed by BB98 to test the results of Rodwell et al. (1999) and Mehta et al. (2000). They forced the model with stochastic noise to obtain SSTs which have no predictability beyond one year. The "observed" SSTs were then used to force the atmospheric component of the model. Doing this six times and applying a 6.5 year low pass filter produced correlations similar to Rodwell et al. (1999). Bretherton and Battisti (2000) thus concluded that the high correlations between the observed and simulated atmospheric responses are due to ensemble averaging which filters out the noise inherent in the atmospheric response. Hence, Bretherton and Battisti (2000) argued the results of Rodwell et al. (1999) and Mehta et al. (2000) are simply consistent with damped thermal coupling and do no prove a robust dynamic response of the extratropical atmosphere to midlatitude SST anomalies. However, Czaja and Marshall (2000) countered that conclusions about the predictability of the atmosphere cannot be drawn from low pass correlations.

1.2.3 Observational evidence of an atmospheric response to midlatitude SST anomalies

The previous sections reviewed the mechanisms by which the extratropical atmosphere might respond to midlatitude SST anomalies and noted that attempts to model such a response have yielded inconclusive results. This section shifts the focus to studies that have sought observational evidence of an extratropical atmospheric response to fluctuations in midlatitude SST anomalies.

One approach to examining the observed relationship between the extratropical atmosphere and midlatitude SSTs involves non-contemporaneous analysis of the statistical relationships between these fields. Results from several studies using this approach exhibit an asymmetry in the relationship between midlatitude SSTs and the overlying atmospheric circulation. Davis (1976) showed that the observed relationship between North Pacific SLP and SST anomalies is significant when the atmosphere leads by ~1 month but not vice versa. Frankignoul (1998) showed the North Atlantic surface fluxes and SST anomalies are positively correlated when the fluxes lead, indicating that the fluxes force the SSTs. The correlation reverses sign when SSTs lead, consistent with the damping of SST anomalies to the atmosphere. It has been observed that the lag time between the NAO and the emergence of the tripole in monthly data is ~1 month (Marshall et al. 2001a).

To determine the degree of covariability between the atmospheric circulation and previously generated SSTs, Czaja and Frankignoul (1999) used lagged Singular Value Decomposition (SVD) analysis between monthly mean North Atlantic SST anomalies and 500 hPa geopotential height (Z_{500}) and surface heat fluxes. They found statistically significant covariability between summertime SST anomalies and the atmospheric circulation ~6 months later. While their results suggest that summertime SST anomalies yield predictive skill for wintertime climate but the correlations are restricted to a small fraction of the Northern Hemisphere winter (Kushnir et al., 2002).

The second method of examining the non-contemporaneous relationship between the midlatitude SSTs and the extratropical atmosphere is to analyze the relationships between variations in one media and the tendency in the other. Realizing that it is impossi-

ble to distinguish the direction of forcing through contemporaneous analysis, Wallace et al. (1990) examined the relationship between Z_{500} and the tendency in mid-winter SSTs over the North Atlantic and North Pacific basins. Using Empirical Orthogonal Function analysis of mid-winter SSTs defined as the SST anomalies averaged from October through March of the previous calendar year, the study showed that changes in the dominant patterns of the midlatitude SST field reflect atmospheric forcing of the ocean.

1.2.4 New approaches

The majority of research in midlatitude ocean-atmosphere interaction has focused primarily on monthly and seasonal mean data. The results are consistent with the models outlined in FH77 and DAT03, confirming that a substantial fraction of midlatitude SST variability owes its existence to the dominant patterns of atmospheric variability. However, the advent of satellite technology offers a new approach to exploring midlatitude ocean-atmosphere interactions. From satellite retrievals, SST data of finer temporal and spatial resolution has become available in recent years. Thus these data can be used to explore ocean-atmosphere interaction on temporal and spatial scales smaller than those used in most observational analyses of extratropical atmosphere-ocean interaction. This section discusses the relevant studies that have analyzed ocean-atmosphere interactions using spatially and temporally dense data.

Using 25-km scatterometer measurements, Chelton et al. (2004) noted previously unresolved small-scale features in the curl and divergence of wind stress which may play a role in midlatitude atmosphere-ocean interaction. Nonaka and Xie (2003) observed a positive relationship between anomalous SSTs and wind speed over the Kuroshio current,

where complex meanders give rise to variability in the SST field which can persist for years. They hypothesized that warm SSTs reduce the static stability of the atmosphere near the surface, leading to enhanced vertical mixing and advection of strong winds aloft to the surface. A similar mechanism was suggested by Wallace et al. (1989), who observed that near-surface winds in the tropical eastern Pacific weakened directly over the cold tongue and strengthened over the warm waters north of the cold tongue. Positive relationships between SSTs and wind speed are also found in the East China Sea and the Southern Ocean (O'Neill et al. 2003; Xie et al., 2002) but basin wide studies noted negative relationships between the SSTs and surface winds (Namias and Cayan 1981; Wallace et al 1990). To what extent these results extend beyond the boundary layer is unclear.

Deser and Timlin (1997) examined the relationships between the extratropical atmosphere and North Atlantic SSTs using 14 years of weekly mean data. They removed the seasonal mean from each winter to eliminate the contribution of year-to-year variability to the analysis. Lagged SVD analysis was used between weekly values of standardized Z_{500} and SST anomalies to examine to the degree of covariability between the midlatitude ocean and atmosphere at weekly lags out to one month.

Figure 1.8 shows the results of the lagged SVD analysis for the North Atlantic. The results exhibit an asymmetry in the lag relationships between the extratropical atmosphere and underlying SSTs. That is, the relationships are strongest when the atmosphere leads by 2-3 weeks but relatively weak when the ocean leads by 2-3 weeks. When the atmosphere leads by 2 weeks (Fig 1.8c) the heterogeneous correlation patterns of Z_{500} and the SST for the first SVD mode reveal the tripole pattern in SST and the NAO in Z_{500}. When SSTs lead by 2 weeks (Fig 1.8a), a small area of correlations exceeding 0.4 is observed

south of Newfoundland. They concluded that the dominant patterns of Northern Hemisphere atmospheric variability lead variations in the SST field by 2-3 weeks, but they did not focus on any patterns in the SST field which lead atmospheric variability.

1.3 Objectives

Much of the previous research on midlatitude ocean-atmosphere interaction has been unable to determine the extent to which the midlatitude SST field impacts the extratropical atmosphere. Satellite data of finer temporal and spatial resolution offers a new approach to exploring these interactions in the observations but these data have been exploited by relatively few studies. The objective of this thesis is to provide a comprehensive analysis of weekly variability in the North Atlantic SST field and associated interaction with the extratropical atmosphere. The rest of this thesis is divided into the following chapters. Chapter 2 describes the data sets used in the analysis and provides background on the relevant statistical tools. Chapter 3 explores the climatology of the oceanic and atmospheric fields in the North Atlantic sector. Chapter 4 investigates the patterns of variability that dominate the North Atlantic SST field on weekly timescales. Chapter 5 expands upon the work of Deser and Timlin (1997) and more closely examines the non-contemporaneous relationships between North Atlantic wintertime SST anomalies and the dominant patterns of Northern Hemisphere variability. Chapter 6 offers a discussion of the major findings in this thesis and presents ideas for future work.

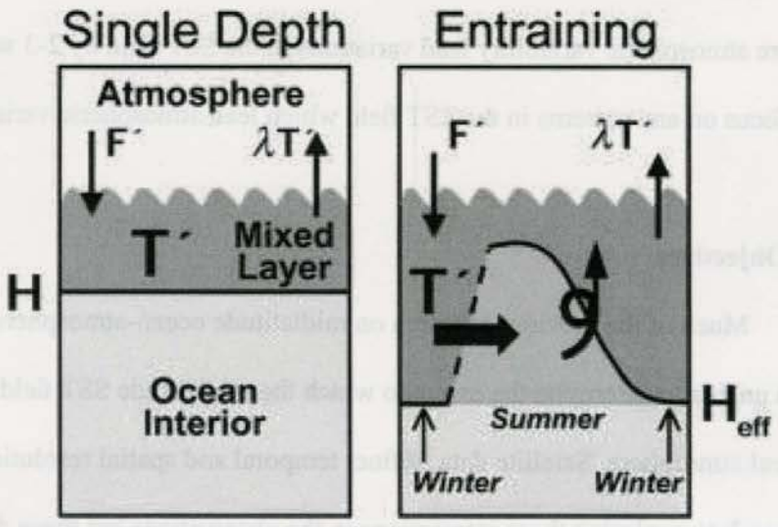

Figure 1.1. From Deser et al. (2003; DAT03). Conceptual schematics of (left) the original simple stochastic climate model of FH77 and (right) extended stochastic climate model of DAT03. In both models, changes in T' are induced by atmospheric forcing F' and damped back to space by $\lambda T'$. In FH77, the mixed layer depth (H) is constant; in DAT03, H varies seasonally with a maximum (minimum) mixed layer depth in the winter (summer). As a result of the varying H, SST anomalies induced in the previous winter are sequestered beneath the mixed layer during the summer and re-entrained in the subsequent winter.

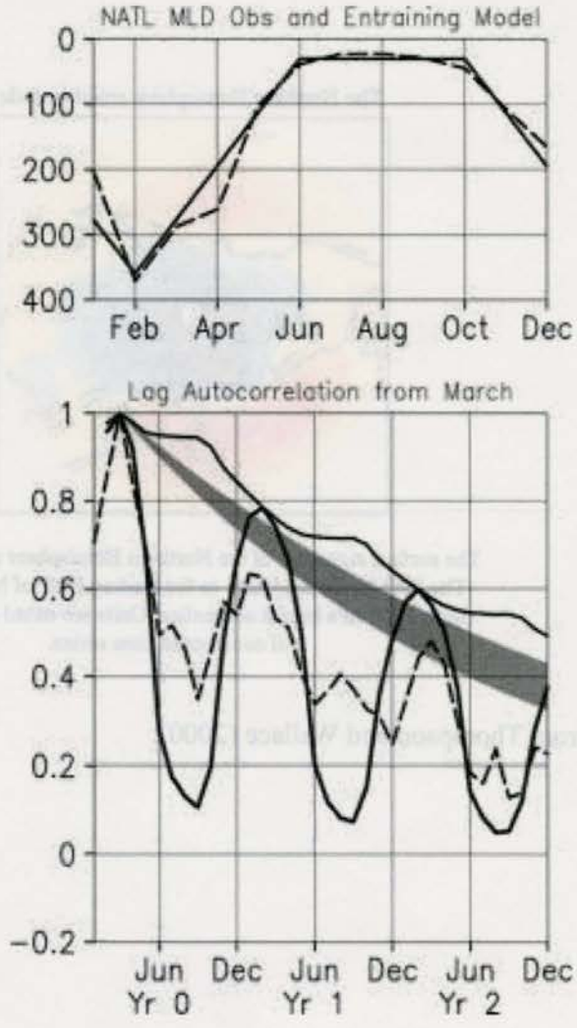

Figure 1.2. From Deser et al. (2003). (Top) Observed (dashed) and simulated (solid) mean seasonal cycle of mixed layer depth (m) for the North Atlantic Ocean. (Bottom) Monthly lag autocorrelation curves from March for heat content (solid step function-like curve), SST from the entraining model (solid), and the observed SST (dashed). The theoretical autocorrelation function for heat content based upon the extended simple stochastic climate model is denoted by shading.

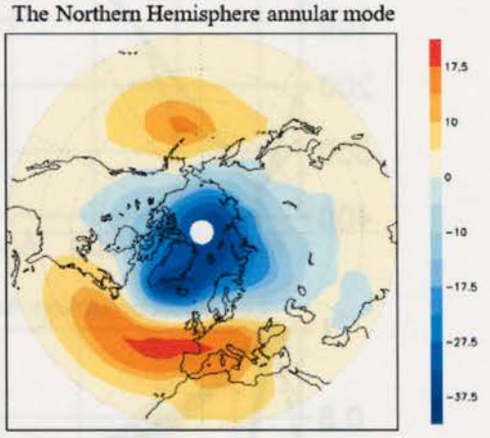

Figure 1.3. From Thompson and Wallace (2000).

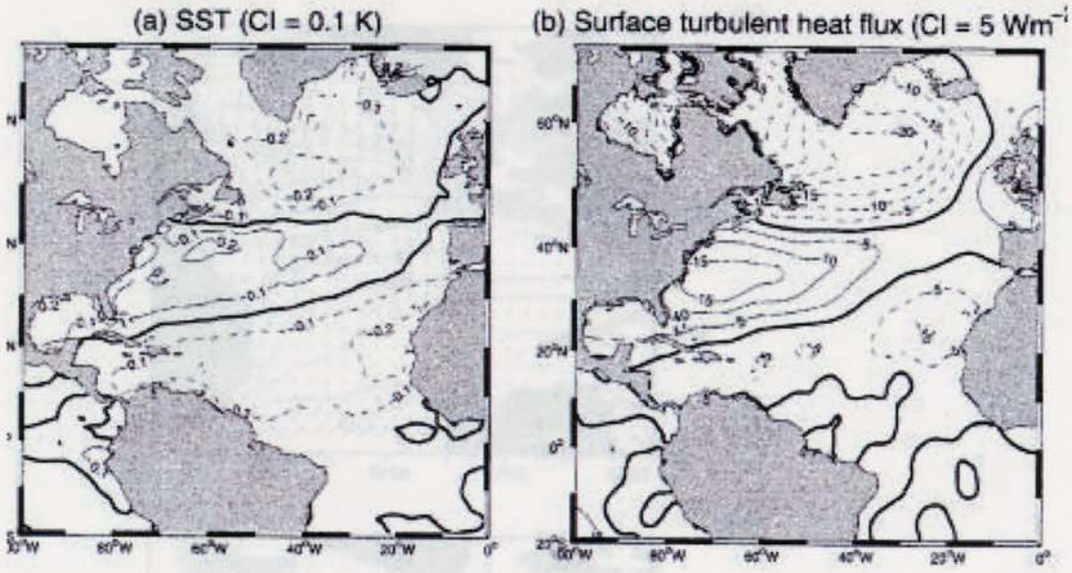

Figure 1.4. From Marshall et al. (2001a). Regressions of North Atlantic (a) SST anomalies and (b) surface turbulent heat flux onto the NAO index. The SST data was provided by the NCEP-NCAR reanalysis project and the surface heat flux data was obtained from Da Silva et al. (1994). The linear trend was removed from the data sets before calculating the regressions. Positive surfaces fluxes are directed into the ocean.

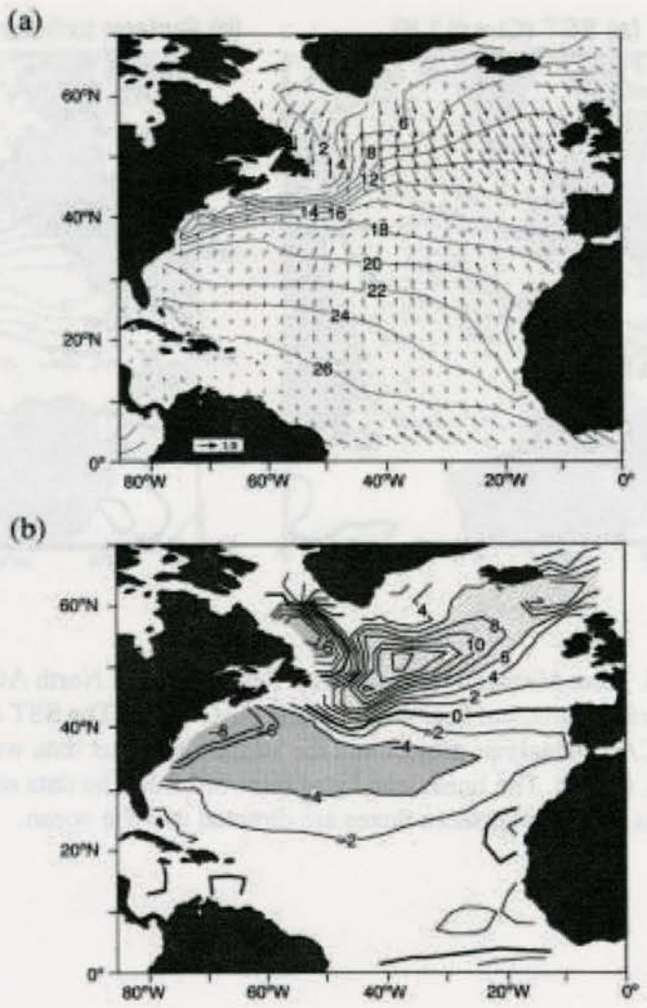

Figure 1.5. From Marshall et al. (2001b). (a) Ekman transport (arrows) induced by the positive phase of the NAO and climatological December-February SST field (solid contours). (b) Pseudo air-sea Ekman heat flux induced by the positive phase of the NAO. Positive fluxes are directed out of the ocean.

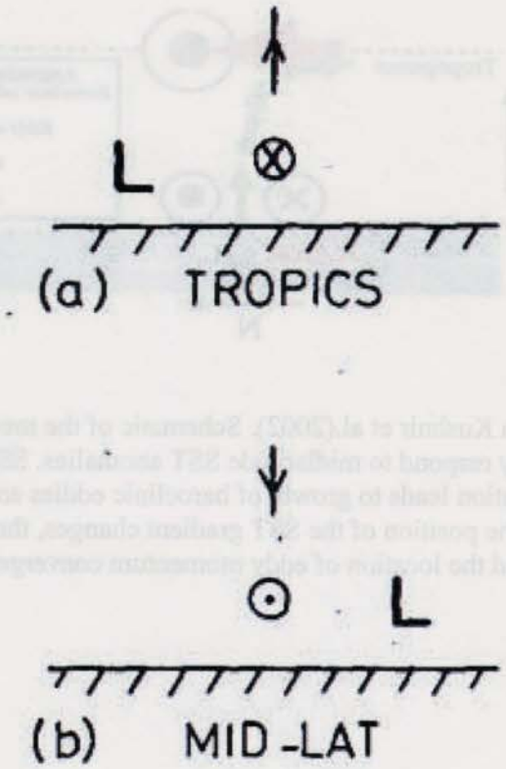

Figure 1.6 From Hoskins and Karoly (1981). Longitude-height sections of the atmospheric response to thermal forcings in (a) the tropics and (b) the midlatitudes. Arrows denote vertical motion. Circled crosses and dots denote motion into and out of the paper, respectively. L represents the low pressure trough.

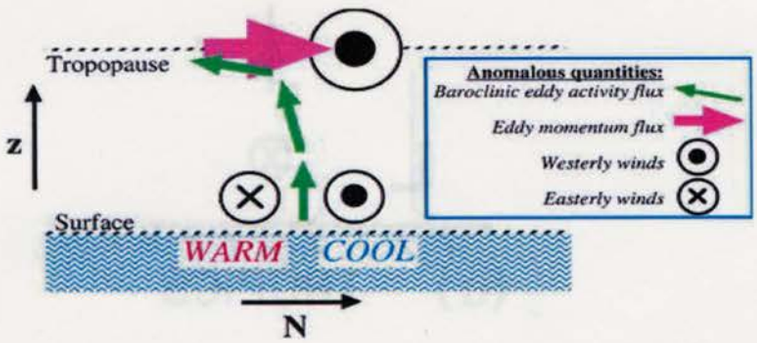

Figure 1.7 From Kushnir et al.(2002). Schematic of the mechanism through which the atmosphere may respond to midlatitude SST anomalies. SST gradient caused by an atmospheric perturbation leads to growth of baroclinic eddies and eddy momentum convergence aloft. If the position of the SST gradient changes, then the position of baroclinic wave growth and the location of eddy momentum convergence will also change.

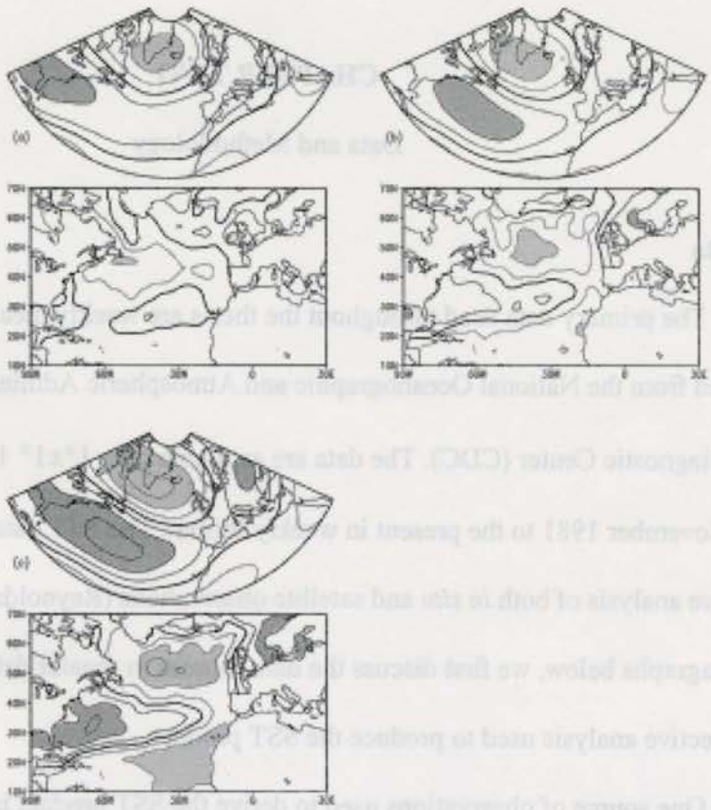

Figure 1.8. From Deser and Timlin (1997). Heterogeneous correlation patterns of intraseasonal (top) 500-mb height and (bottom) SST of the leading wintertime SVD mode in the North Atlantic for lags (a) -2 weeks (SST leads), (b) 0 weeks, and (c) +2 weeks (SST lags). Contour intervals are at (-0.2, 0, +0.2,...). Positive (negative) correlations are solid lines (dashed) and the zero contour is darkened. Dark (light) shading indicates correlations >0.4 (<-0.4).

CHAPTER TWO

Data and Methodology

2.1 Data

The primary data used throughout the thesis are weekly mean values of SST obtained from the National Oceanographic and Atmospheric Administration (NOAA) Climate Diagnostic Center (CDC). The data are available on a $1°x1°$ latitude/longitude grid from November 1981 to the present in weekly format. The SST data are produced by objective analysis of both *in situ* and satellite observations (Reynolds et al. 1995, 2002). In the paragraphs below, we first discuss the data sources in greater detail and then describe the objective analysis used to produce the SST product.

One source of observations used to derive the SST product is *in situ* data. These data consist primarily of SST observations on ships from insulated buckets, hull contact sensors and engine intakes with additional observations from drifting and moored buoys in regions of sparse ship observations. SST observations from buoys are measured using thermistors and hull contact sensors and are then relayed back to shore in real-time by satellites. Prior to 1998, *in situ* data are obtained from the Comprehensive Ocean-Atmosphere Data Set (COADS; Woodruff 1998). After 1998, the observations were obtained from the Global Telecommunication System (GTS), a communications network that transmits SST observations from ships and buoys to ground stations via satellite (Colwell and Turner 1999).

Another source of data used to derive the SST product is satellite retrievals from the Advanced Very High Resolution Radiometer (AVHRR). The weekly AVHRR satellite retrievals are centered about Wednesday. The retrievals cover roughly three times as much area as *in situ* observations and allow higher resolution of small scale features such as Gulf Stream eddies. The resolution of the AVHRR is 1.1km at nadir.

One disadvantage of satellite retrievals is the inability of the satellite to "see" through the clouds to the surface. As a result, retrievals cannot be made in 100% cloud-covered regions. They are made in partially cloud-covered regions but the cloud contamination creates a negative bias in SSTs since cloud top temperatures are colder than SSTs. Increased aerosol concentrations (e.g. from volcanic eruptions) also create a negative bias in the satellite retrievals. Although the satellite biases are reduced by techniques described in Reynolds et al. (1989, 1993), they cannot be completely eliminated. Thus, *in situ* data is not only critical for satellite calibration and validation but for final bias corrections as well.

The AVHRR satellite did not retrieve data prior to 1989, and during this period the SST data were supplemented with the analysis of the National Environmental Satellite, Data and Information Service (NESDIS) satellite retrievals at the University of Miami's Rosenstiel School of Marine And Atmospheric Sciences (RSMAS). The weekly NESDIS satellite retrievals are centered about Sunday. Thus, the center of the week is defined as Sunday for the 1981-1989 and Wednesday from January 1990 to the present.

Once the satellite biases are removed, the *in situ* and satellite data are analyzed using an optimum interpolation (OI) technique outlined in Gandin (1963). The OI technique corrects the SST value from the previous week by incorporating observations,

weighted according to their distance from SST value. At each time step, the analyzed SST is found as follows: first, the differences between the data and the SST value from the previous week are calculated. The differences, called data increments, are weighted according to the following: 1) the distance between the location of the first guess estimate and the observed data point and 2) the covariance and variance errors of the first guess and data increments. The weighted data increments are summed to form an analysis increment. The analyzed SST value is then calculated by adding the analysis increment to the SST value from the previous week.

There are several problems that could impact the quality of the SST analyses. First, the quality of the SST values may be poor in areas of high cloud cover and sparse *in situ* observations. This is especially true in the Southern Ocean where there are few ship observations and the percentage of annual mean cloud coverage exceeds 75% (O'Neill et al. 2003). The second problem is that values of -1.8°C represent any SST measurement less than -1.8°C (assuming that the average salinity in the polar regions is 34 practical salinity units (psu), the freezing point of water is -1.8°C. In the analysis, any SST value below the freezing point is considered to be too low to be a physical value of SST). Third, the satellite bias correction adds noise to the SST analyses product. To reduce the noise, a 3 point binomial filter is typically applied to the SST field in space and time (O'Neill et al. 2003; Reynolds et al. 2002).

The atmospheric variables used throughout the study are produced by the National Centers for Environmental Prediction-National Center for Atmospheric Research (NCEP-NCAR) reanalysis project obtained from the NOAA CDC (Kalnay et al. 1996; Kistler et

al. 2001). The reanalysis consists of land surface, ship, rawinsonde, aircraft, satellite and other data sources, all of which are quality controlled and then assimilated with a data assimilation system. As part of the assimilation system, the NCEP operational model dynamically interpolates the data using 6 hr. forecasts. The NCEP operational model contains 28 vertical levels and has a spatial resolution of ~210 km. The data assimilation system is frozen over the period 1957-1995 to prevent climatic jumps resulting from changes in the model.

The NCEP reanalysis data are available on 17 vertical levels of 6 hourly $2.5° x 2.5°$ latitude/longitude grids from 1948-present. The variables have been separated into four categories, based on the relative influence of the observations and the model on the analysis values. Variables in Class A, such as geopotential height and zonal wind, strongly depend on the observations and are considered to be the most reliable. Class B variables, e.g. surface pressure, also rely on the observations but the NCEP model strongly affects the analysis values. Class C variables are entirely model dependent and Class D variables are derived solely from the climatological fields, with no influence from data assimilation. Variables in the last two classes, e.g. soil temperature and precipitation rate, are less reliable than the first two. In our analysis, only Class A and B variables are used.

In addition to the NCEP reanalysis, the daily NAM index provided by the NOAA Climate Prediction Center (CPC) is used. The index is constructed by projecting daily fields of 1000 hPa height anomalies onto the leading Empirical Orthogonal Function (EOF) of monthly mean 1000 hPa height anomalies for the period 1979-2002 (Thompson and Wallace 2001). We use daily values of the NAM index from 1981-2002. The index

values are standardized by subtracting the long-term mean and dividing by the long-term standard deviation.

2.2 Methodology

Our analysis investigates the North Atlantic region, 20° – 80° N, 90°W-30°E for the full record of the OI SST analysis (November 1981-December 2002). As mentioned in the previous section, any SST values below the threshold $-1.8°C$ were considered unphysical and are omitted from the analysis. We computed the weekly means of daily values of the NCEP reanalysis fields and the NAM index. The seasonal cycle is removed from the SST and NCEP reanalysis fields by subtracting the long term weekly mean from each week at each grid point.

We explore the variability in the mid-latitude North Atlantic SST field and associated interaction with the overlying circulation by making extensive use of statistical tools such as regression/correlation analyses and Empirical Orthogonal Function analysis. The remainder of this section describes these techniques in greater detail.

2.2.1 Regression and correlation analyses

We use univariate linear regression analysis to describe the linear relationship between two variables using the following equation:

$$\hat{y}(t) = a_0 + a_1 x(t), \tag{2.1}$$

where $x(t)$ is an independent variable and $\hat{y}(t)$ is the estimate of the observed $y(t)$. Linear regression determines the slope of the line that produces the smallest error in estimating

the observed data $y(t)$. The most common method of determining the error is the least squares method which minimizes the sum of the squared error $(y - \hat{y})$ at each time step. Using the least squares method, the regression coefficient a_1 is given as:

$$a_1 = \frac{\overline{x'y'}}{\overline{x'^2}}, \tag{2.2}$$

where the prime denotes the deviation from the mean and the overbar represents the mean. If the independent variable *x(t)* is standardized then the regression coefficient will have units of change in *y(t)* per one standard deviation change in *x(t)*.

Correlation analysis is a useful tool for determining the statistical significance of the linear relationship between *x(t)* and *y(t)*. In the linear case described above, the correlation coefficient *r* can be calculated as a function of the regression coefficient:

$$r = a_1 \frac{\sqrt{\overline{x'^2}}}{\sqrt{\overline{y'^2}}}. \tag{2.3}$$

The square of *r* indicates what fraction of the total variance in *y(t)* is explained by the linear relationship with *x(t)*. The statistical significance of all correlation coefficients is assessed using the *t*-statistic defined as:

$$t = \frac{r\sqrt{N_{eff} - 2}}{\sqrt{1 - r^2}}, \tag{2.4}$$

where *r* is the correlation coefficient and N_{eff} is effective sample size. The effective sample size accounts for the persistence in the data. If the data exhibit substantial persistence, then each sample may not be independent from the previous sample and the number of independent samples will not be equal to *N*. Assuming the data follows a first order auto

regressive process, Bretherton et al. (2002) outlined a method for determining the effective sample size N_{eff} as:

$$N_{eff} = N\left[\frac{1 - r_1 r_2}{1 + r_1 r_2}\right], \tag{2.5}$$

where N is the sample size; and r_1 and r_2 are the lag-one autocorrelations of the time series being correlated. Note that as the persistence increases in the time series, effective sample size decreases.

2.2.2 Empirical Orthogonal Function (EOF) analysis

We use Empirical Orthogonal Function (EOF) analysis to examine the dominant patterns in the North Atlantic midlatitude SST field. EOF analysis decomposes any data matrix, A_{MxN}, into a series of orthogonal spatial patterns and time series such that the variance in the new phase space is organized entirely along the diagonal of the dispersion matrix. The EOFs are found by solving the eigenvalue problem:

$$C_{NxN} E_{NxN} = E_{NxN} L_{NxN} \ , \tag{2.6}$$

where C is the covariance matrix ($A^T A$), E is the matrix of eigenvectors e_i of length N and L is a diagonal NxN matrix containing the eigenvalues λ_i. If M is the number of timesteps and N is the number of grid points then C corresponds to the spatial covariance matrix. In this case, the largest eigenvector corresponding to the largest eigenvalues λ_i is that pattern which explains more variance than any other pattern. The fraction of the total variance explained by each eigenvector is given as:

$$fraction\ of\ variance\ explained = \frac{\lambda_i}{\sum_{i=1}^{N} \lambda_i}. \tag{2.7}$$

The largest eigenvalue in L, λ_1, corresponds to the first eigenvector in E, e_1. The first EOF (often called the leading EOF) is the pattern that explains the largest fraction of variability, the second EOF is the pattern that explains the second largest fraction of variability, etc. Because the eigenvectors are linearly independent of each other, each EOF must be orthogonal to all other EOFs before and after it. As a result of the orthogonality constraint, higher order EOFs are increasingly affected by the mathematical constraints of the analysis.

Projecting the original data matrix A onto each eigenvector at each time step produces the Principal Component (PC) time series, which depicts how each EOF evolves with time. The PC time series can also be found by solving equation (2.6) where C is the temporal covariance matrix (AA^T). In this case, e_i will represent the i^{th} PC time series and L will still be the diagonal matrix containing the eigenvalues.

To assess the statistical significance of EOF/PC pairs, the robustness (i.e. reproducibility) of each pair is determined. A common method estimates robustness of EOF/PC pairs by calculating the degree of separation between eigenvalues (North et al., 1982). The 95% confidence errors bars $\Delta\lambda$ for each eigenvalue λ can be calculated using:

$$\Delta\lambda = \lambda\sqrt{\frac{2}{N}}, \tag{2.8}$$

where N is the number of independent samples. EOFs are considered to be distinct and statistically significant at the 95% confidence level if the error bars do not overlap. EOF anal-

ysis of subdivided data can also indicate the robustness of EOF/PC pairs. A robust EOF/PC pair should emerge in EOF analysis of both the full record and its subsets.

Several steps are necessary to prepare the data for EOF analysis. First, we use the anomalous fields so that the seasonal cycle will not emerge as an EOF. The grid boxes must also be weighted by the square root of the cosine of the latitude. Weighting takes into account the fact that polar grid boxes are smaller than grid boxes near the equator and therefore have less influence on the results. The data is weighted by the square root of the cosine (rather than the cosine) of the latitude because EOF analysis eigenanalyzes the covariance matrix A^TA. Generally, the EOFs themselves are not displayed for interpretation because they are weighted and are dimensionless. Therefore, the original data is regressed onto standardized values of the associated PC time series.

CHAPTER THREE

Climatology of North Atlantic Oceanic and Atmospheric Fields

The primary objective of this thesis is to investigate weekly midlatitude North Atlantic SST variability and its relationship with the extratropical atmospheric circulation. Before examining midlatitude ocean-atmosphere interaction, we first explore the key features of the general circulation of the ocean and atmosphere. The goal of this chapter is to provide a description of the climatology of the SST field and the overlying atmospheric circulation.

3.1 North Atlantic SST Field

This section explores the climatology of North Atlantic SST field. We first examine the main features of the climatological mean SST field. We then explore the total variance maps of weekly SST anomalies to determine where the most pronounced variability in this field is observed.

The climatological mean SST field for each calendar month is represented by the solid contours in Figure 3.1. Note that the maps in Fig. 3.1 are column oriented (i.e., November, December, January, and February are displayed in the first column, etc.). During the winter months, the SST field south of ~35^{o}N exhibits a zonally symmetric banded structure in which SSTs decrease monotonically with latitude. During the summer

months, the isotherms in this region shift northward due to increased solar insolation and also tilt from the northwest to the southeast. Poleward of 35°N, the isotherms continue to decrease with latitude but are also characterized by a distinct southwest-northeast orientation. In all months, the climatological mean SST field exhibits a sharp gradient in SSTs along the eastern coast of the United States, extending from Cape Hatteras to east of Newfoundland. The SST gradient is enhanced in the winter months. During the summer and fall, the gradient weakens as the temperatures of the coastal waters to the north of the SST gradient increase.

The strong SST gradient and fanning out of SSTs into the subpolar North Atlantic mark an oceanic frontal boundary between cool subpolar waters and warm water transported poleward by the Gulf Stream, the intense western boundary current located along the western flank of the North Atlantic subtropical gyre. The SST gradient is largest poleward of the Gulf Stream and is coincident with the sharp transition from warm waters in the Sargasso Sea to cooler waters along the east coast of Canada.

Because the Gulf Stream plays an important role in the structure of the SST field, it is worth describing in greater detail. Figure 3.2 shows a satellite image of the SSTs over the western North Atlantic during June 1984. The shading denotes the amplitude of the SSTs: the warmest SSTs are represented by red; blue represents the coldest SSTs. The purpose of the satellite image is to show features of the Gulf Stream that are averaged out in the long-term climatological mean maps. South of Cape Hatteras, the Gulf Stream current is marked by the narrow band of dark red SSTs beginning roughly near the Straits of Florida. It moves along the Blake Plateau where the flow is limited to a depth of 800m.

SSTs between the Gulf Stream and the coast of southeast United States are slightly cooler than those within the Gulf Stream but this feature is not evident in Fig. 3.1.

Downstream of Cape Hatteras, the Gulf Stream broadens as it leaves the continental shelf and moves into relatively deeper water (4000-5000m). The lack of topographic constraints gives rise to a more complex flow with respect to the region south of Cape Hatteras. Meanders in the flow can exceed 350 km and eddies can break off from the meanders, forming independent circulations called Gulf Stream eddies (Brown et al. 1989). There are two types of eddies: cold core and warm core eddies. An example of a cold core Gulf Stream eddy is evidenced by the small green disk within the warm waters of the Sargasso Sea east of Cape Hatteras. It is characterized by a cyclonic circulation of cold water extending to a depth of ~4000-5000 m. Cold core Gulf Stream eddies tend to move towards the south, southwest and can persist anywhere from months to years. At any give time, up to 15% of the Sargasso Sea contains cold core eddies (Brown et al. 1989). Fig. 3.2 shows an example of the formation of a warm core eddy in the cooler subpolar water south of Nova Scotia at ~40°N. Warm core Gulf Stream eddies are regions of independent anticyclonic circulation and occupy ~40% of the region between the Gulf Stream and the eastern coast of Canada (Brown et al. 1989). In most cases, warm core eddies last only a few months before they are entrained back into the Gulf Stream. As the Gulf Stream continues across the North Atlantic, water is advected from the Labrador Sea into the region between the Gulf Stream and the coast. These coastal waters are much cooler than the Gulf Stream waters, as evidenced by the strong SST gradient in Fig. 3.1.

The shading in Figure 3.1 represents the total variance of SST anomalies. In all months, the largest variance occurs primarily within the zone of pronounced SST gradi-

ents in the region from Cape Hatteras to east of Newfoundland (the region is also referred to as the Gulf Stream extension). In the winter months (November-April), a weak secondary variance maximum is also observed to the south and east of the region of largest SST gradients. The amplitude of the variance within the region of largest SST gradients is comparable in the summer months (May-October) but is zonally elongated toward the western coast of Europe during the fall months. A region of enhanced variance is also observed near the zero SST contour in the Labrador and Greenland Seas between June and October, possibly arising from year-to-year variations in the timing of the melting sea ice. Comparison of the region of strongest SST variance in Fig. 3.1 to the pattern of SSTs in Fig. 3.2 shows that the strong SST variance occurs in the region of relatively complex flow. This suggests that the source of enhanced SST variance in the SST gradient is the existence of the complex, meandering current and Gulf Stream eddies. Temperature advection and Ekman currents may also contribute to SST variance.

To determine the relative contribution of week-to-week and year-to-year SST variability to the total variance, the SST anomaly field is decomposed into intraseasonal and seasonal mean components, respectively (Figure 3.3). The amplitude of the (top) intraseasonal and (bottom) seasonal mean SST variance are comparable. The top panels in Figure 3.3 show the intraseasonal variance of (left) November-April and (right) May-October SST anomalies. During the winter, the maximum intraseasonal SST variance lies within the zone of pronounced SST gradients but very little intraseasonal variance is observed in any other region. During the summer, the intraseasonal variance within the SST gradient extends further east toward the coast of Europe. Variance is also enhanced in the Great Lakes and the Mediterranean Sea during the summer.

The bottom panels of Fig. 3.3 show the variance of the seasonal mean (i.e., variance from one season to the next; left) November-April and (right) May-October SST anomalies. Similar to the variance of intraseasonal SST anomalies, the year-to-year variance is strongest within the region of largest SST gradients and extends eastward during the summer season. In contrast to the top panels of Fig. 3.3, the year-to-year variance is enhanced in the subtropical North Atlantic and the Labrador and Greenland Seas, possibly arising from processes such as mean advection by ocean currents and deep water formation (the latter more likely in the Labrador and Greenland Seas).

3.2 North Atlantic Atmospheric Circulation

This section provides an overview of the general atmospheric circulation over the North Atlantic sector by examining the observed climatological mean of several atmospheric fields. The figures also include the climatological mean SST field so we can compare where key features of the atmospheric circulation occur with respect to those of the SST field.

We first examine the distribution of mass over the North Atlantic sector by calculating the monthly mean maps of sea level pressure (SLP, Figure 3.4). In all months, the mean SLP field exhibits a region of relatively high pressure located over the eastern subtropical North Atlantic (hereafter referred to as the Azores high). The Azores high is coincident with the descending branch of the Hadley cell, which is centered at 30^{o}N and gives rise to strong subsidence there (James 1994). The maximum SLP occurs on the eastern side of the ocean basin where the air temperature is colder relative to the zonal mean. In the winter months, the mean SLP field also exhibits a region of relatively low pressure

located over Iceland (hereafter referred to as the Icelandic low). This feature occurs as the results of the almost daily passage of wintertime storm systems across the North Atlantic.

The Azores high (Icelandic low) steers the clockwise (counterclockwise) movement of water in the North Atlantic known as the subtropical (subpolar) gyre. As the wind blows clockwise over the subtropical North Atlantic, the direction of the oceanic Ekman transport is 90° to the right of the wind stress (Gill 1982). As a result, water converges under the center of the anticyclonic atmospheric circulation, creating a horizontal pressure gradient force that drives water outward from the center. The Coriolis force deflects the outward moving water to the right until the ocean currents attain geostrophic balance. The result is the anticyclonic flow of water under the Azores high called the subtropical gyre (Brown et al. 1989). The opposite argument can be used in the case of the subpolar gyre which lies beneath the Icelandic low.

Figure 3.5 shows the climatological monthly mean maps of the zonal wind at 300hPa (u_{300}). During the winter months, the u_{300} field is characterized by westerlies over much of the North Atlantic basin. Regions of maximum zonal wind are located over North Africa at ~20°N and off the east coast of the northern United States at ~40°N. During the spring and summer months, the strength of u_{300} weakens considerably.

The zonal wind maximum centered on the eastern coast of the United States is commonly called the North Atlantic jet and is driven by the convergence of eddy momentum fluxes in the atmosphere (Holton 1992). Note the region of strong SST gradient is located under the jet. By the thermal wind relation, in regions of enhanced horizontal temperature gradients, the zonal wind must increase with height (Wallace and Hobbs 1977). The surface barotropic signature of the jet is evidenced by the westerly winds implied by

the gradients in SLP in Fig. 3.4. Meridional meanders in the jet reflect variability in the NAM.

The North Atlantic jet plays an important role in the development of storms off the coast of the eastern United States (Holton 1992). In the poleward flank of the jet exit region, the curvature of the jet and the changing wind speed produces a region of divergence aloft. To compensate, air rises from the surface. As more air aloft is swept away by the jet than can be supplied from below, a low pressure develops at the surface. Note the region of divergence aloft and surface convergence occurs over the region of enhanced SST variability in the Gulf Stream extension.

The zonal wind maximum over North Africa is part of the subtropical jet which occurs as the result of the conservation of angular momentum of air moving poleward from the deep tropics (Grotjahn 1993). In the tropics, surface heating is balanced by rising motion. As air parcels reach the tropopause they spread northward. The Coriolis force deflects air to the right in the Northern Hemisphere and thus the zonal wind accelerates as the air moves poleward. As the air parcels continue to move poleward, the radius of each latitude band decreases. To conserve angular momentum, the zonal wind continues to increase until it reaches the poleward extent of the Hadley cell at ~30°N. At this latitude, the flow becomes unstable and the atmosphere is disturbed by eddies that cause the zonal wind to decrease poleward. In contrast to the North Atlantic jet, the subtropical jet does not extend to the surface.

Figure 3.6 shows climatological mean maps of the meridional heat transport due to stationary and transient eddies at 700hPa ($v^*T^*_{700}$) where '*' denotes departure from the zonal mean. In the winter, a band of positive heat flux is located along 45°N, with a maxi-

mum centered over the eastern coast of the United States. This maxima lies near the poleward exit of the North Atlantic jet, as evidenced in Fig 3.5 and over the region of the most pronounced SST gradients. A secondary weaker maximum is located over eastern Europe. The amplitude of the meridional eddy heat transport decreases throughout the spring and summer. A small region of negative heat transport is observed over the midwestern United States.

The presence of enhanced poleward (i.e., positive) heat transport in the Gulf Stream extension is indicative of cyclogenesis there (James 1994) and is consistent with the strong surface baroclinicity evidenced in the SST field. Growing baroclinic waves are characterized by the conversion of available potential energy into eddy kinetic energy (Hartmann 1994). Associated with this conversion is the westward displacement of the temperature wave with respect to the pressure wave (Wallace and Hobbes 1977). Thus, in growing baroclinic waves over the Gulf Stream extension, warm air is advected towards the pole and cold air is advected towards the equator. As baroclinic waves move across the North Atlantic, the conversion of eddy kinetic energy into zonal kinetic energy becomes important and the poleward heat flux weakens (James 1994). In the summer, the baroclinicity in the northwest Atlantic weakens and cyclogenesis becomes less frequent.

Finally, we examine the climatological mean surface fluxes due to sensible and latent heat (Figure 3.7). Note the orientation of the fluxes is positive when the flux is out of the ocean into the atmosphere. During the winter months, the positive surface heat flux is stronger over the ocean than over land. The opposite is true in the summer months. The strongest region of positive surface heat fluxes is near the east coast of the United States, along the southern flank of the strongest SST gradient that marks the Gulf Stream.

Surface fluxes are the predominant mechanism through which the ocean and atmosphere communicate. Because the heat capacity of the ocean is larger than the atmosphere, relatively warm SSTs persist throughout the winter while air temperature decreases. Hence, during the winter, midlatitude SSTs are generally warmer than the air temperature, giving rise to a positive net heat flux into the atmosphere. This effect is strongest in the Gulf Stream. The difference between the air temperature and the underlying SSTs grows as the air is swept off the North American continent by the westerlies and moves over increasingly high SSTs. As a result, the largest fluxes are observed over the southern edge of the pronounced SST gradient.

3.3 Concluding Remarks

This chapter demonstrated that the largest variance in weekly wintertime SST anomalies occurs within a region of pronounced SST gradients in the Gulf Stream extension and underlies a region of strong cyclogenesis off the coast of the northeast United States. In Chapter One, we described a mechanism for a possible extratropical atmospheric response to midlatitude SST through anomalous eddy feedbacks in the region of the storm track. Because the Gulf Stream extension exhibits maximum variance in the SST field and underlies a region of intense cyclogenesis, it may be a potential region where the atmosphere is sensitive to variations in SSTs.

In the next chapter, we continue to explore variability in the midlatitude North Atlantic SST field using EOF analysis. Based on the SST variance observed in Figure 3.1, a pattern capturing variability along the Gulf Stream extension is expected.

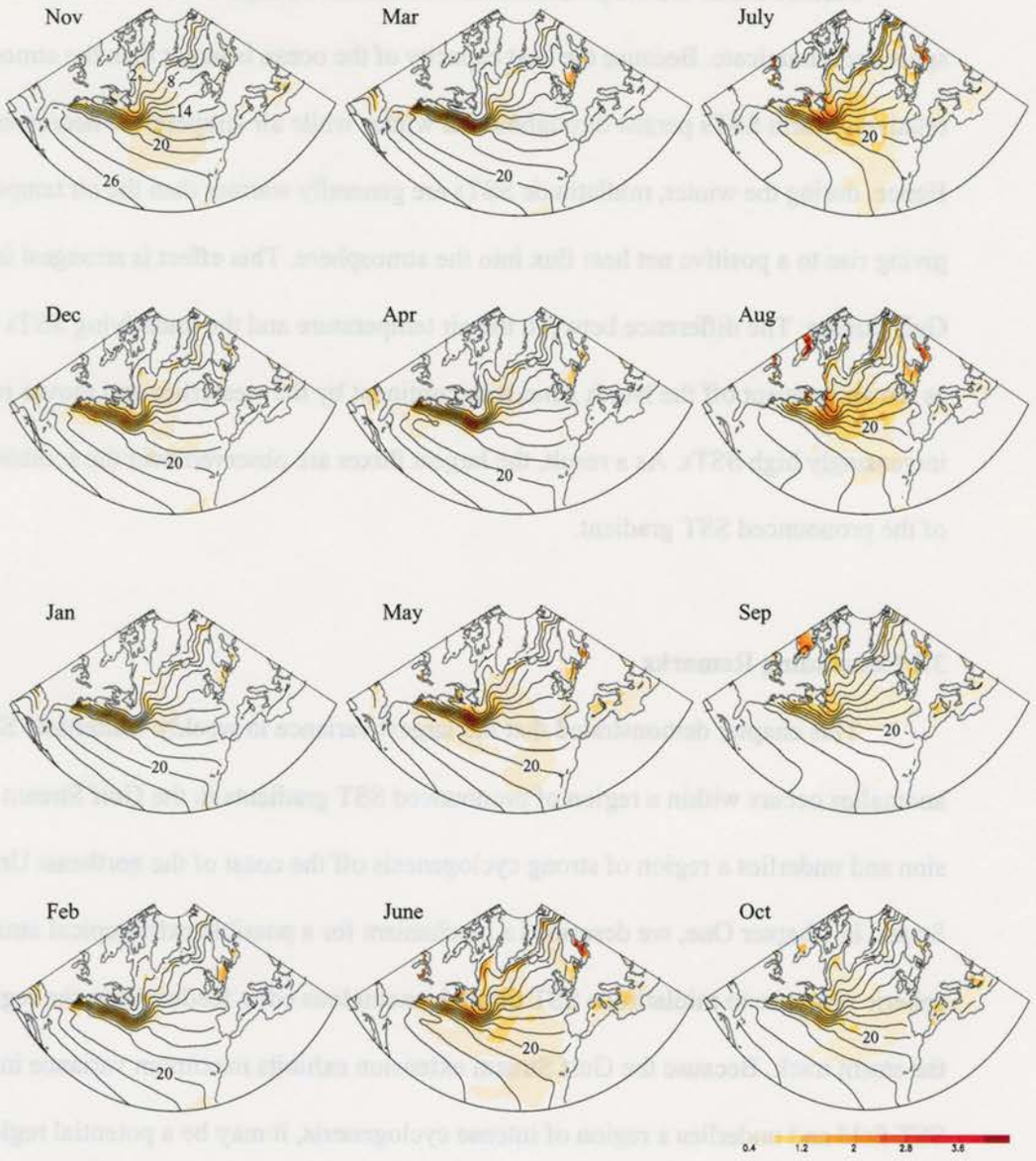

Figure 3.1. Climatological variance of weekly mean SST anomalies (shading) and climatological mean SSTs (solid contours) shown as a function of the month based on the period from 1981-2002. Contour intervals are drawn at (0°C, 2°C, 4°C, etc....). The 20°C contour interval is marked on all maps.

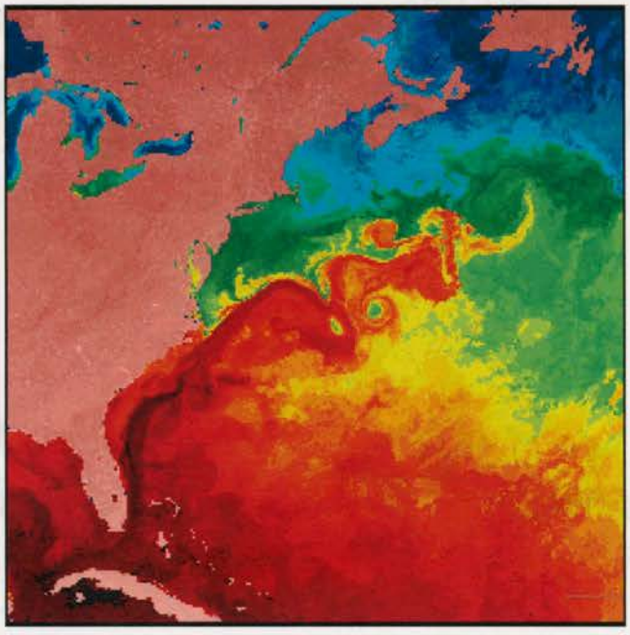

Figure 3.2. Satellite image of SSTs in the Gulf Stream and the western North Atlantic from June 1984. SSTs represented by computer-generated color. Red denotes the warmest SSTs, followed by orange, yellow, green, and blue. Photo courtesy of O. Brown, R. Evans, and M. Carle, University of Miami, Rosenstiel School of Marine and Atmospheric Science.

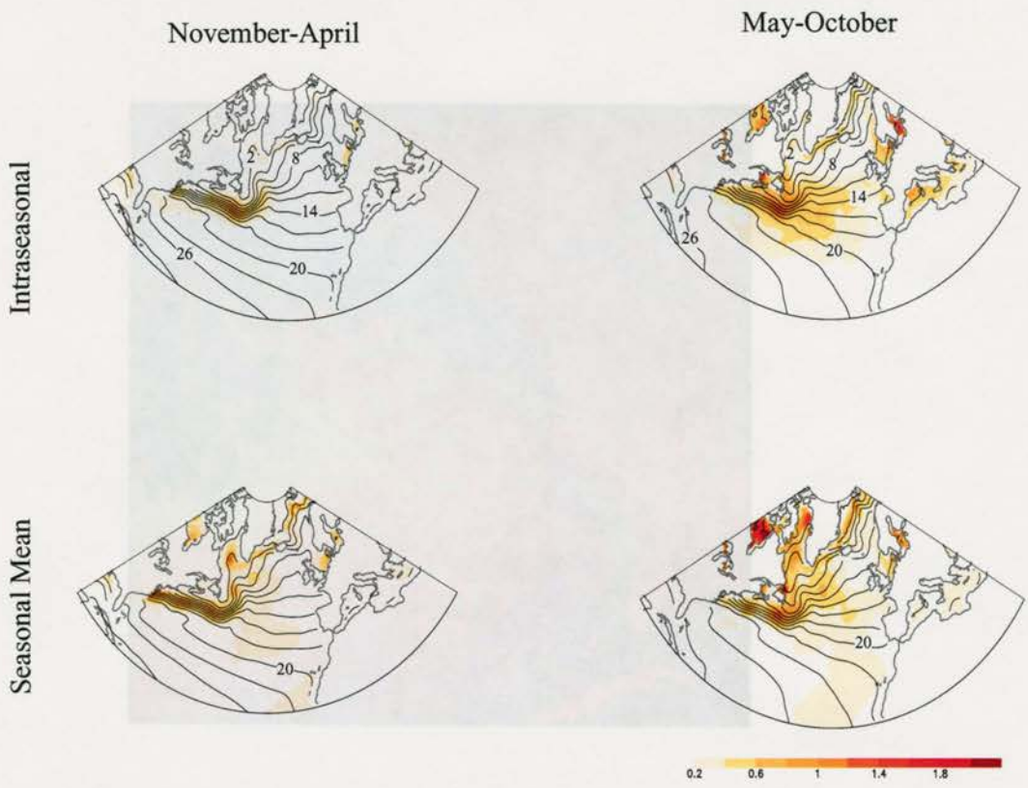

Figure 3.3. Decomposition of the variance of SST anomalies (shaded) into (top panels) intraseasonal and (bottom panels) seasonal mean components for (left panels) November-April and (right panels) May-October. Mean SST contour intervals are as in Figure 3.1. Units are in ^{o}C. Note that shading contours have been reduced by half relative to Fig. 3.1.

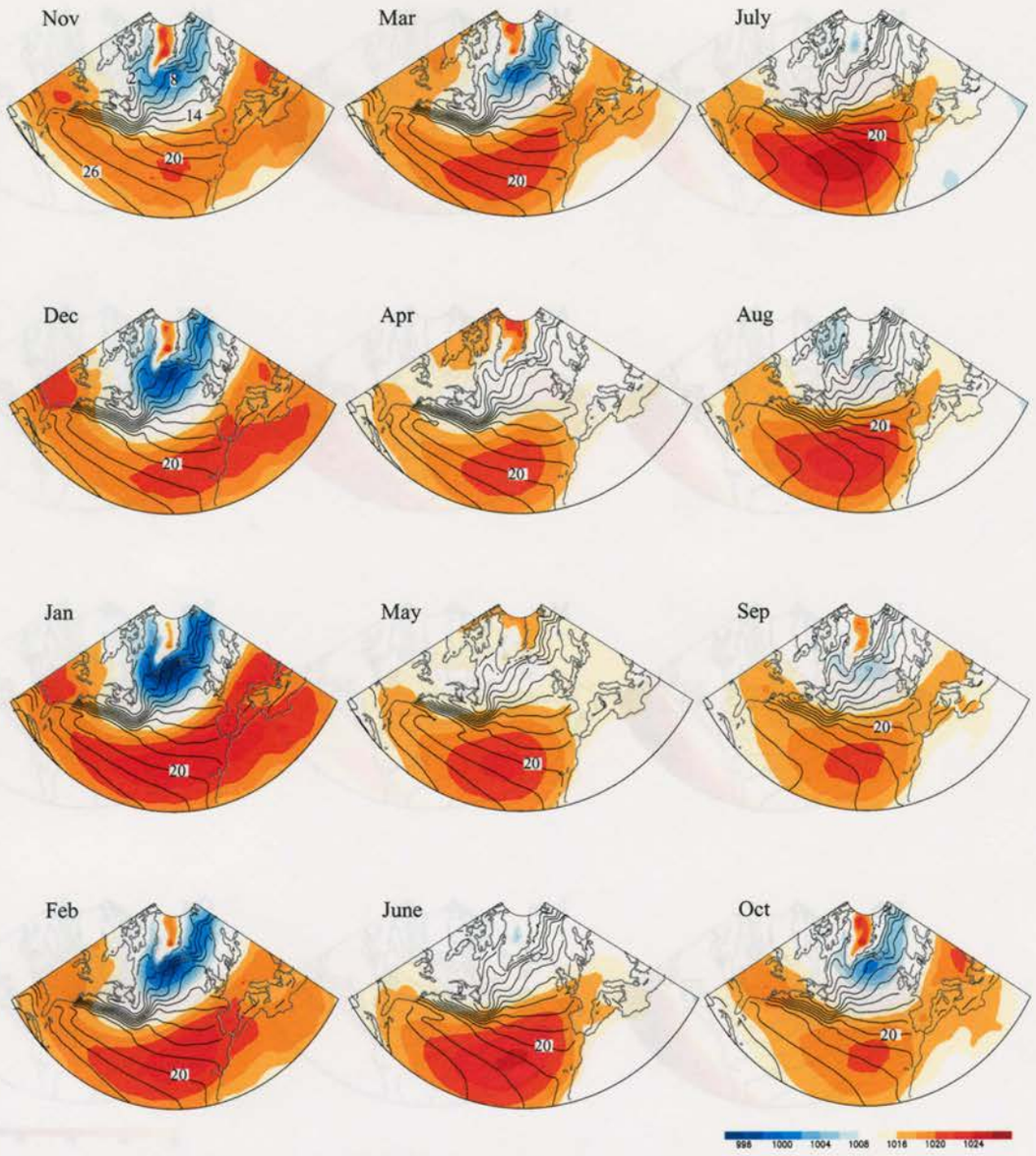

Figure 3.4. As in Figure 3.1 but shaded contours denote climatological monthly mean sea level pressure (SLP). Units of SLP are in millibars (mb).

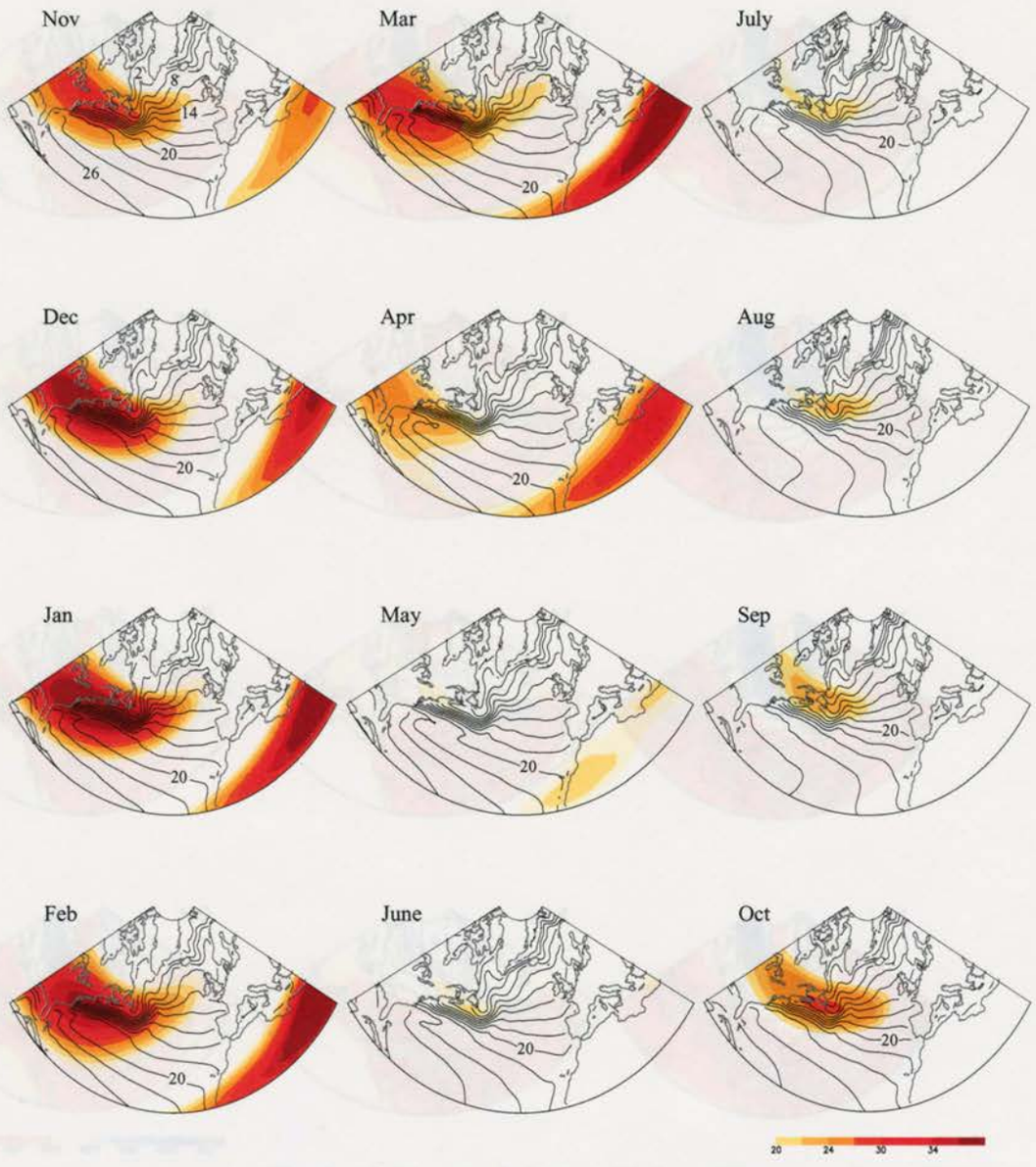

Figure 3.5. As in Figure 3.1 but shaded contours denote climatological monthly mean zonal wind at 300hPa (u_{300}). Units of zonal wind are in ms^{-1}.

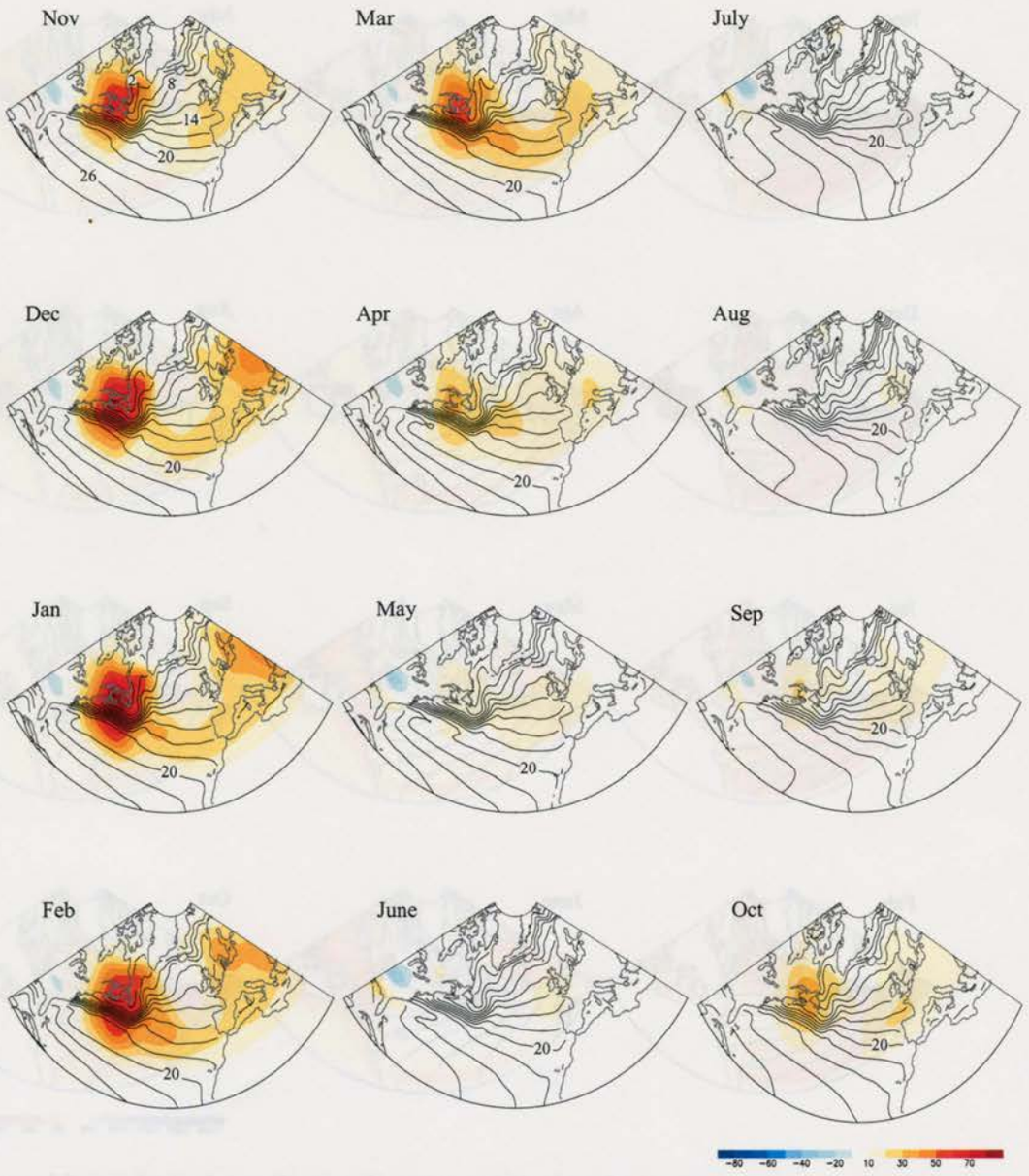

Figure 3.6. As in Figure 3.1 but shaded contours denote climatological monthly mean meridional heat flux due to eddies at 700 hPa ($v^*T^*_{700}$). Units of heat flux are in $ms^{-1}K$.

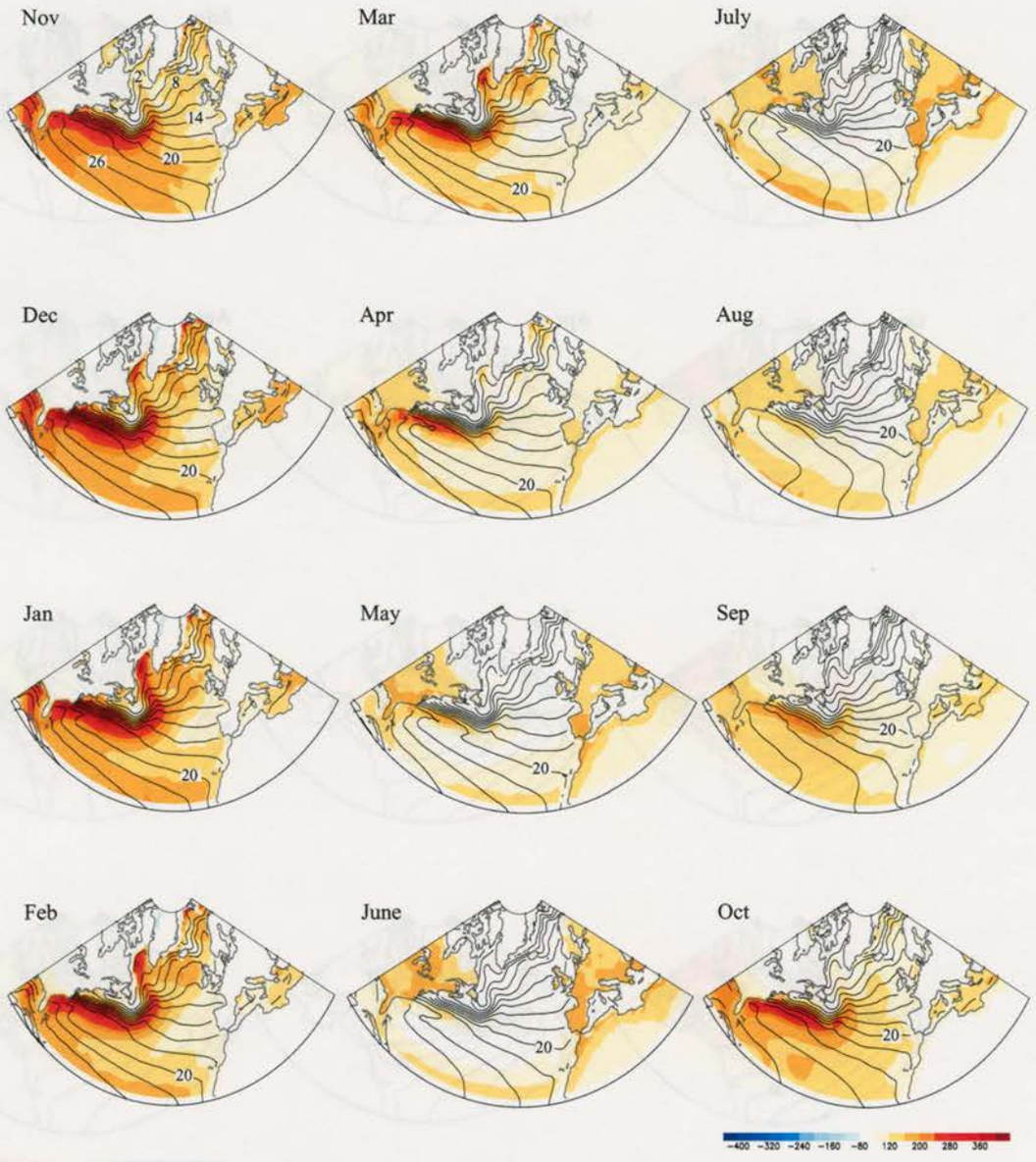

Figure 3.7. As in Figure 3.1 but shaded contours denote climatological monthly mean surface heat fluxes due to sensible and latent heat fluxes. Units of heat flux are in Wm^{-2}.

CHAPTER FOUR

Dominant Patterns of Weekly North Atlantic SST Variability

The previous chapter provides a description of the climatological mean and variance of the midlatitude North Atlantic atmospheric and oceanic fields. The results show that the largest variance in the SST field is located within a zone of pronounced SST gradients that coincides with the poleward side of the Gulf Stream extension. The area of maximum SST variance also underlies a region of enhanced wintertime cyclogenesis over the western edge of the North Atlantic storm track. This chapter more closely examines the patterns of variability that dominate the weekly midlatitude SST field. The next chapter will focus on how the patterns of variability found in the present chapter interact with the overlying atmospheric circulation.

The dominant patterns of midlatitude North Atlantic SST variability are investigated using Empirical Orthogonal Function (EOF) analysis. Before analyzing the SST field, the weekly mean data were converted to anomalies by subtracting the long-term weekly mean values from each week. The data were then weighted by the square root of the cosine of latitude as per discussion in Section 2.2. The patterns of variability resulting from EOF analysis of the weighted SST anomalies are displayed as the regression of the anomalous SST field onto the associated standardized Principal Component (PC) time series. In the following discussion, EOFs and PCs are denoted by 'E' or 'P', respectively,

followed by the corresponding number (e.g., EOF is denoted E1) and a subscript denoting what form of the data was used in the analysis. For example, the first EOF of detrended SST anomalies is denoted $E1_{detrend}$.

Statistical significance of each EOF/PC pair is assessed using the method outlined in North et al. (1982). 95% confidence errors for the first 10 eigenvalues are calculated using equation (2.8). If the error bars for eigenvalue λ_i do not overlap with the error bars for eigenvalues λ_{i-1} and λ_{i+1}, then the associated EOF/PC pair is considered well-separated and statistically significant at the 95% confidence level. Note that a statistically significant EOF/PC pair is not necessarily representative of a physical pattern of variability: EOF analysis always finds spatial structures that explain more variance than subsequent EOFs. Therefore, we look for structures in the EOFs of SST anomalies that are consistent with *a priori* expectations based on results either previously published or in this thesis. We only discuss the first three EOF/PC pairs because in none of the cases were higher order EOFs statistically significant.

The following patterns are expected *a priori* to dominate North Atlantic SST variability:

1) The "tripole". As discussed in Chapter One, the tripole is the direct response of the ocean mixed layer to anomalous sensible and latent heat fluxes associated with the NAM. The tripole has been widely documented as the leading pattern of North Atlantic SST variability on monthly and seasonal mean time scales (Marshall et al. 2001); therefore, we expect it should also be evident in the EOFs of weekly SST anomalies. We use the structure of the tripole pattern exhibited in Figure 1.4a as a basis for comparison of our results.

2) Variability in the Gulf Stream extension region. The variance maps of SST anomalies shown in Figure 3.1 exhibit enhanced SST variability in the region of the Gulf Stream from Cape Hatteras to east of Newfoundland. Thus, we also expect to see an EOF/PC pair capturing variability within this region.

The chapter is divided into the following sections. EOF analysis is first performed on weekly North Atlantic SST anomalies for all weeks in the calendar year. The calendar year is then broken down into two seasons consisting of summer and winter weeks. Finally, the SST field is decomposed into seasonal mean and intraseasonal components to isolate variability in the year-to-year and week-to-week midlatitude SST fields, respectively.

4.1 EOF/PC pairs of Weekly SST Anomalies: All Weeks of the Calendar Year

The examination of the North Atlantic weekly SST variability begins with EOF analysis of the "raw" SST anomalies (i.e., only the seasonal cycle has been removed). Each EOF/PC pattern is denoted by the subscript "raw".

Figure 4.1 (top three panels) shows the EOF/PC pairs of North Atlantic SST anomalies calculated for all weeks of the calendar year. Figure 4.1 (bottom panel) shows the percent variance explained by the first 10 EOF/PC pairs and their respective error bars. The error bars between the first three EOF/PC pairs do not overlap; therefore, they are considered well-separated as per the criterion outlined in North et al. (1982).

The first EOF ($E1_{raw}$) exhibits a horseshoe-like pattern, characterized by centers of action located over the North Atlantic subtropical and subpolar regions and a relatively weak area of opposite sign located in the Sargasso Sea. The features of $E1_{raw}$ bear some

resemblance to the tripole pattern seen in Fig. 1.4a. Both structures exhibit centers of action in the subtropical and subpolar regions; however, in Fig. 1.4a, the subtropical and subpolar centers of action are not connected along the coast of Europe and North Africa. Another noticeable difference between $E1_{raw}$ and the tripole is the strength of the center located in the Sargasso Sea. In the tripole, the amplitude of this center of action is comparable to the amplitude of the subpolar and subtropical centers in; in $E1_{raw}$ it is relatively weak. Because of the differences discussed above, we hesitate to call $E1_{raw}$ the tripole pattern and hereafter refer to it as the horseshoe pattern.

The PC time series corresponding to $E1_{raw}$ ($P1_{raw}$) exhibits variability on a range of time scales, including a sharp transition from predominantly negative values to predominantly positive values ~1994 and considerable memory from one year to the next (e.g., the predominantly positive values from ~1987-1991). The sharp transition ~1994 (hereafter referred to as the regime shift) is more clearly evident in summertime segments of $P1_{raw}$ (Figure 4.2) and will be discussed further in the following section.

The second EOF, $E2_{raw}$, is dominated by a strong center of action within the region of the Gulf Stream extension. A region of weak amplitude of opposite sign is observed along the coast of Europe and Africa which bears some resemblance to the loadings in the subpolar and subtropical nodes exhibited in the tripole. $E3_{raw}$ exhibits a dipole structure with centers of opposite sign southeast of Newfoundland and east of Cape Hatteras. $P2_{raw}$ and $P3_{raw}$ exhibit variability on interannual and intraseasonal timescales, but do not exhibit any sharp transitions.

The first three EOF/PC pairs are well-separated but are not entirely consistent with the *a priori* expectations stated in the introduction to this chapter. Instead, the EOF/PC

pairs reflect a mix of the expected patterns, i.e., the tripole and variability in the Gulf Stream extension region. For example, the first EOF of North Atlantic SST anomalies exhibits some elements of the tripole but lacks amplitude in the Sargasso Sea. The second EOF captures variability in the Gulf Stream extension but also exhibits a hint of the tripole in the subpolar and subtropical regions.

Why does the tripole not emerge as a distinct pattern of SST variability in the year-round weekly mean data? One possible explanation is that the tripole is evident primarily in the winter, when the midlatitude ocean-atmosphere interaction that drive the tripole is strongest. Further investigation of the tripole and other patterns of SST variability will thus be explored in the summer and winter seasons separately.

4.2 EOF/PC Pairs of Weekly Summertime SST Anomalies

This section investigates the dominant patterns of midlatitude North Atlantic weekly summertime SST anomalies and more closely examines the "regime shift" most clearly evident in the summer season segments of the time series in Fig. 4.2. EOF analysis of May-October (MO) SST anomalies is used to explore what patterns of variability dominate summertime North Atlantic SST variability. The EOF/PC pairs are denoted by the subscript "*MO*".

Figure 4.3 (top three panels) shows the EOF/PC pairs of North Atlantic May-October weekly SST anomalies. Only the first two EOF/PC pairs are statistically significant at the 95% confidence level (Figure 4.3 bottom panel). The horseshoe pattern and associated regime shift evident in the first EOF for the full year (Figure 4.1 top panel) also emerge as the first EOF/PC pair for the summer season. It explains roughly 19.0% of the total May-

October variance. The associated PC time series exhibits the 1994 regime shift in which the values jump from below -1σ to above 1σ. After 1994, the values are predominantly positive. $P1_{MO}$ is highly correlated with the time series in Fig. 4.2a (r~0.95). $E2_{MO}$ exhibits similar features as the second EOF in Fig. 4.1.

The results in Fig. 4.3 confirm that the horseshoe pattern and associated regime shift are statistically significant and robust features of the summertime EOFs. However, based on the literature reviewed in Chapter One, there is no *a priori* reason to expect the structure. The rest of this section more closely examines the regime shift and its impact on the EOFs of summertime SST anomalies.

The structure of SST anomalies associated with the regime shift is investigated in the following two data sets: 1) the weekly mean SSTs used in EOF analysis throughout this chapter and 2) monthly mean SSTs obtained from the Comprehensive Ocean-Atmosphere Data Set (gridded on $2^{o}x2^{o}$ latitude/longitude boxes). Figure 4.4 shows the difference maps between the 1991-1993 and 1995-1997 periods averaged over May-October for both monthly and weekly SST data. The purpose of these maps is to compare the amplitude and location of the regime shift in both data sets. Despite the coarser resolution of the monthly COADS SST field, the difference maps are very similar. They both exhibit a horseshoe pattern with the largest amplitude south of Greenland and east of Newfoundland. The patterns in Figure 4.4 bear a strong resemblance to the horseshoe pattern evidenced in $E1_{MO}$ and $E1_{raw}$.

The effect of the regime shift on the structure of summertime EOFs is examined by computing the leading EOFs of weekly May-October SST anomalies with the years 1993-1995 removed from the data (Figure 4.5; denoted by the subscript "cut"). In this case, no

statistically significant EOF emerges from the analysis. The horseshoe pattern is no longer evident and variability in the Gulf Stream extension evident in $E2_{raw}$ emerges as the first EOF.

This section demonstrates that: 1) the leading EOF of summertime SST anomalies is characterized by a horseshoe pattern reminiscent of $E1_{raw}$, 2) variability in this pattern is dominated by a regime shift ~1994 and 3) the leading EOF in data with the regime shift removed captures variability along the Gulf Stream extension but it is not statistically significant. The regime shift is associated not with uniform changes in SST but by a large-scale pattern resembling $E1_{raw}$ and $E1_{MO}$. This pattern is also evident in a data set that does not contain satellite observations. Thus, the horseshoe pattern is not an artifact of the satellite data. However, because both monthly and weekly data sets used in the analysis contain the same *in situ* measurements, we cannot conclude that the horseshoe pattern and its attendant regime shift are not artifacts of the data. Since the focus of this thesis is primarily on variability of wintertime SST anomalies, a season in which the regime shift is much less evident, further analysis of the summer SST variability and the regime shift is left for future work.

4.3 EOF/PC Pairs of Weekly Wintertime SST Anomalies

This section investigates patterns of weekly mean wintertime North Atlantic SST variability. Figure 4.6 (top three panels) shows the EOF/PC pairs of North Atlantic November-April SST anomalies (denoted with subscript "*NA*"). Note that only the third EOF/PC pair is well-separated from adjacent EOF/PC pairs (Figure 4.6 bottom panel). The first two EOF/PC pairs are well-separated from the third but not from each other. The

first EOF exhibits a horseshoe pattern similar to $E1_{raw}$ but the amplitude is much stronger in the subpolar region, especially near the Gulf Stream extension, than in the subtropical region. The first EOF also exhibits features similar to the tripole in Fig. 1.4a but the amplitude of the middle node is relatively weak and the subtropical and subpolar nodes are joined along the coast of Europe and Africa.

The corresponding PC time series $P1_{NA}$ is highly correlated with the time series in Fig. 4.2b (r~0.96). The sharp regime shift exhibited in $P1_{MO}$ and Fig. 4.2a is less evident in the winter PC time series. Instead, the variability of wintertime North Atlantic SST anomalies is characterized by a gradual transition from negative values to predominantly positive values ~1988-2000, contributing to an overall positive trend for the full record 1981-2002.

$E2_{NA}$ exhibits a pattern that is reminiscent of both the tripole pattern and variability in the Gulf Stream extension evidenced in $E2_{raw}$. $P2_{NA}$ is characterized by a strong peak ~1998. $E3_{NA}$ shows a dipole pattern along the Gulf Stream that bears a strong resemblance to $E3_{raw}$.

The results in Figure 4.6 demonstrate that the leading EOF of wintertime SST variability is associated with a positive trend. Because we are interested primarily in variability on interannual and intraseasonal time scales, we also examine the EOFs after the overall trend is subtracted from each gridpoint in the SST data. In doing so, we can infer the impact of the 1981-2002 trend on wintertime SST variability. The EOF/PC pairs are denoted by the subscript "detrend".

Figure 4.7 (top three panels) shows the EOFs for detrended November-April weekly North Atlantic SST anomalies. The first two EOF/PC pairs are not well-separated

from each other but are well-separated from the higher order EOF/PC pairs (Figure 4.7 bottom panel). $E1_{detrend}$ explains 19.0% of the total variance $E2_{detrend}$ explains 14.9% of the total variance. $E1_{detrend}$ bears a strong resemblance to $E2_{NA}$ but is slightly weaker in amplitude. Similarly, $E2_{detrend}$ bears resemblance to $E3_{NA}$. It exhibits a dipole along the Gulf Stream with centers of opposite sign south of Newfoundland and east of Cape Hatteras. The gradual transition from negative values in the mid-1980s to predominantly positive values in the 1990s which contributed largely to the PCs in Fig. 4.6 are, by construction, not evident in PCs in Fig. 4.7. However, the peak ~1998 exhibited in $P2_{NA}$ is evident in $P1_{detrend}$.

The lack of separation between the first two EOF/PC pairs of the detrended SST anomalies may arise because they reflect the same phenomenon at different stages of its temporal evolution. Figure 4.8 shows the lag correlations between $P1_{detrend}$ and $P2_{detrend}$ at lags out to +8 ($P1_{detrend}$ leading) and -8 weeks ($P2_{detrend}$ leading). The lag correlations are not statistically significant at the 95% confidence level but they exhibit an asymmetry in which the values are strongest when $P1_{detrend}$ leads by 8 weeks.

4.4 EOF/PC Pairs of Intraseasonal and Seasonal Mean Wintertime SST Anomalies

In order to isolate week-to-week and year-to-year variability, the SST field is decomposed into intraseasonal and seasonal mean components, respectively. Intraseasonal SST anomalies are calculated by subtracting the seasonal (November-April) mean from each week in the November-April season. Removal of year-to-year variability isolates processes that occur on subseasonal time scales from those that occur on longer time scales, such as the re-emergence mechanism and mean advection by large scale ocean currents.

The EOF/PC pairs of seasonal mean and intraseasonal SST anomalies are denoted by the subscripts "*sm*" and "*is*", respectively.

Figure 4.9 (top three panels) shows the EOF/PC pairs of seasonal (November-April) mean SST anomalies. The first EOF/PC pair explains 23% of the total variance and is well-separated from the higher order EOFs. Similar to $E2_{NA}$ and $E1_{detrend}$, $E1_{sm}$ captures variability along the Gulf Stream extension mixed with elements of the tripole pattern: it is dominated by a center of action along the Gulf Stream extension juxtaposed by two centers of opposite sign in the subtropical and subpolar North Atlantic. The corresponding PC time series exhibits predominantly positive values during the mid-1980s, predominantly low values during the late 1980s and early 1990s, and a peak ~1996. Similar features are exhibited in $P1_{detrend}$.

Figure 4.10 (top three panels) shows the EOF/PC pairs of intraseasonal November-April North Atlantic SST anomalies. Note that the shading and contour intervals are smaller compared to previous EOF figures. In contrast to the results of previous EOF analyses in this chapter, the pattern capturing variability in the Gulf Stream extension and the tripole are evident as separate EOFs. The first EOF bears a strong resemblance to the structure evidenced in Fig. 1.4a; the second EOF, $E2_{is}$, captures variability along the Gulf Stream with strong negative values in the Gulf Stream extension and weaker positive values around Florida. By construction, both $P1_{is}$ and $P2_{is}$ exhibit variability only within each November-April season. These first two EOF/PC pairs are well-separated from the higher order EOF/PCs but not from each other as per the criteria outlined in North et al. (1980).

The lack of separation between the first two EOF/PC pairs is similar to the results found in EOF analysis of detrended SST anomalies. To examine whether the first two

EOFs reflect the same phenomenon at different stages of its temporal evolution, lag correlations are calculated between $P1_{is}$ and $P2_{is}$ at lags out +8 and -8 weeks. Figure 4.11 shows significant correlations when $P2_{is}$ (variability in the Gulf Stream extension) leads $P1_{is}$ (the tripole) by six weeks. The results suggest variability in the Gulf Stream extension ($E2_{is}$) precedes variability in the tripole by ~ 5-6 weeks.

4.5 Concluding Remarks

At the beginning of the chapter, we stated the following patterns are expected *a priori* to dominate North Atlantic SST variability: 1) the so-called tripole pattern because it has been well-documented in the literature presented in Chapter One and 2) a pattern capturing the variability in the Gulf Stream extension because it is evident in variance maps of SST anomalies in Chapter 3. The key results in this chapter are as follows:

- The leading EOFs of weekly SST anomalies for all weeks in the calendar year exhibit a mix of the expected patterns. The first EOF is characterized by a horseshoe pattern with largest loadings in the subtropical and subpolar regions of the North Atlantic. The associated PC time series is characterized by a sharp transition from negative to positive values around ~1994. The second EOF captures variability along the Gulf Stream extension but also exhibits relatively weak variability in the subtropical and subpolar regions.
- The leading EOF of weekly summertime SST anomalies is characterized by the horseshoe pattern and its associated regime shift. Further analysis could not ascertain if this pattern is a physical mode of variability. Once the regime shift was removed from the data, no patterns emerged as statistically significant EOFs.

- The leading EOFs of weekly wintertime SST anomalies are characterized by the tripole and variability in the Gulf Stream extension; however, the patterns often emerge as mixed structures in the EOFs.
- The tripole and variability in the Gulf Stream extension are most clearly separated in the EOFs of intraseasonal wintertime SST anomalies. In this case, the first two EOF/PC pairs are not well-separated. However, it is notable that the corresponding PC time series are correlated at a statistically significant level when variability in the Gulf Stream extension leads the tripole by roughly 6 weeks. The results suggest that variability in the weekly wintertime North Atlantic SST field should not be described in terms of a single spatial pattern, but perhaps two patterns that reflect the evolution of the SST field over a period of several weeks.

In the next chapter we will continue to look at the relationship between variability in the Gulf Stream extension and tripole pattern but focus primarily on their interaction with the overlying atmospheric circulation.

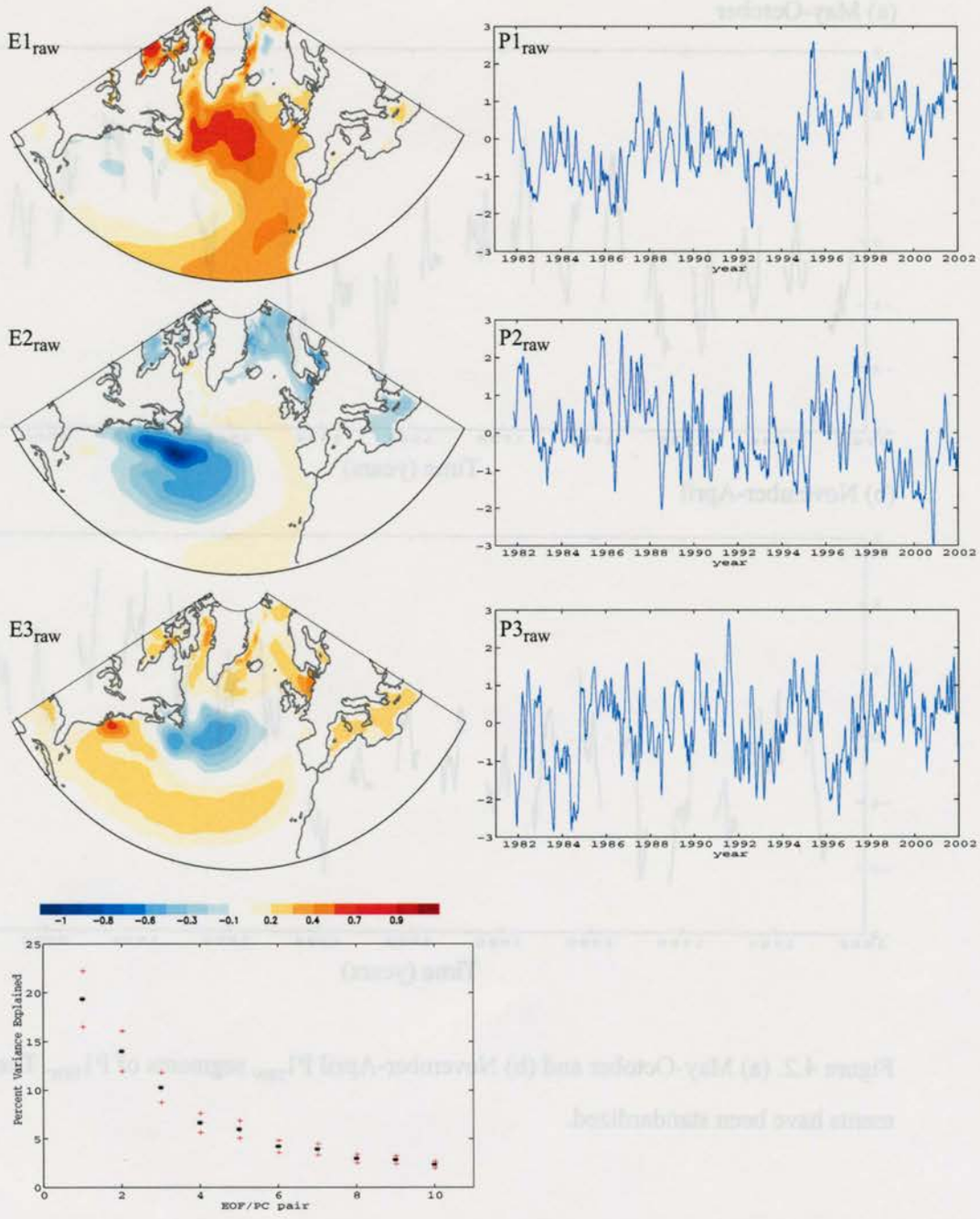

Figure 4.1 (Top three panels; left) Empirical Orthogonal Functions (EOFs) and (right) Principal Components (PCs) of North Atlantic SST anomalies for all weeks in the calendar year, November 1981- December 2002. (Bottom panel) Percent variance explained by each EOF/PC pair (black stars) and 95% confidence levels (red crosses).

(a) May-October

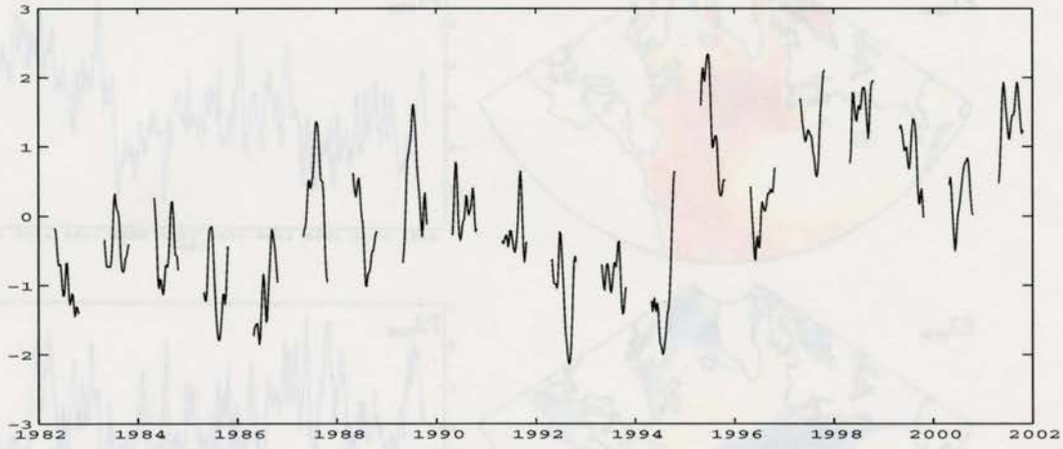

(b) November-April

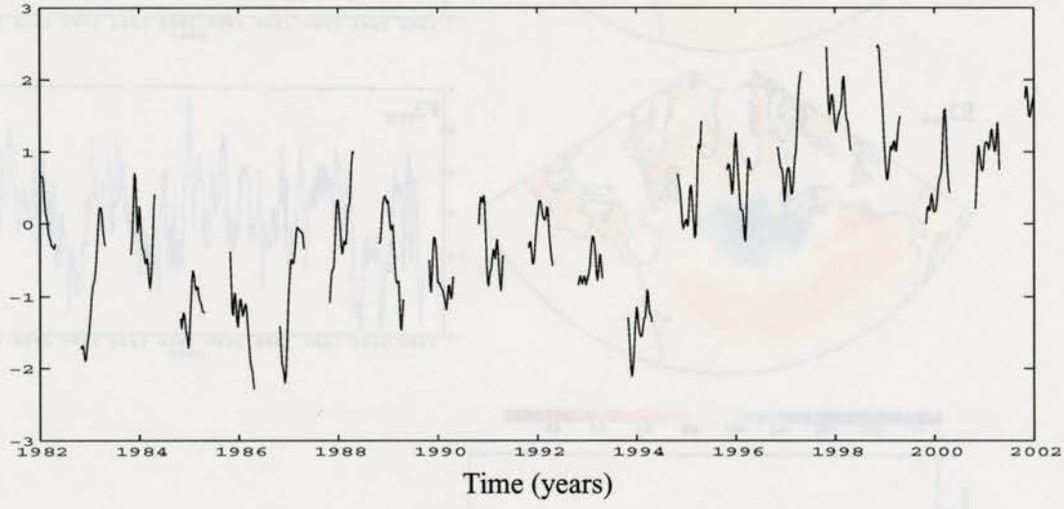

Figure 4.2. (a) May-October and (b) November-April $P1_{raw}$ segments of $P1_{raw}$. The segments have been standardized.

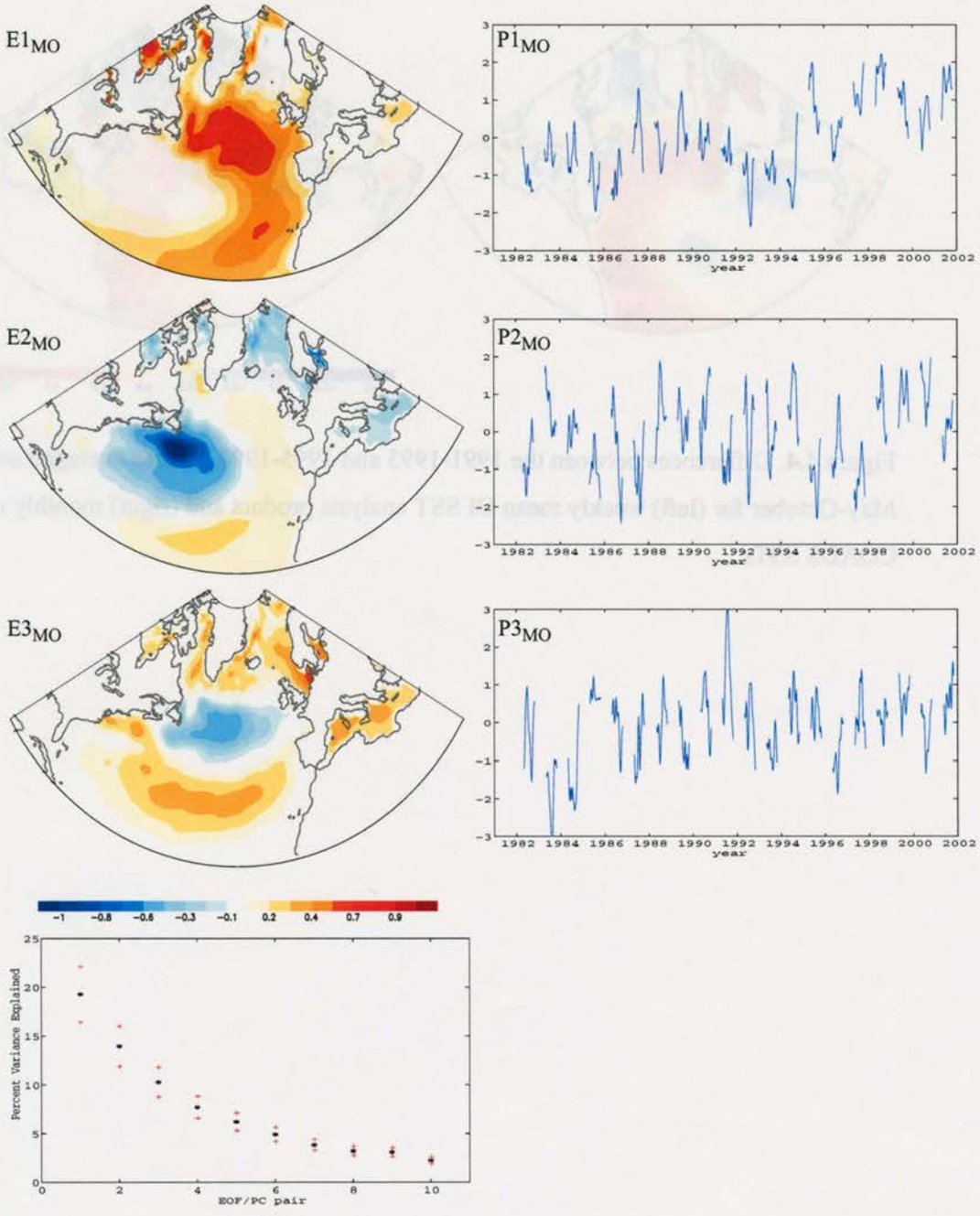

Figure 4.3. As in Figure 4.1 but for May-October weekly SST anomalies. PC time series are displayed with gaps between summer seasons.

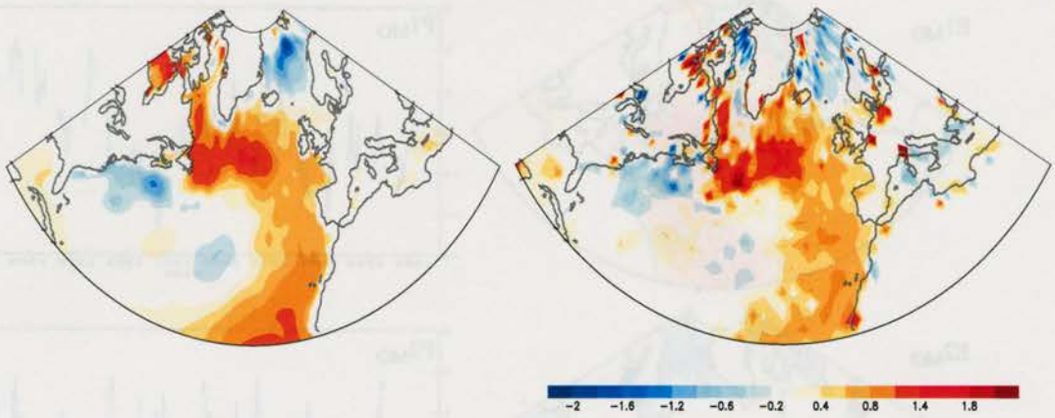

Figure 4.4. Differences between the 1991-1993 and 1995-1997 periods averaged over May-October for (left) weekly mean OI SST analysis product and (right) monthly mean COADS SSTs.

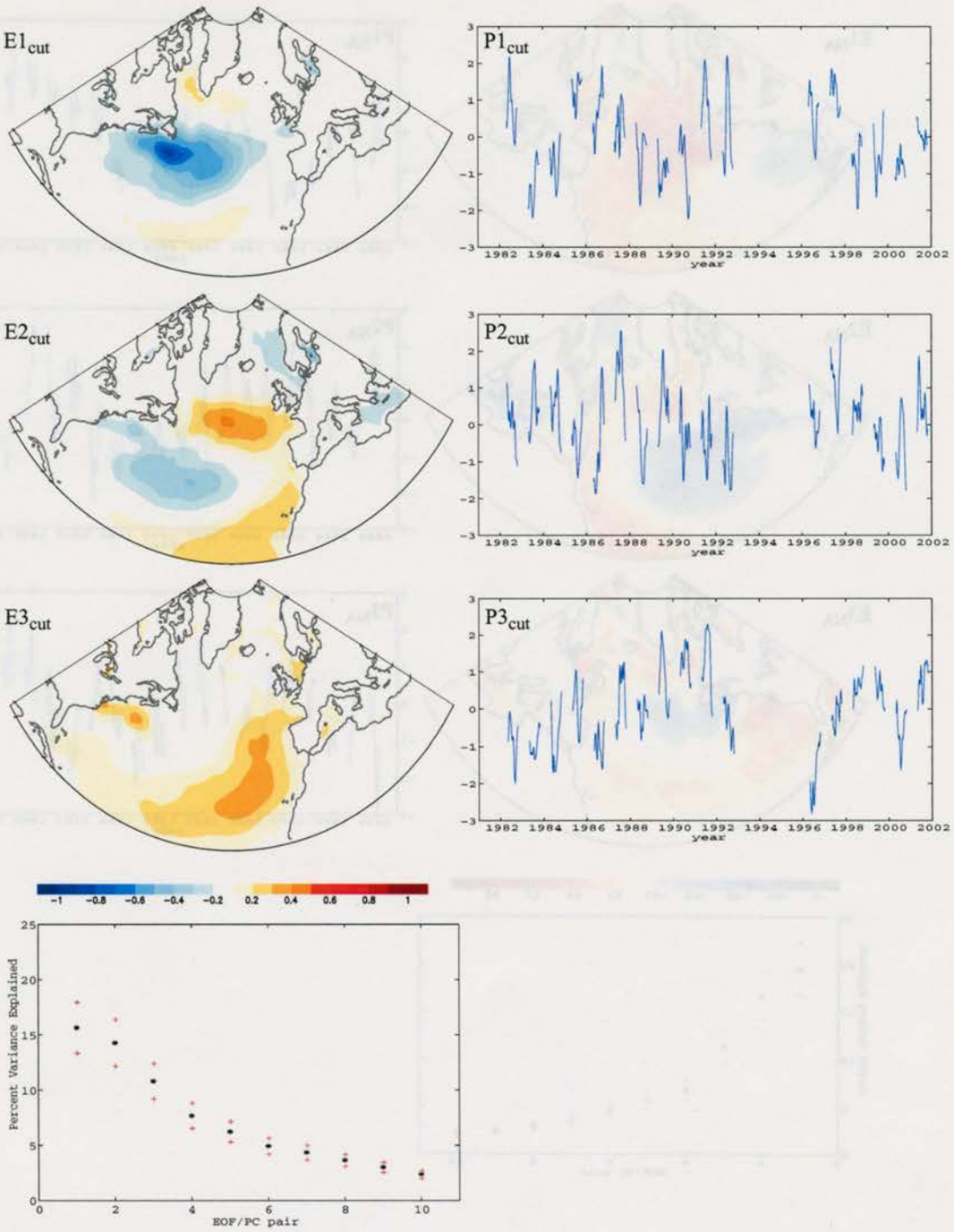

Figure 4.5. As in Figure 4.3 but the years 1993-1995 have been removed before performing EOF analysis.

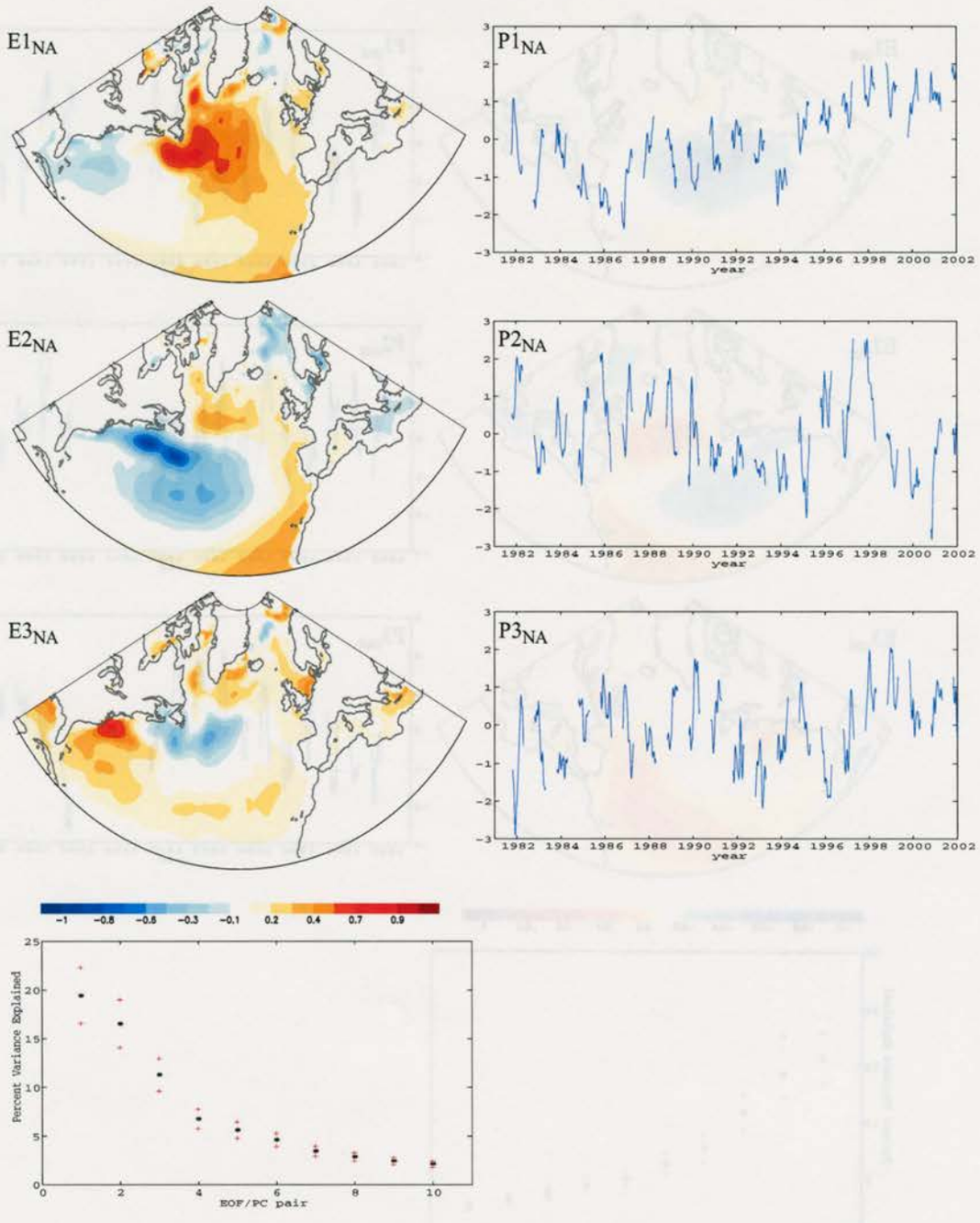

Figure 4.6. As in Figure 4.1 but for November-April weekly SST anomalies. PC time series are displayed with gaps in between winters.

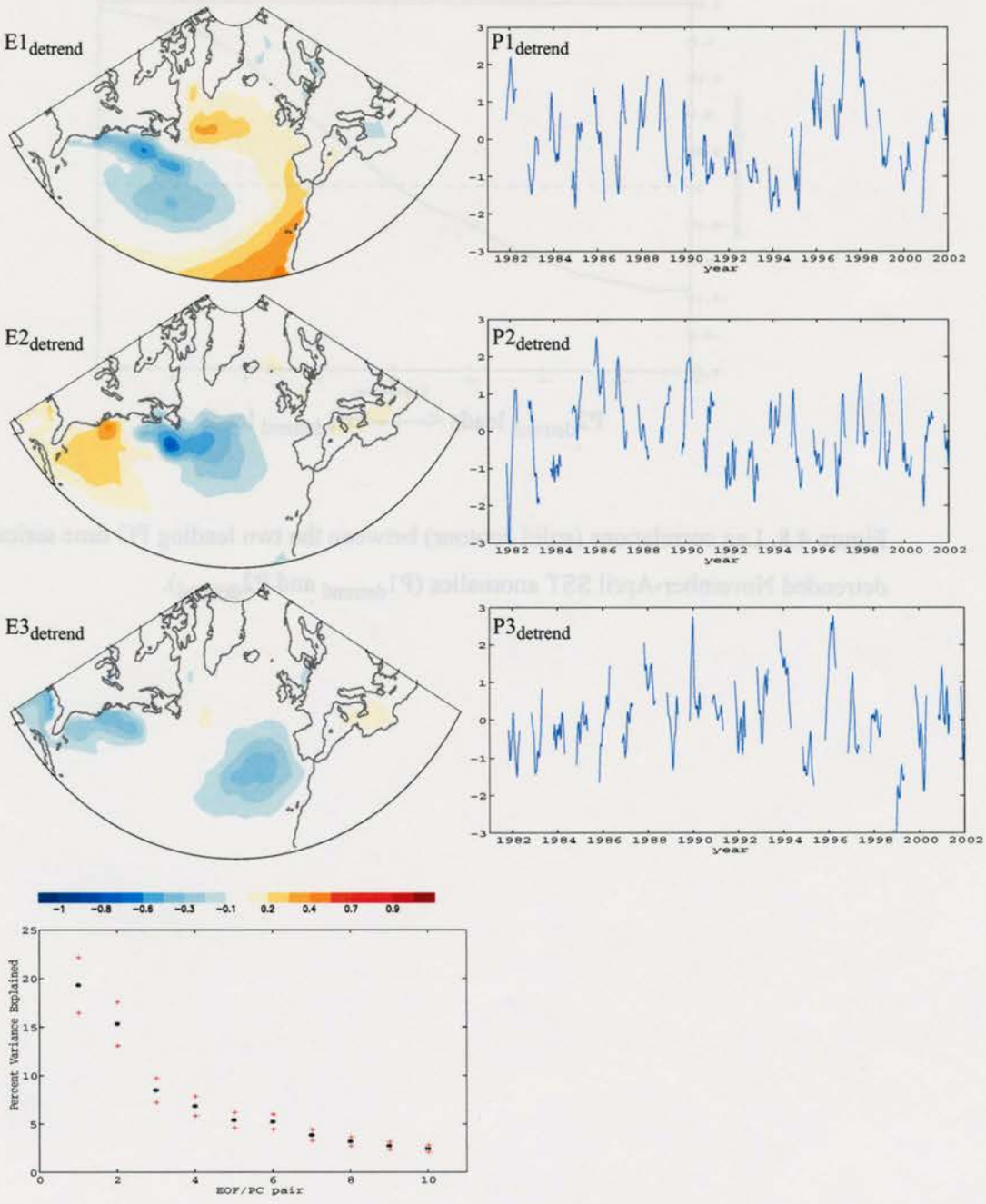

Figure 4.7. As in Figure 4.6 but the SST anomalies have been detrended.

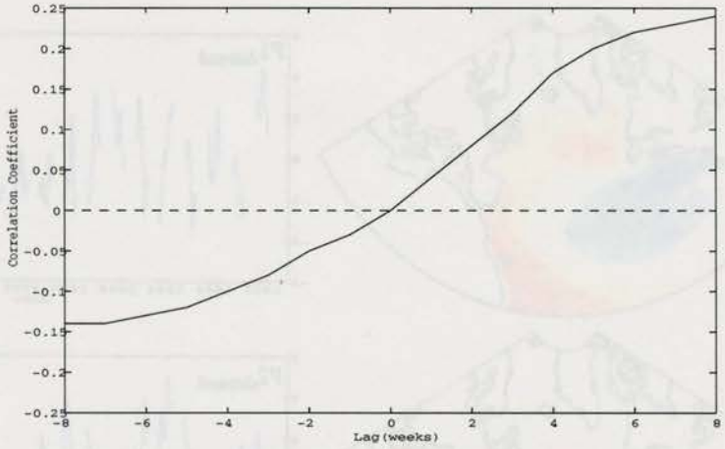

Figure 4.8. Lag correlations (solid contour) between the two leading PC time series of detrended November-April SST anomalies ($P1_{detrend}$ and $P2_{detrend}$).

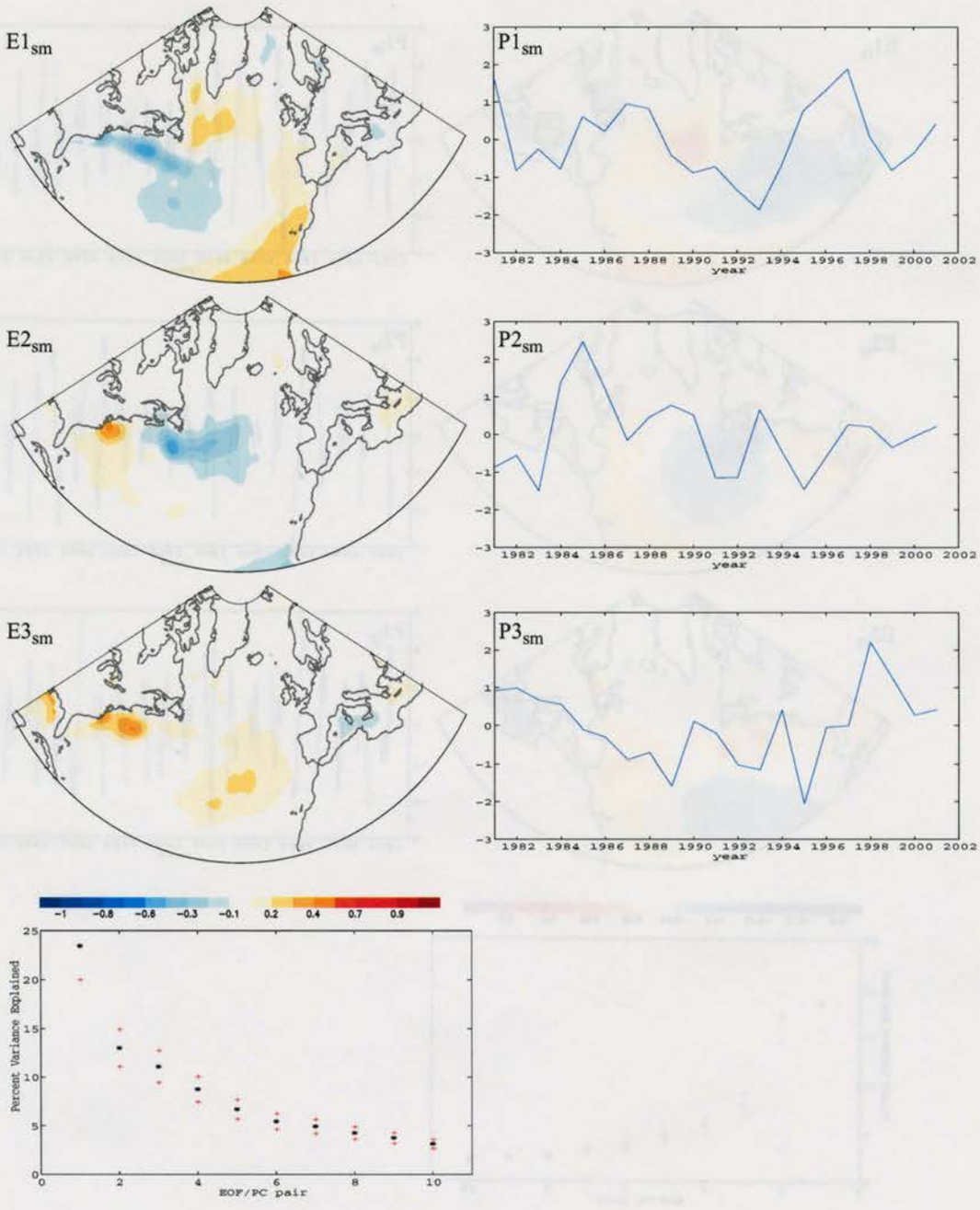

Figure 4.9. As in Figure 4.7 but for November-April seasonal mean SST anomalies.

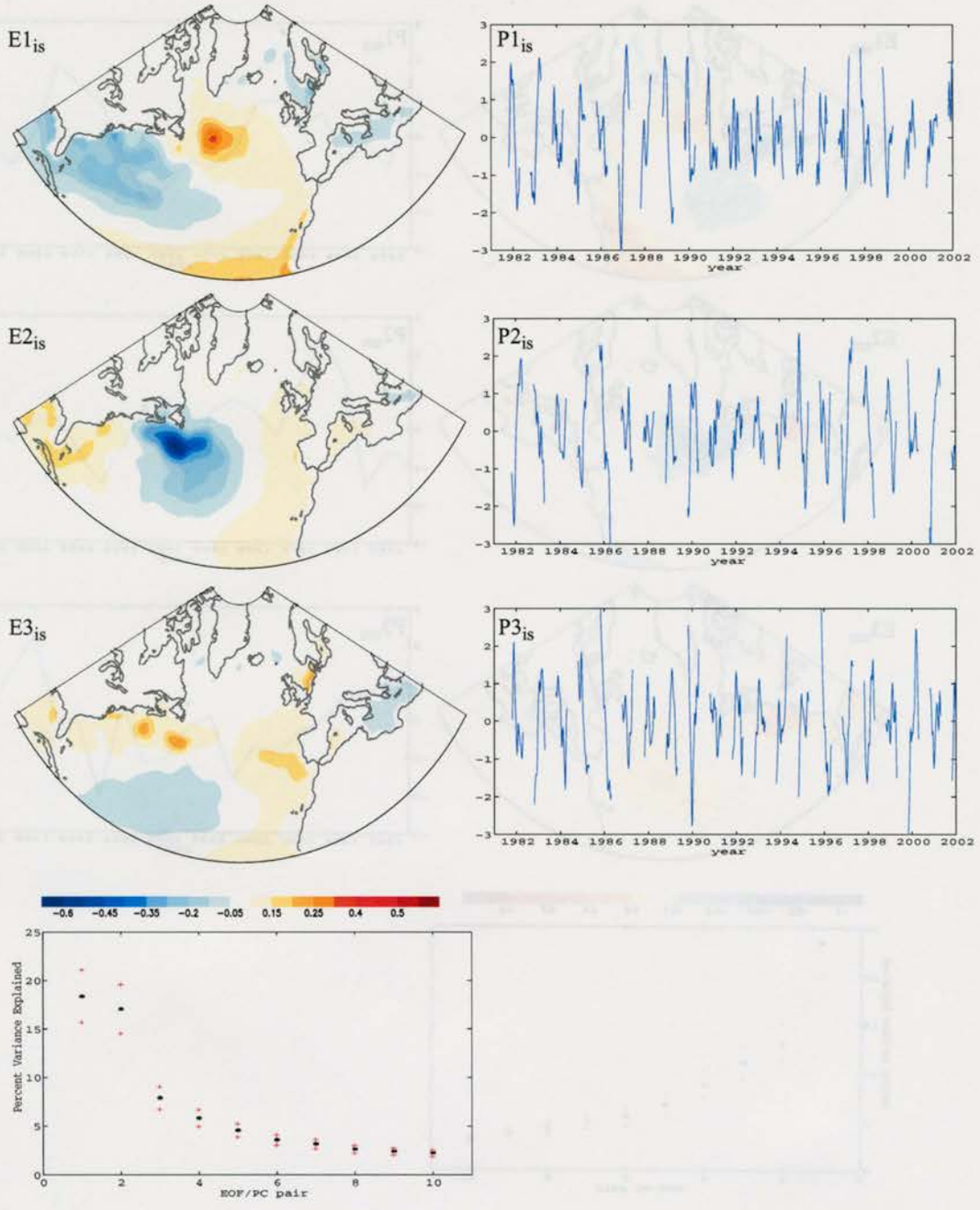

Figure 4.10. As in Figure 4.7, but for November-April intraseasonal SST anomalies. Note that shading contours have been reduced relative to Figure 4.7.

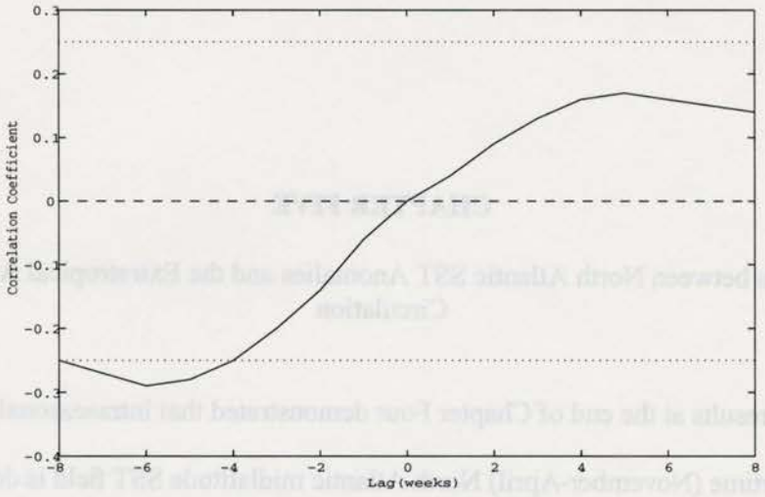

$P2_{is}$ leads <---|--->$P1_{is}$ leads

Figure 4.11. As in Figure 4.8 but for the leading two PC time series of intraseasonal November-April SST anomalies ($P1_{is}$and $P2_{is}$). Dotted line denotes the 95% confidence level (r=0.25).

CHAPTER FIVE

Interactions between North Atlantic SST Anomalies and the Extratropical Atmospheric Circulation

The results at the end of Chapter Four demonstrated that intraseasonal variability in the wintertime (November-April) North Atlantic midlatitude SST field is dominated by the following two patterns of variability: 1) the tripole pattern and 2) variability in the Gulf Stream extension region. As evidenced in Chapter Three, variability in the Gulf Stream extension lies under a region of pronounced cyclogenesis along the western edge of the North Atlantic storm track. Furthermore, the analyses in Chapter Four suggest that variability in the Gulf Stream extension precedes variations in the tripole pattern by ~six weeks. This chapter focuses on understanding the relationship between these two patterns and the NAM, the leading pattern of Northern Hemisphere atmospheric variability.

As mentioned in Chapter One, Deser and Timlin (1997, hereafter DT97) examined midlatitude ocean-atmosphere interactions on intraseasonal time scales using lagged SVD analysis between 14 years of normalized midlatitude SST anomalies and the 500hPa height field. Our analysis deviates from DT97 by using lag correlation/regression analysis between the NAM and the SST field. The latter field will not be standardized in order to retain the amplitude of variability in the ocean. In contrast to DT97, our record of analysis extends to 22 years.

The chapter is divided into two main sections. First we more closely examine the non-contemporaneous relationships between midlatitude North Atlantic SST anomalies and the NAM. If the extratropical atmosphere responds to midlatitude SST anomalies, the response should be evidenced in the NAM, the dominant pattern of Northern Hemisphere atmospheric variability. Then we offer possible explanations for the observed relationships.

5.1 Non-contemporaneous Relationships between North Atlantic SSTs and the NAM

In this section, the non-contemporaneous relationships between the midlatitude North Atlantic ocean and extratropical atmospheric circulation are examined. DT97 demonstrated that the strongest covariability between the midlatitude ocean and atmosphere occurs when the atmosphere leads by ~ 2 weeks. Here we examine to what extent such covariability exists when the atmosphere lags the SST field. We investigate North Atlantic ocean-atmosphere relationships using two methods: 1) lagged regression/correlation analysis at lags out to one month and 2) regression of the tendency of one field onto contemporaneous time series from the opposing field.

5.1.1 Lagged correlation/regression analysis

The investigation of midlatitude ocean-atmosphere interaction begins with lagged regression/correlation analysis between intraseasonal values of North Atlantic winter SST anomalies and standardized values of the NAM index. Results are based on the 23 week winter season extending from the first week in November to the last week in March. Lag regressions/correlations are centered about the months December, January and February.

Thus the intraseasonal SST anomalies (hereafter referred to as SST_{is}) are formed by subtracting the November-March mean from each winter season. As mentioned in Chapter Four, removing the seasonal mean from each winter isolates processes that occur on intraseasonal time scales from those that occur on interannual and longer time scales. Note that subtracting the seasonal mean from each winter season does not impact the asymmetry of the lag regressions or the tendency regressions.

Figure 5.1 shows the regression of SST_{is} onto the standardized time series of the NAM at lags ranging from -4 to +4 weeks. At positive lags (when the ocean lags the atmosphere), the regression maps are marked by SST anomalies that are significantly lower than normal to the south of Greenland, higher than normal over the region extending eastward from the coast of the United States, and lower than normal in the subtropical North Atlantic. Significantly higher than normal SST anomalies are also observed along the coast of northwestern Europe. The meridionally banded structure evidenced in Figs. 5.1d,e strongly resembles the tripole pattern documented in Figure 1.4a. This pattern also resembles the first EOF of intraseasonal winter North Atlantic SST anomalies (Figure 4.10).

At negative lags (when the ocean leads the atmosphere), the tripole is no longer evident and a different pattern of SST_{is} anomalies emerges. In contrast to the pattern evident in Fig. 5.1d,e, the regression maps in Figs. 5.1a,b exhibit largest amplitude along the Gulf Stream extension. The largest and most significant SST anomalies in the Gulf Stream extension occur ~ 2 weeks prior to the peak in the NAM and have an amplitude comparable to that observed in the subpolar center of the tripole (~0.25 ^{o}C). A similar pattern is evident in DT97 (see Figure 1.8), but this feature is not highlighted in their SVD analysis of standardized data. The patterns in Figs. 5.1 a,b also bear a strong resemblance to vari-

ability in the Gulf Stream extension captured in the second EOF of intraseasonal wintertime North Atlantic SST anomalies (Figure 4.10).We hereafter refer to the pattern evidenced in 5.1b and the second EOF of intraseasonal wintertime SST anomalies (Figure 4.10) as G.

The lag zero regression map (i.e., the contemporaneous regression of SST_{is} onto the NAM), can be interpreted as the linear combination of the lag -2 and +2 regression maps. Similar to the lag +2 map, Figure 5.1c exhibits higher than normal SSTs extending east from the coast of the United States and along the coast of northwestern Europe, whereby, similar to the lag -2 map, Fig. 5.1c exhibits lower than normal SSTs in the Gulf Stream extension region.

Expansion coefficient time series of G in Fig. 5.1b and the tripole pattern in Fig. 5.1d were formed by projecting the respective regression maps onto SST_{is} data. Figures 5.2a,b shows the November-March expansion coefficient time series of the tripole pattern and G evidenced in Figure 5.1d,b, respectively. The time series in Fig. 5.2a is highly correlated with the leading PC time series of intraseasonal wintertime SST anomalies from Section 4.4 of Chapter Four ($r \sim -0.93$) and the time series in Fig. 5.2b is highly correlated with the second PC time series of intraseasonal wintertime SST anomalies ($r \sim 0.96$). In practice, the corresponding time series for G is also highly correlated with intraseasonal SST anomalies averaged over the box indicated in Fig. 5.1 ($r = -0.91$).

Figure 5.3 a,b shows the lag correlations between the NAM and the two time series of SST_{is} (i.e. G and the tripole). Consistent with the results presented in DT97, the lag correlations between the NAM and the tripole (Fig. 5.3a) are largest and most significant

when the NAM leads by ~2-3 weeks. The attendant asymmetry in the lag correlations implies that variability in the NAM precedes variations in the tripole, but not vice versa.

In contrast to Fig. 5.3a, the lag correlations between the NAM and G (Fig. 5.3b) are largest and most significant when G leads by 1-2 weeks, and drop to near zero at positive lags. The asymmetry in the lag correlations between the NAM and G implies that changes over the Gulf Stream extension region tend to precede changes in the NAM on intraseasonal time scales.

Figure 5.3c shows the lag correlations between the expansion coefficient time series of the tripole and G. Consistent with Figs. 5.3a,b, the strongest and most statistically significant correlations occur when G leads the tripole by ~3-4 weeks. The result is similar to the lag correlations between the leading two PC time series of intraseasonal wintertime SST anomalies evidenced in Figure 4.11.

The results presented thus far demonstrate that two patterns of SST anomalies emerge in association with the NAM: G precedes changes in the NAM which, in turn, precedes changes in the tripole. These patterns also correspond to the leading patterns of intraseasonal wintertime North Atlantic SST anomalies investigated at the end of the previous chapter. But while the relationships between the NAM and the patterns of SST_{is} anomalies revealed in Fig. 5.1 are statistically significant, the results do not prove that the midlatitude North Atlantic ocean drives variations in the extratropical atmosphere. The causality between the two fields will be discussed further in section 5.2.

5.1.2 Regression of the tendency in atmospheric variables onto contemporaneous time series of SSTs

If SST anomalies in the Gulf Stream extension region are associated with changes in the overlying atmospheric circulation, the relationship should be evident in the regression of the tendency in various atmospheric parameters onto contemporaneous values of G. The tendency is defined as the difference in data between +2 and -2 weeks. In practice, the results in this section are qualitatively similar to the results derived when the tendency is defined as the difference in data between +3 and -3 weeks and between +4 and -4 weeks.

Figure 5.4a shows the regression of the tendency in SLP onto contemporaneous values of G. The regression map bears evident similarity to the NAM evidenced in Figure 1.3: positive values of G (i.e., lower-than-normal SSTs over the Gulf Stream extension) are characterized by falling pressures over the Arctic/subpolar North Atlantic juxtaposed against rising pressure over the central North Pacific and North Atlantic. Figures. 5.4b,c shows that the tendency regression map is dominated by the atmosphere-lagging component of the tendency. When SLP leads G by 2 weeks (i.e, the atmosphere-leading component of the tendency), the regression map exhibits a low pressure over the central North Atlantic and high pressure over the North Pacific (Fig. 5.4b). In contrast, when SLP lags G by 2 weeks (i.e., the atmosphere-lagging component of the tendency), the regression map has evolved into a pattern bearing a strong resemblance to the structure of the NAM (Fig. 5.4c). The results in Fig. 5.4 thus demonstrate that the regression of the tendency in SLP onto G reflects increasing amplitude of the NAM with time. The pattern derived by regressing the tendency in zonal mean zonal wind onto G also reflects the increasing

amplitude of the NAM with time (Figure 5.5). It is characterized by easterlies at ~30°N and equivalent barotropic strengthening of the westerlies at ~55°N.

Figure 5.6a shows the regression of the tendency in SLP onto contemporaneous values of the tripole. In this case, the regression map bears a strong resemblance to the negative phase of the NAM: positive values of the tripole (warmer-than-normal SSTs in the Sargasso Sea juxtaposed by cooler-than-normal SSTs in the subpolar and subtropical regions) are characterized by rising pressure in the Arctic/subpolar region and falling pressure in the central North Pacific and North Atlantic. In contrast to the regressions based on G, Figures. 5.6b,c reveals that the tendency in SLP regressed onto the tripole is dominated by the atmosphere-leading component of the tendency. When SLP leads the tripole by 2 weeks, the regression map bears a strong resemblance to the positive phase of the NAM. But when SLP lags tripole by 2 weeks, the regression map is characterized by relatively weak low pressure over Europe and the central North Pacific. Hence, in contrast to the relationship between the NAM and G, the tripole is associated with decreasing amplitude of the NAM with time.

The results in Figs. 5.1-5.6 support the conclusion reached by DT97 that on intraseasonal time scales the strongest covariability between the extratropical atmosphere and ocean occurs when the atmosphere leads by ~ 2 weeks. However, the results also demonstrate a distinct and statistically significant pattern of variability over the Gulf Stream extension region that precedes changes in the leading mode of Northern Hemisphere atmospheric variability. As noted in the previous chapter, this pattern emerges in conjunction with the tripole as the leading EOFs of intraseasonal wintertime SST anomalies, each explaining ~18% of the total variance. The structure of G is also hinted at in DT97 but is

not accentuated in their SVD analysis of 14 yr of standardized data. The correlations between G and the NAM exceed the 95% confidence level when the ocean leads by 2 weeks, and the asymmetry in the lag correlations is evident in more than 95% of 500 randomized subsamples of the data consisting of 10 randomly chosen winters each.

5.2 Interpretation of the Observed Relationship between G and the NAM

The previous section demonstrated that the strongest correlations between the ocean and atmosphere occurs when the atmosphere leads. The previous section also showed that a coherent and statistically significant pattern of SST anomalies located over the Gulf Stream extension precedes changes in the leading mode of Northern Hemisphere atmospheric variability by ~2 weeks. However, statistical tools such as lag correlation/ regression analysis do not prove causality, and hence the results in the previous section do not prove that the midlatitude ocean is forcing the atmosphere. In this section, we more closely explore the possible causal mechanisms that underlie the observed relationship between G and the NAM. The relationship between the NAM and the tripole has been explored in numerous studies (e.g., Cayan 1992a,b; Kaplan 1998) and will not be discussed further in this chapter.

When trying to understand the causal relationship between the NAM and G, two questions arise: 1) What drives variability in G? and 2) What is the nature of the physical relationship between the NAM and G? To explore these questions, we will continue to look at lead-lag relationships between G and various atmospheric fields. In part, the purpose of these analyses is to understand how G is related to atmospheric variability other than the NAM.

5.2.1 What drives variability in G?

On intraseasonal time scales, variations in the overlying atmosphere must contribute to variability in G. Figure 5.7 shows the regression of intraseasonal wintertime SLP anomalies regressed onto G at lags ranging from -4 to +4 weeks. When the SLP field leads G by 2-4 weeks, the regression map is marked by a region of low pressure centered between Newfoundland and England, juxtaposed with relatively weak regions of high pressure located in the western subtropical Atlantic and over Europe (Figs. 5.7a,b; also shown in Fig. 5.4b). The anomalously low pressure center is consistent with the advection of cold continental air from the north into the region of G. In contrast, as evidenced in Fig. 5.4c, when SLP lags G by 2-4 weeks, the regression map bears a strong resemblance to the NAM: lower than normal pressure over the Arctic region and higher than normal pressure in the central North Atlantic. The contemporaneous relationship between SLP and G can be interpreted as a linear combination of the structure of the NAM and the pattern that precedes variability in G.

The pattern of atmospheric variability that precedes G by 2-4 weeks does not project strongly onto the NAM at any stage in its lifecycle. Lag regressions of SLP onto the NAM (Figure 5.8) show that the patterns preceding the peak in NAM project only weakly onto the pattern of surface circulations that precedes G (i.e., compare Fig. 5.7a,b with Fig. 5.8 b,c). Hence, the results in Figs. 5.1b and 5.3 (bottom) do not reflect the evolution of the NAM. Furthermore, when SLP leads G by 2-4 weeks, the regression maps are marked by an apparent poleward propagation of the low pressure in the North Atlantic and the attendant zonal westerlies. This feature is only weakly exhibited in regressions of

SLP onto NAM. Further discussion of the atmospheric pattern that precedes variations in G is provided in the next subsection.

The intraseasonal wintertime sensible and latent heat fluxes regressed onto G (Figure 5.9) are consistent with the atmosphere driving intraseasonal variability in G. At negative lags, the regression maps are marked by positive fluxes (i.e. flux out of the ocean into the atmosphere) in the region of G (Figs. 5.9a-c), consistent with cold air advection over the Gulf Stream extension from the anomalous low pressure observed in Fig. 5.7. At positive lags, when G leads the surface heat fluxes, the regression maps are marked by a meridionally banded structure with positive fluxes in the subtropical and subpolar North Atlantic and negative fluxes in the Sargasso Sea, consistent with the damping of G to the overlying atmosphere at lag 0 and the development of the tripole ~lags 2-4.

Another possible mechanism whereby the atmosphere may impact variability in G is through Ekman heat transport in the region of G. As mentioned in Section 1.2, Marshall et al. (2001b) demonstrated how NAO-induced Ekman transport contributes to variability in midlatitude SST anomalies (Figure 1.5). In future studies, we will calculate the Ekman transport and the associated pseudo heat flux to determine the effects of the Ekman transport induced by the pattern that precedes variability in G.

There may also be possible contributions to variability in G from ocean dynamics. By subtracting the seasonal mean from each week from the data, mechanisms such as re-emergence and mean advection by large-scale ocean currents have presumably been removed from the analysis. But in the region of the Gulf Stream extension, mechanisms such as mean advection by small-scale ocean currents may contribute to driving variability in G on intraseasonal time scales; mesoscale ocean eddies such as the Gulf Stream

rings (Chapter Three) are highly variable on weekly time scales and can persist anywhere from months to years.

5.2.2 What is the nature of the physical relationship between G and the NAM?

Thus far we have found that variations in G precede variations in the NAM by ~2 weeks using various statistical analyses and have explored possible atmospheric contributions to variability in G. However, that atmospheric variability contributes to intraseasonal variations in SST over the Gulf Stream extension does not preclude SSTs in this region from providing a feedback to the extratropical atmospheric circulation. Potential explanations for the observed relationship between G and NAM include: 1) Variations in G reflect forcing by the NAM at a previous lag and 2) Variations in G give rise to variations in the NAM.

If variations in G reflect forcing by the NAM at a previous lag, the structure of the atmospheric circulation anomalies associated with increasing amplitude in G should resemble the forcing of the NAM at an earlier stage. As noted in the previous section (Figs. 5.7, 5.8), the SLP pattern that precedes variations in G is not consistent with the structure of the NAM at a previous lag. This can also be demonstrated by comparing the zonal winds averaged over the North Atlantic basin ($[u_{300}]_{ATL}$) regressed onto NAM and G at lags ranging from -4 weeks to +4 weeks (Figure 5.10). The contemporaneous regression of $[u_{300}]_{ATL}$ onto the NAM is characterized by strong westerlies at ~50°-60°N, consistent with the enhanced SLP gradient between the Azores High and Icelandic low. Enhanced anticyclonic flow about the Azores gives rise to strong easterlies located at

~30°N. The relationship between $[u_{300}]_{ATL}$ and the NAM is strongest at lag 0 and drops to ~1/e at a lag of ±2 weeks.

A different picture emerges when $[u_{300}]_{ATL}$ is regressed onto G at lags -4 to +4 (Figure 5.10b). At negative lags ($[u_{300}]_{ATL}$ leads), the regression map is marked by strong westerlies at ~40°N and easterlies at 20°N and 55°N. At lag +2 (when G leads by 2 weeks), the regression of $[u_{300}]_{ATL}$ onto G projects strong onto the NAM. There are two ways of interpreting the results of Figure 5.10: 1) as a single atmospheric pattern that evolves in time or 2) as two distinctive atmospheric patterns that peak at lag -2 and +2 respectively. Note that the results in Fig. 5.10b are not the evolution of the NAM itself: otherwise, the propagation of zonal wind anomalies evident in Fig. 5.10b would project strongly onto the regression coefficients in Fig. 5.10a. A similar propagation of zonal wind anomalies is observed in Feldstein et al. (1998), but in that case the propagation only extends over ~10-15 degrees of latitude.

On the other hand, it is possible that variations in G influence variations in the NAM. Variations in G underlie a region of marked cyclogenesis over the western edge of the North Atlantic storm track. Thus, the anomalous surface heat fluxes which must accompany G as it decays on weekly time scales (Fig. 5.9) are uniquely positioned to perturb the extratropical atmospheric circulation. The expected steady-state, linear atmospheric response to SST anomalies in the Gulf Stream extension can be determined using the equations outlined by Hoskins and Karoly (1981; see section 1.2.1). Positive G (i.e., colder than normal SSTs in the Gulf Stream extension) creates a vertical temperature gradient between the ocean and the overlying atmosphere. Because cooling in the midlatitudes is balanced by horizontal temperature advection, warm air is transported poleward

into the region of the Gulf Stream extension. Thus the observed response would exhibit northward flow over G associated with either a high (low) pressure centered downstream (upstream). The tendency in SLP regressed onto G (Fig. 5.4) is consistent the expected response to anomalous SSTs in the Gulf Stream extension. It exhibits poleward flow in the region of G associated with a high pressure centered downstream of the SST anomaly.

5.3 Concluding Remarks

In summary, the results in this chapter demonstrate that variations in G tend to precede variations in the NAM which, in turn, precede variations in the tripole. These two patterns of SST variability also emerge as the leading EOFs of intraseasonal wintertime SST anomalies. Further analysis has shown that on the timescales considered in this study, variations in G are forced by anomalies in the fluxes of latent and sensible heat at the ocean surface. Mesoscale ocean eddies, mean advection by ocean currents, and anomalous Ekman currents may also contribute to variability in G.

Two possible explanations for the observed relationship between the NAM and G were provided. The first explanation is that the relationship merely reflects the evolution of the NAM. However, the results showed that the pattern that precedes variability in the G projects weakly onto the NAM at any lag, and thus this explanation does not appear to hold. The second explanation (i.e., G gives rise to variations in NAM) is more interesting because it suggests that variability in the extratropical atmospheric circulation is influenced by midlatitude North Atlantic SST variability. The observed tendency in SLP based upon G is generally consistent with the expected steady-state linear atmospheric response outlined by Hoskins and Karoly (1981) but the vertical structure of the tendency is not

baroclinic, and thus not consistent with the linear response. It is also worth noting several caveats to the latter explanation. One example is the amplitude of the associated atmospheric and SST anomalies. A typical ~0.5K fluctuation over the Gulf Stream extension region only projects weakly onto the climatological SST gradient there (Figure 3.1), and the largest anomalies in Figure 5.1 and 5.6 account for only 20% of the variance in their respective fields. Also the atmospheric change associated with G is large for a relatively small change in SST. According to Figs. 5.1 and 5.4 a typical of 0.1K in SST is associate with 10-15 Z_{1000} change.

Another caveat is the inconsistency of the GCM response to midlatitude SST anomalies. Palmer and Sun (1985), Ferranti et al. (1994), and Peng et al. (1995) all examine the GCM response to a pattern of SST anomalies reminiscent of G, but the amplitude and structure of the simulated responses varies not only from model to model but from season to season as well (Peng et al. 1995; Kushnir et al. 2002). In light of these caveats, we are hesistent to conclude that the results in this chapter reveal that the NAM is responding to variations in SSTs over the Gulf Stream extension. However, it is equally difficult to interpret the tendency toward increasing amplitude of the NAM in Figs. 5.4, 5.5 as the response of the ocean to atmospheric forcing.

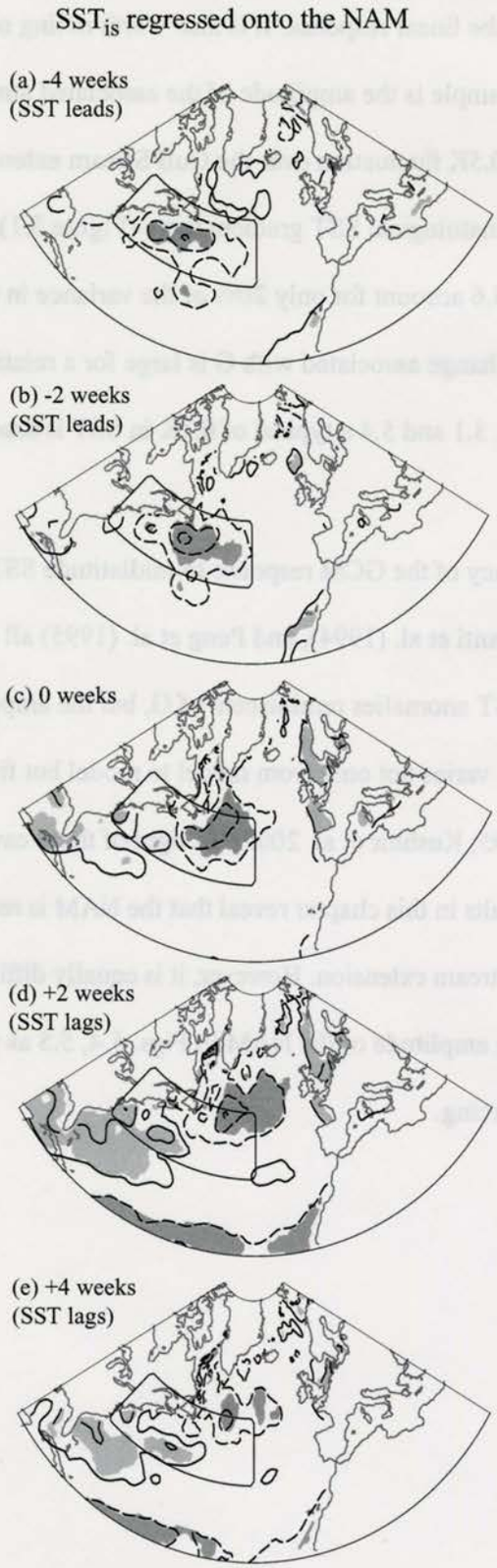

Figure 5.1. Intraseasonal wintertime SST anomalies regressed on the NAM index at (a) lag -4 weeks (SST leads NAM), (b) lag -2 weeks, (c) lag 0 weeks, (d) lag +2 weeks (SST lags NAM), (e) lag +4 weeks. Positive (negative) contours are denoted by solid (dashed) lines and are drawn at (-0.05°C, 0.05°C, 0.15°C...). Areas that exceed the 95% confidence level (r~0.25) are shaded. The box denotes the region (35°-50° N, 30°-75° W).

(a) Tripole

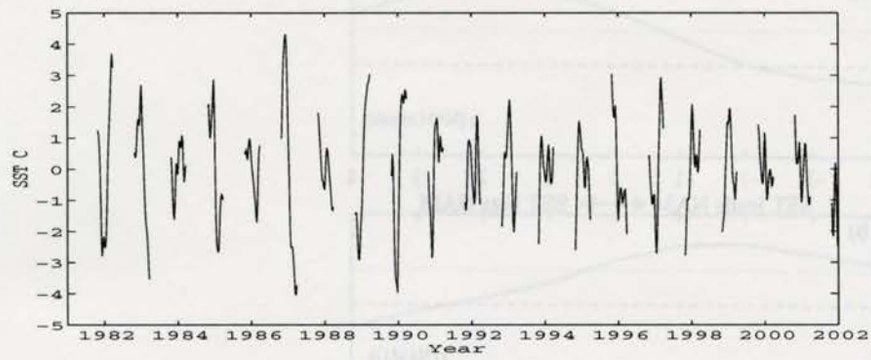

(b) G

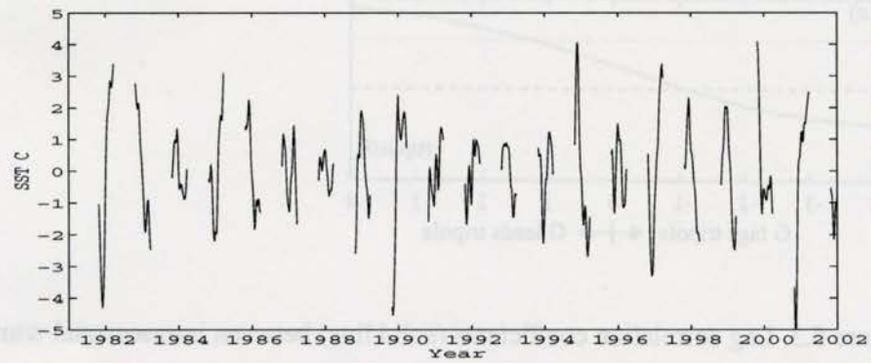

Figure 5.2. Expansion coefficient time series of the patterns in (a) Fig. 5.1d and (b) Fig. 5.1b.

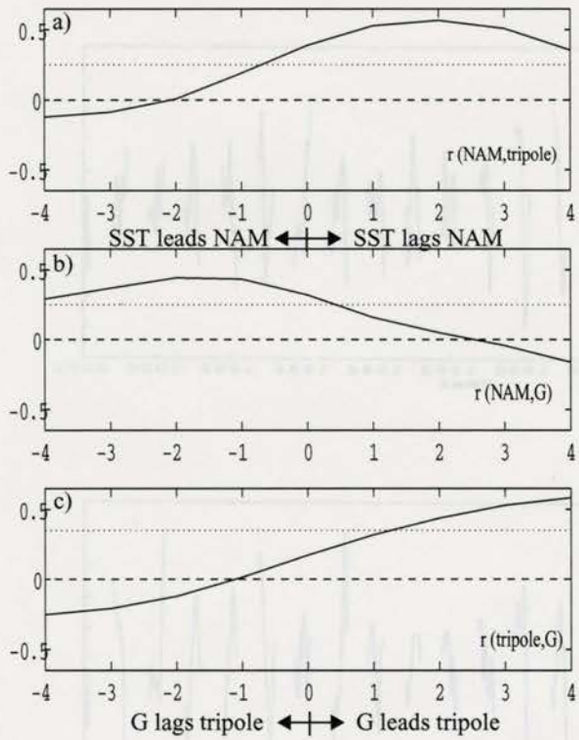

Figure 5.3. Lag correlation coefficients (solid line) between intraseasonal wintertime values of the NAM index and the expansion coefficient time series of the patterns in (a) Fig. 5.1d, (b) Fig. 5.1b, and (c) between the expansion coefficient time series of Fig 5.1d and Fig 5.1b. The 95% confidence level is denoted by the dotted line.

Tendency in SLP regressed onto G

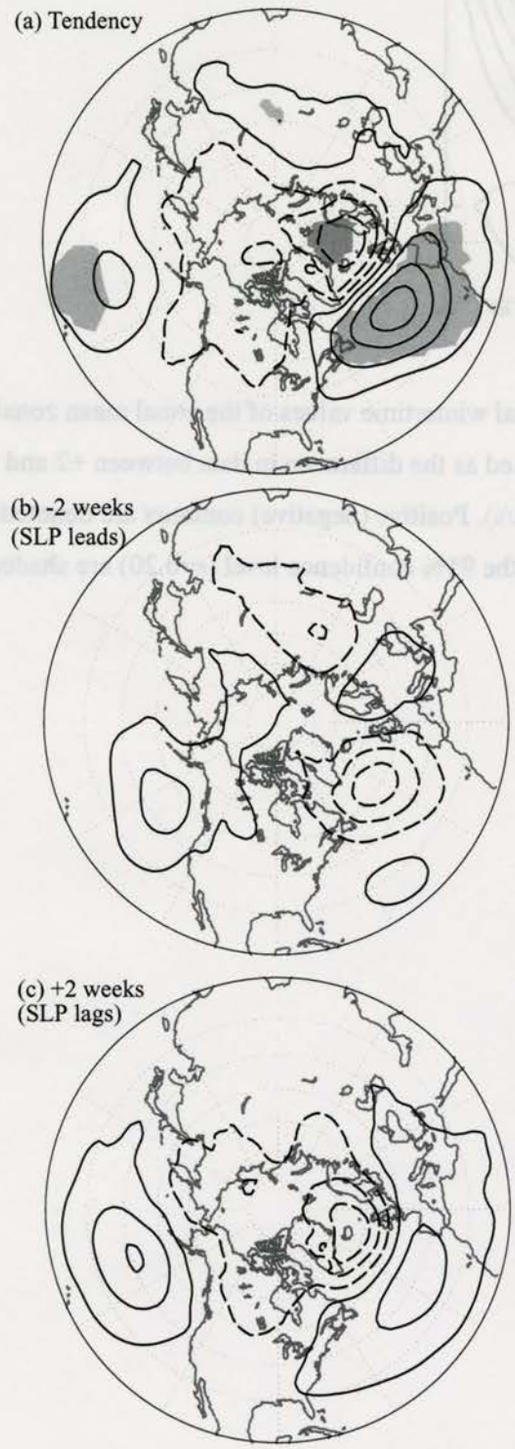

Figure 5.4. (a) The tendency in intraseasonal wintertime values of SLP (expressed as Z_{1000}) regressed onto G, (b) the atmosphere-leading component of the tendency and (c) the atmosphere-lagging component of the tendency. The tendency in panel (a) is defined as the difference in data between +2 and -2 weeks. Contours are at (-5, 5, 15....m). Positive (negative) contours are denoted by solid (dashed) lines. Areas in (a) that exceed the 95% confidence level (r~0.20) are shaded.

Zonal mean wind tendency regressed onto G

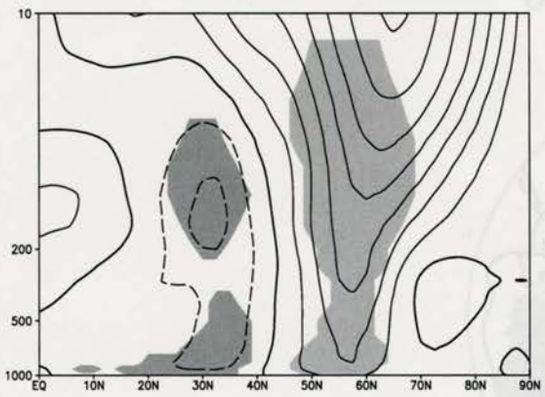

Figure 5.5. The tendency in intraseasonal wintertime values of the zonal mean zonal wind regressed onto G. The tendency is defined as the difference in data between +2 and -2 weeks. Contours are at (-0.5, 0, 0.5... m/s). Positive (negative) contours are denoted by solid (dashed) lines. Areas that exceed the 95% confidence level (r~0.20) are shaded.

Tendency in SLP regressed onto tripole

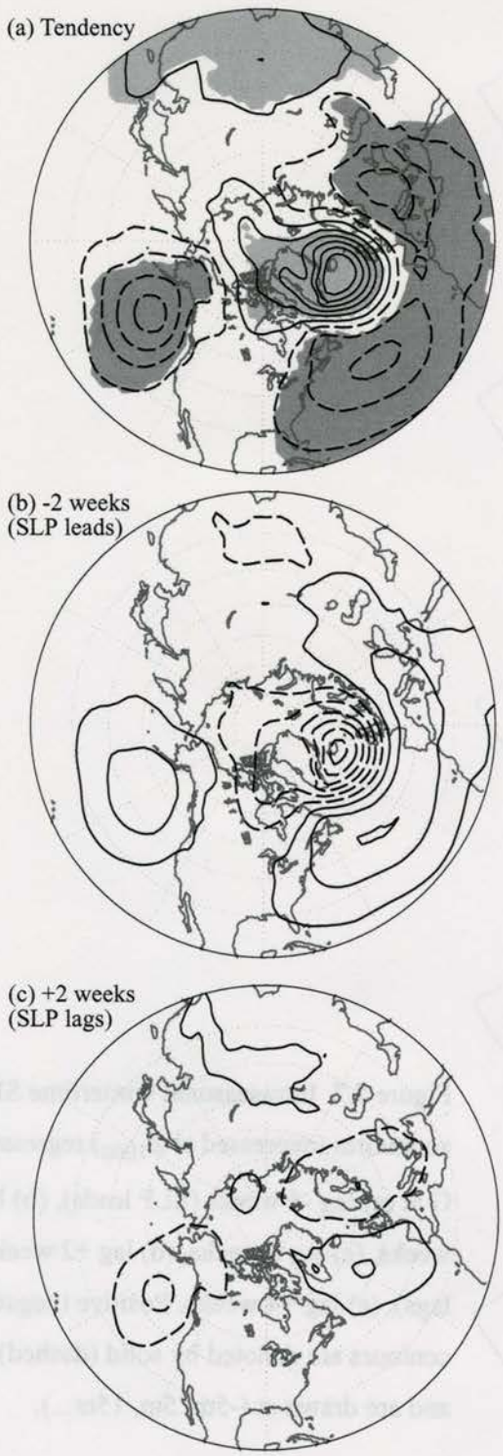

Figure 5.6. (a) The tendency in intraseasonal wintertime values of SLP (expressed as Z_{1000}) regressed onto the tripole, (b) the atmosphere-leading component of the tendency and (c) the atmosphere-lagging component of the tendency. The tendency in panel (a) is defined as the difference in data between +2 and -2 weeks. Contours are at (-5, 5, 15....m). Positive (negative) contours are denoted by solid (dashed) lines. Areas in (a) that exceed the 95% confidence level (r~0.20) are shaded.

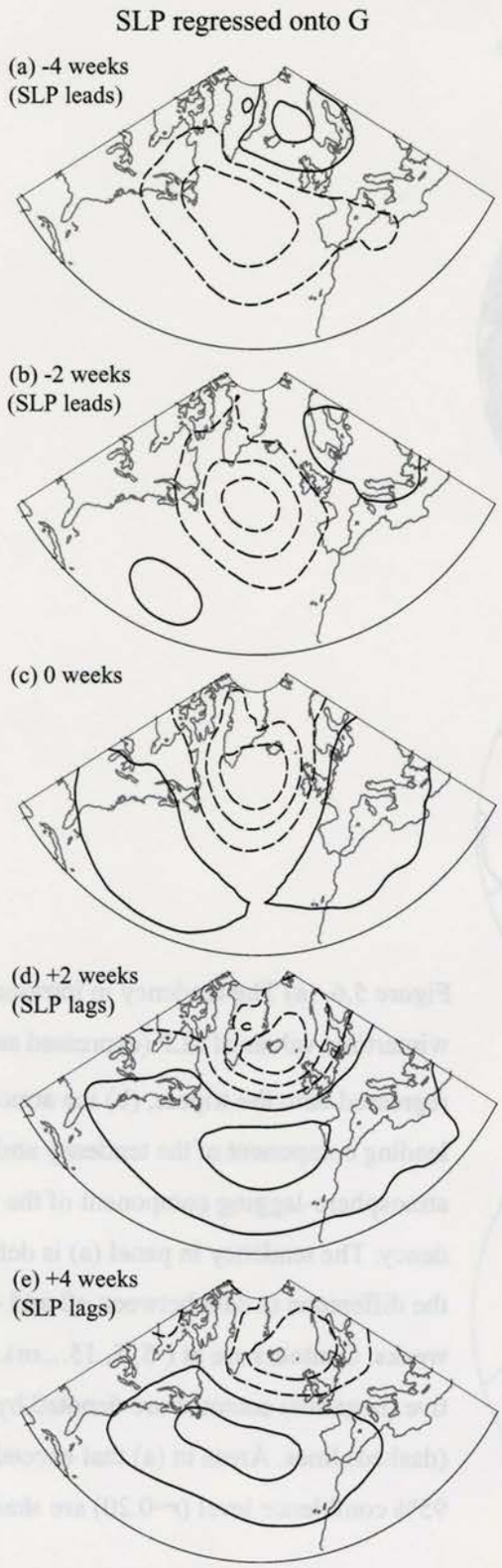

Figure 5.7. Intraseasonal wintertime SLP anomalies (expressed at Z_{1000}) regressed onto G at (a) lag -4 weeks (SLP leads), (b) lag -2 weeks, (c) lag 0 weeks, (d) lag +2 weeks (SLP lags), (e) lag +4 weeks. Positive (negative) contours are denoted by solid (dashed) lines and are drawn at (-5m, 5m, 15m...).

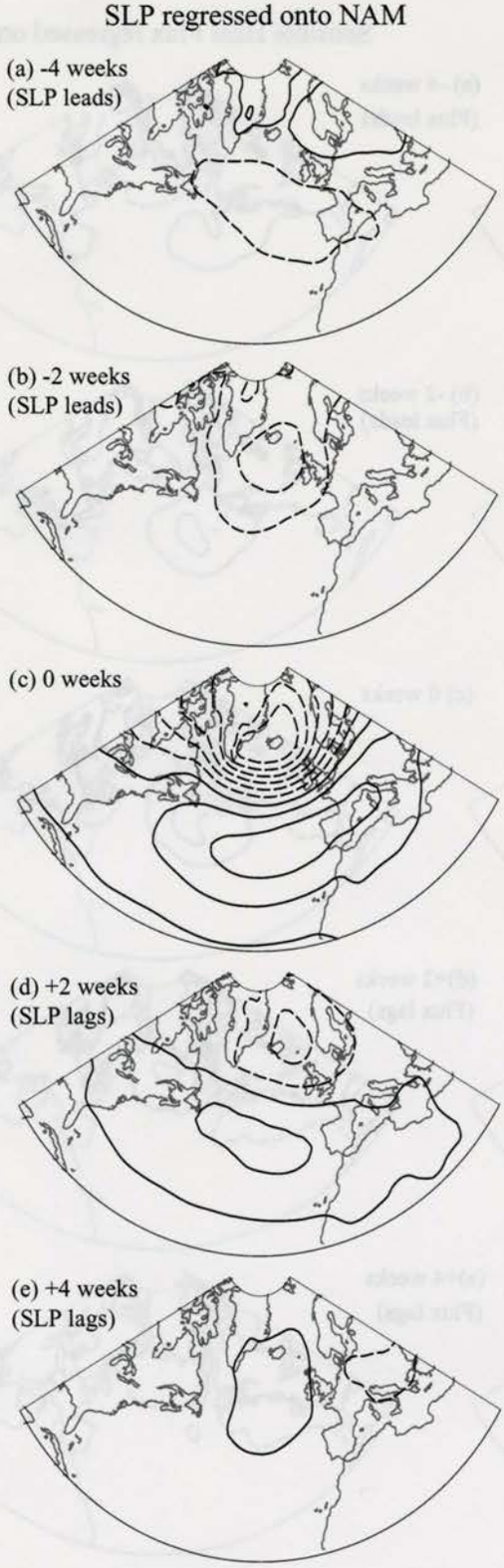

Figure 5.8. Intraseasonal wintertime SLP anomalies (expressed as Z_{1000}) regressed on the NAM at (a) lag -4 weeks (SLP leads), (b) lag -2 weeks, (c) lag 0 weeks, (d) lag +2 weeks (SLP lags), (e) lag +4 weeks. Positive (negative) contours are denoted by solid (dashed) lines and are drawn at (-5m, 5m, 15m...).

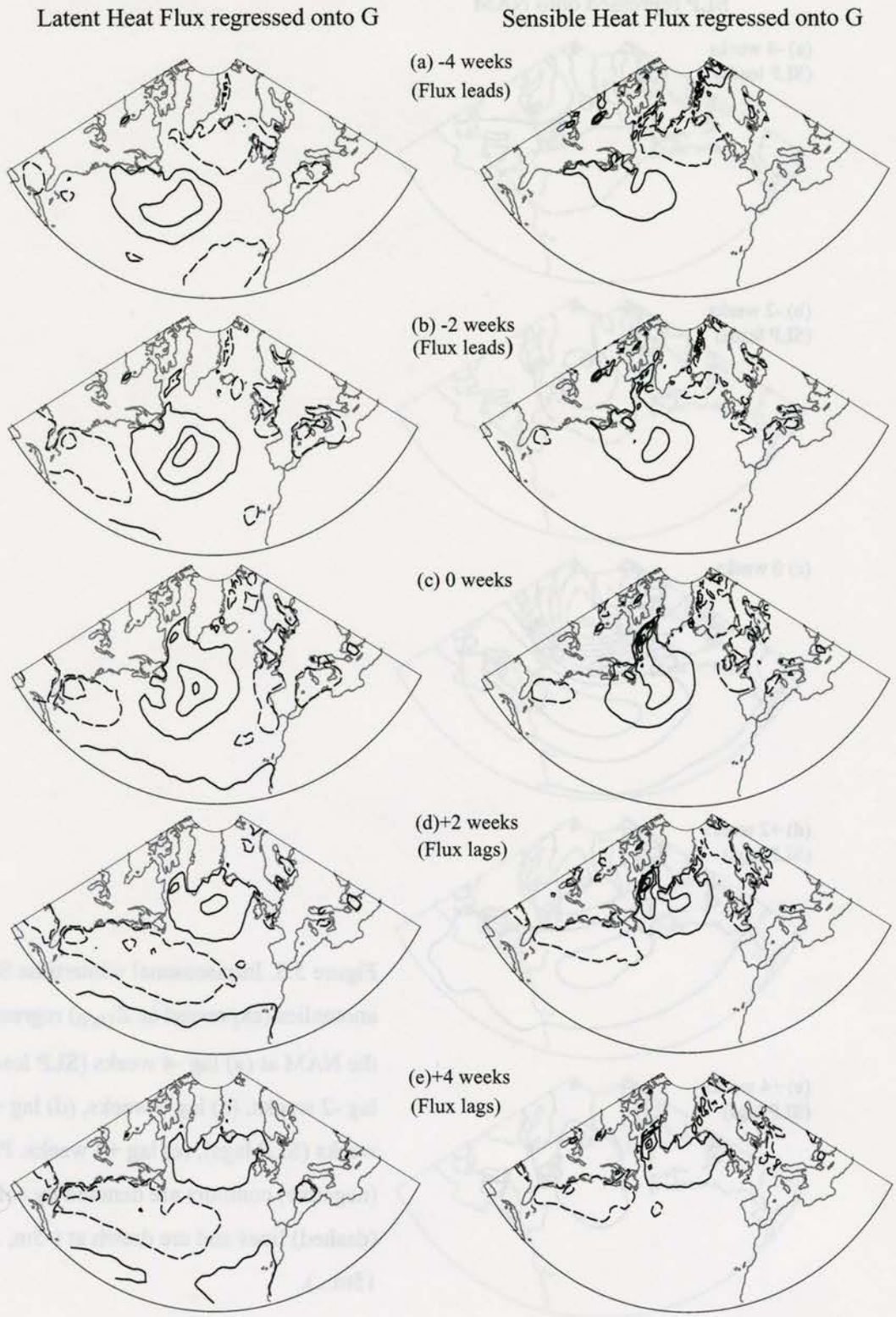
Latent Heat Flux regressed onto G
Sensible Heat Flux regressed onto G
(a) -4 weeks
(Flux leads)
(b) -2 weeks
(Flux leads)
(c) 0 weeks
(d)+2 weeks
(Flux lags)
(e)+4 weeks
(Flux lags)

Figure 5.9. Intraseasonal wintertime latent heat flux anomalies (left panel) and sensible heat flux anomalies (right panel) regressed onto G at (a) lag -4 weeks (flux leads), (b) lag -2 weeks, (c) lag 0 weeks, (d) lag +2 weeks (flux lags), (e) lag +4 weeks. Positive (negative) contours are denoted by solid (dashed) lines and are drawn at (-5 Wm^{-2}, 5 Wm^{-2}, 15W m^{-2}...). Positive fluxes are directed out of the ocean.

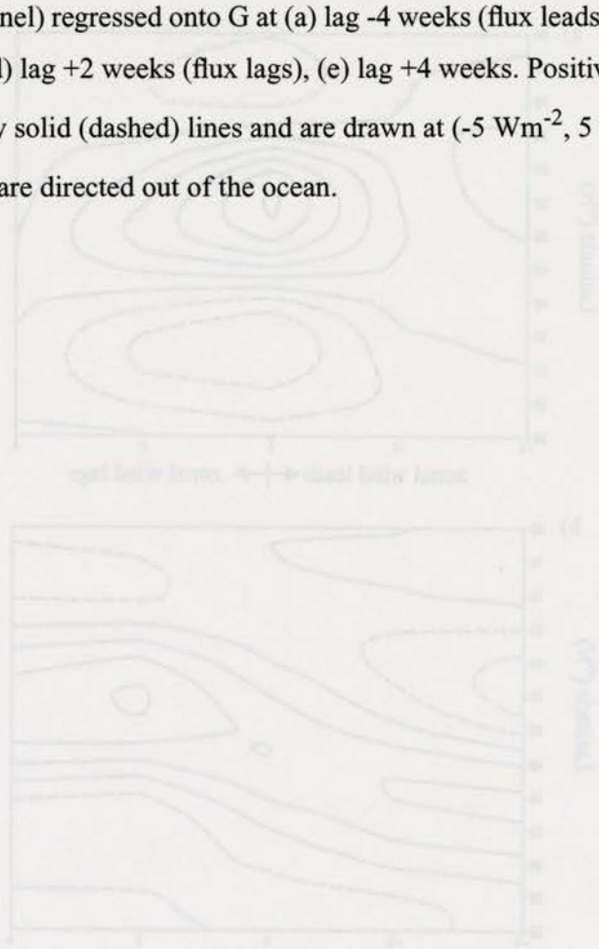

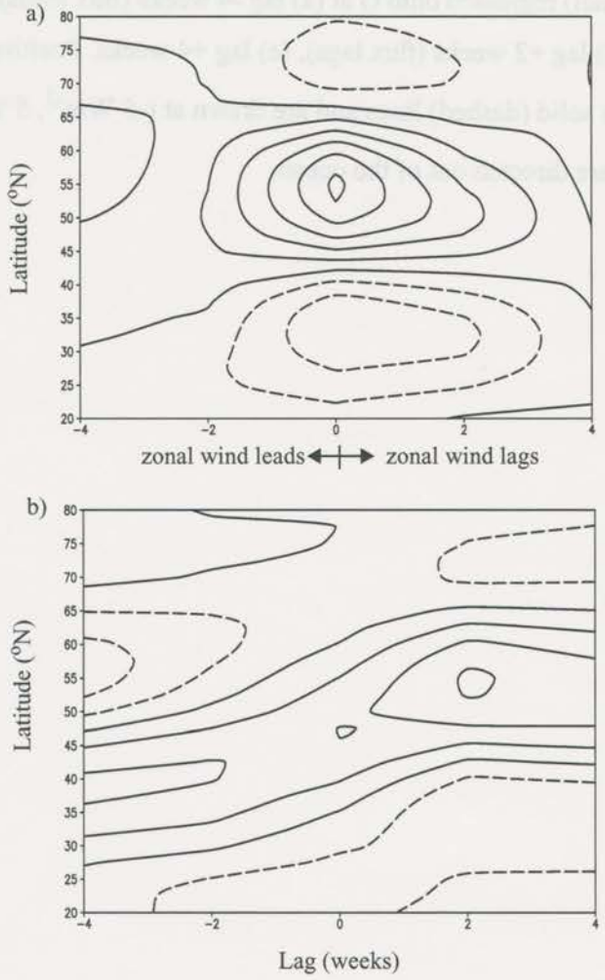

Figure 5.10. Lag regression coefficients of intraseasonal wintertime values of u_{300} zonally averaged over the North Atlantic basin onto values of (a) the NAM and (b) G. Contours are at (-1, 0, 1... m/s). Positive (negative) contours are denoted by solid (dashed) lines.

Chapter Six

Conclusions

In this section, we summarize and discuss the key results of the thesis and offer some avenues for future research.

Much of the research concerning midlatitude ocean-atmosphere interaction has used monthly and seasonal mean data to examine the role of the ocean in the climate system. The stochastic climate models of Frankignoul and Hasselman (1977) and Deser et al. (2003) conclude that midlatitude SST variability on time scales ranging from months to years is consistent with the passive thermodynamic response of the ocean to stochastic atmospheric variability. Observed relationships between the midlatitude ocean and atmosphere are consistent with this null hypothesis, demonstrating that the dominant patterns of Northern Hemispheric atmospheric variability gives rise to the dominant patterns of variability in the North Atlantic SST field.

To what extent midlatitude SSTs, in turn, give rise to the dominant patterns of Northern Hemisphere atmospheric variability remains unclear. General circulation models run with prescribed SST anomalies suggest that the amplitude of the extratropical atmospheric response to realistic midlatitude SST anomalies is modest compared to internal atmospheric variability (Kushnir et al. 2002). Previous literature reveals that the observed relationship between the extratropical atmosphere and midlatitude ocean is strongest when

the atmosphere leads by ~1 month and negligible when the ocean leads by ~1 month.

Because the heat capacity of the troposphere is low, the dynamics of an atmospheric response to midlatitude SSTs should occur on relatively short time scales, i.e., shorter than the monthly and seasonal means used in most observational analyses of extratropical ocean-atmosphere interaction. The thesis thus focuses on interactions between North Atlantic SST variability and the extratropical atmospheric circulation on intraseasonal time scales.

We first examined the climatology of the SST field and the atmospheric circulation over the North Atlantic sector. The largest variance in both seasonal mean and intraseasonal SST anomalies is observed in the region of pronounced gradients in SST, poleward of the Gulf Stream extension. This result was somewhat unexpected because previous literature characterizes the tripole as the leading pattern of SST variability, which does not exhibit variability along the Gulf Stream extension. The region of largest SST gradients are associated with enhanced baroclinicity over the Gulf Stream extension, creating a zonal wind maximum at 300hPa referred to as the North Atlantic jet. The barotropic signature of the jet is evidenced as a belt of surface westerlies at ~40°N implied by the gradients in SLP in Fig. 3.4. Strong poleward heat fluxes by eddies, an indication of cyclogenesis, are also observed over the Gulf Stream extension. If the location of the storm track is set by the gradients in the climatological SST field, then it seems plausible that variations in the horizontal SST gradient might drive variations in the location of the storm track.

In Chapter Four, we further investigated variability in the North Atlantic SST field using Empirical Orthogonal Function (EOF) analysis. Based on the literature reviewed in Chapter One and results in Chapter Three, we expected the tripole and variability captured

along the Gulf Stream extension to emerge as EOFs. The EOF/PC pairs of SST anomalies for all weeks in the calendar year reflect a mix of the expected patterns. For example, the first EOF exhibits a horseshoe pattern with largest loadings in the subtropical and subpolar regions. The pattern bears some resemblance to the tripole but lacks amplitude in the Sargasso Sea. The corresponding time series is dominated by a sharp transition from primarily negative to primarily positive values around ~1994 (we refer to this transition as a regime shift). The second EOF captures variability in the Gulf Stream but also exhibits loadings in the subtropical and subpolar regions.

Because descriptions of summertime SST variability in previous studies are sparse, we also examined EOFs of summertime SST anomalies. The leading EOF/PC pair of summertime SSTs anomalies is characterized by a horseshoe pattern and the regime shift also evidenced in the first EOF/PC of year-round SST anomalies. The results of the analysis were unable to determine if the regime shift is a physical feature of summertime SST variability or an artifact of the data. It was noted that once the regime shift is removed from the analysis, no patterns of summertime SST variability emerged as statistically significant EOFs.

The leading EOFs of wintertime SST anomalies also reflect a mix of the expected patterns, i.e. the tripole and variability in the Gulf Stream extension. These patterns are most clearly evident in EOF analysis of intraseasonal wintertime SST anomalies. Correlation analysis between the two leading PC time series exhibit a statistically significant relationship when variability in the Gulf Stream extension leads the tripole by ~6 weeks. The correlations suggest that the wintertime intraseasonal EOFs of North Atlantic SST field should not be viewed as separate phenomena.

In Chapter Five, non-contemporaneous analysis between midlatitude oceanic and atmospheric fields demonstrated that the two dominant EOFs of wintertime intraseasonal SST anomalies emerge in association with the dominant pattern of Northern Hemisphere atmospheric variability. Lag regression/correlation analysis showed that variability in the Gulf Stream extension region precedes variations in the NAM by ~2 weeks and, in turn, variations in the NAM precede variations in the tripole on a similar time scale. Regressions of the tendency in SLP onto G showed that the regressions are dominated by the atmosphere-lagging component of the tendency and thus reflect increasing amplitude in the NAM with time. In contrast, regressions of the tendency in SLP onto the tripole showed that the regressions are dominated by the atmosphere-leading component of the tendency and thus reflect decreasing amplitude in the NAM with time.

The results in Figs. 5.1-5.6 demonstrate a statistically significant relationship between the NAM and G, but the analyses do not prove an extratropical atmospheric response to variations in midlatitude SSTs. We discussed several possible explanations for the nature of the physical relationship between NAM and G. We first tested against the possibility that the temporal evolution of the NAM at earlier stages in its lifecycle drives variability in G. However, Figures 5.7 and 5.8 showed that the pattern preceding peak amplitude in G projects weakly onto the NAM.

Another explanation is that variations in G give rise to variations in the NAM. Given that the amplitude of G is modest, we are skeptical about whether a 0.25°C anomaly in the Gulf Stream extension could influence variations in the NAM. We also note that the atmospheric response of AGCMs forced with SSTs in the Gulf Stream region are highly model dependent.

The observed relationship between G and the NAM and the questions associated with the relationship offer many directions for future research. Several possible avenues are discussed below.

Because surface heat fluxes are the predominant mechanism through which the ocean and atmosphere communicate, we intend to investigate the surface heat fluxes associated with variations in G and the NAM. However, as noted in Peng and Robinson (2002), the fluxes do not necessarily reveal the direction of cause and effect, thus complicating the interpretation of the results (i.e., both G and the tripole act to damp anomalies in the overlying atmosphere as they decay, but this result does not necessarily reveal a deep, dynamic response of the atmosphere; it is simply consistent with damped thermal coupling).

Another direction for future research is to test the possible mechanisms through which SSTs in the Gulf Stream extension region might contribute to variability in the NAM. As described in Chapter One, Peng and Whitaker (1999) proposed a mechanism in which midlatitude SSTs impacts the overlying atmospheric circulation through anomalous eddy feedback onto the midlatitude storm track. Similarly, we hypothesized that the steady-state linear atmospheric response would be characterized by positive meridional flow over G associated with a high pressure centered downstream. This expected response is consistent with the tendency regression map evidenced in Figure 5.4. However, the amplitude of the atmospheric tendency is large for a relatively small change in midlatitude SSTs. The next step, thus, is to calculate the theoretical temperature advection necessary to wipe out the temperature gradient created by G and compare it to the observed values.

Another approach to understanding the nature of the physical relationship between the NAM and G is to model the atmospheric response to time-varying SSTs in the Gulf Stream region. Several studies have forced AGCMs with prescribed SSTs in a similar region but the structure and amplitude of the atmospheric response varies considerably between models. Because climate models have large grid boxes and do not completely resolve the region of pronounced SST gradients in the Gulf Stream extension, it is plausible that GCMs may not fully capture the relevant interactions between the ocean and atmosphere. One idea is to force both a GCM and a mesoscale model with SST anomalies in the Gulf Stream region and compare the atmospheric response. A similar atmospheric response would imply that the GCM is able to capture the same dynamics as those represented in the mesoscale model. A different atmospheric response would suggest that climate model is missing key elements of the response.

The primary results of this thesis reveal relationships between the North Atlantic intraseasonal SST field and extratropical circulation that are not well-documented in previous observational analyses of monthly and seasonal mean data. In future studies we would like to extend the non-contemporaneous analysis technique used in Chapter Five to investigate weekly ocean-atmosphere interactions in the following three ocean basins:

1) The North Pacific. Analogous to the Gulf Stream in the North Atlantic basin, the Kuroshio current lies under a region of intense cyclogenesis on the western edge of the North Pacific storm track. Several studies have examined North Pacific ocean-atmosphere interactions but with the exception of Deser and Timlin (1997) few studies have used weekly data to investigate non-contemporaneous relationships between the midlatitude ocean and atmosphere.

2) The tropical Atlantic (20°S-20°N). Recent studies have suggested that the sub-tropical node of the tripole may play a role in tropical atlantic variability (Marshall et al. 2001a). Non-contemporaneous analysis of weekly tropical SSTs may shed light on the relationships between the NAM and variability in the tropics. We note that the mechanism through which the atmosphere would respond to a tropical heating source differs from how it responds to a midlatitude heating source.

3) The Southern Ocean. Because of relatively few SST observations, very little research has focused on ocean-atmosphere interactions in the Southern Hemisphere. The OI SST product does include data in the Southern Ocean basins but we are skeptical of SST quality in the southern tropics where cloud cover exceeds 75% and ship observations are sparse (O'Neill et al. 2003).

In addition to extending our analysis to other ocean basins, we plan to continue exploring ocean-atmosphere interactions using satellite data that provides both dense spatial and temporal resolution. For example, the QuikScat scatterometer measures near-surface wind speed and direction on a spatial resolution of 25-km. Chelton et al. (2004) observed that wind stress curl and divergence derived from the QuikScat data exhibit previously unresolved persistent small-scale features which may play an important role in ocean-atmosphere interaction.

REFERENCES

Alexander, M. A., and C. Deser, 1995: A mechanism for the recurrence of wintertime midlatitude SST anomalies. *J. Phys. Oceanogr.*, **25**, 122-137.

Alexander, M. A., C. Deser, and M. S. Timlin, 1999: The reemergence of SST anomalies in the North Pacific Ocean. *J. Climate*, **12**, 2419-2433.

Bjerknes, J., 1959: The recent warming of the North Atlantic. *The Atmosphere and Sea in Motion*, B. Bolin, Ed., Rockefeller Institute Press and Oxford University, 65-73.

Bjerknes, J., 1962: Synoptic survey of the interaction of sea and atmosphere in the North Atlantic. *Geophysica Norvegica*, **24**, 115-145.

Bjerknes, J., 1964: Atlantic air-sea interaction. *Adv. Geophys.*, **10**, 1-82.

Bretherton, C. S., M. Widmann, V. P. Dymnikov, J.M. Wallace, and I. Bladé, 1999: The effective number of spatial degrees of Freedom of a Time-Varying Field. *J. Climate*, **12,** 1990-2009.

Bretherton, C. S., and D. Battisti, 2000: An interpretation of the results from atmospheric general circulation models forced by the history of observed sea surface temperature distribution. *Geophys. Res. Lett.*, **27**, 767-770.

Brown, E., A. Colling, D. Park, J. Phillips, D. Rothery, and J. Wright, 1989: *Ocean Circulation/ Prepared by an Open University Course Team*, New York: Pergamon Press, 238 pp.

Cayan, D. R., 1992a: Latent and sensible heat-flux anomalies over the Northern Ocean- the connection to monthly atmospheric circulation. *J. Climate*, **5**, 354-369.

Cayan, D. R., 1992b: Latent and sensible heat flux anomalies over the northern oceans: driving the sea surface temperature. *J. Phys. Oceanogr.*, **22**, 859-881.

Chelton, D.B., M. G. Schlax, M. H. Freilich, and R. F. Milliff, 2004: Satellite measurements reveal persistent small-scale features in ocean winds. *Science*, **303**, 978-983.

Colwell, S. and J. Turner, 1999: Antarctic Meteorological Observations on the GTS during the FROST project. *Weather and Forecasting*, **14**, 811-816.

Czaja A., and C. Frankignoul, 1999: Influence of the North Atlantic SST on the atmospheric circulation. Geophys. Res. Lett., **26**, 2969-2972.

Czaja A., and C. Frankignoul, 2002: Observed impact of t Atlantic SST anomalies on the North Atlantic Oscillation. *J. Climate*, **15**, 606-623.

Czaja A., A. W. Robserton, and T. Huck, 2003: The role of the Atlantic ocean-atmosphere coupling in affecting North Atlantic Oscillation variability. *The North Atlantic Oscillation: Climatic Significance and Environmental Impact,* J. W. Hurrell, Y. Kushnir, G. Ottersen M. Visbeck, American Geophysical Union, 147-172.

Da Silva, A., A. C. Young and S. Levitus, 1994: *Atlas of surface marine data: algorithms and procedures*. US Department of Commerce: Washington, DC.NOAA Atlas NESDIS 6.

Davis, R. E., 1976: Predictability of sea surface temperature and sea level pressure anomalies over the North Pacific Ocean. *J. Phys. Oceanogr.*, **6**, 249-266.

Deser C., 2000: On the teleconnectivity of the Arctic Oscillation. *Geophys. Res. Lett.*, **27**, 779-782.

Deser, C. and M. L. Blackmon, 1993: Surface climate variations over the North Atlantic Ocean during winter: 1900-1989. *J. Climate*, **6**, 1743-1753.

Deser, C. and M. S. Timlin, 1997: Atmosphere-ocean interaction on weekly timescales in the North Atlantic and Pacific. *J. Climate*, **10**, 393-408.

Deser, C., M. A. Alexander, and M.S. Timlin, 2003: Understanding the Persistence of Sea Surface Temperature Anomalies in Midlatitudes. *J. Climate*, **16**, 57-72.

Dickson, R. R., T. J. Osborn, J. W. Hurrell, J. Meincke, J. Blindheim, B. Adlandsvik, T. Vigne, G. Alekseev, and W. Maslowski, 2000: The Arctic Ocean response to the North Atlantic Oscillation. *J. Climate*, **13**, 2671-2696.

Feldstein, S. B., 1998: An observational study of the intraseasonal poleward propagation of zonal mean flow anomalies. *J. Atmos. Sci*, **55**, 2516-2529.

Feldstein, S. B., 2000: The timescale, power spectra and climate noise properties of teleconnection patterns. *J. Climate,* **13**, 4430-4440.

Ferranti, L., F. Molteni, and T. N. Palmer, 1994: Impact of localized tropical and extratropical SST anomalies in ensembles of seasonal GCM integrations. *Quart. J. Roy. Met. Soc.*, **120**, 1613-1645.

Frankignoul, C., and K. Hasselman, 1977: Stochastic climate models. Part II: Application to sea-surface temperature variability and thermocline variability. *Tellus*, **29**, 289-305.

Frankignoul, C., 1985: Sea surface temperature anomalies, planetary waves, and air-sea feedback in the middle latitudes. *Rev. Geophys.*, **23**, 357-390.

Frankignoul, C., A. Czaja, and B. L'Heveder, 1998: Air-sea feedback in the North Atlantic and surface boundary conditions for ocean models. *J. Climate*, **11**, 2310-2324.

Gandin, L. S., 1963: *Objective Analysis of Meteorological Fields*. Gidrometeorizdar, 238 pp. (Translated from Russian by Israeli Program fro Scientific Translations in 1965.)

Gill, A. E., 1982: *Atmosphere-Ocean Dynamics*. Academic Press, 662 pp.

Grotjahn, R., 1993:*Global Atmospheric Circulation: Observations and Theories*. New York: Oxford University Press, 430pp.

Hartmann, D. L., 1994: *Global Physical Climatology.* Academic Press, 411 pp.

Holton, J. R., 1992: *An Introduction to Dynamic Meteorology.* 3d Ed. New York: Academic Press, 511 pp.

Hoskins, B. J., and D. J. Karoly, 1981: The steady linear response of a spherical atmosphere to thermal and orographic forcing. *J. Atmos. Sci.*, **38**, 1179-1196.

Hurrell, J. W., 1995: Decadal trends in the North Atlantic oscillation: Regional temperature and precipitation. *Science*, **269**, 676-679.

Hurrell, J. W., Y. Kushnir, G. Ottersen, and M. Visbeck, 2003: The Ocean s Response to North Atlantic Oscillation Variability. *The North Atlantic Oscillation: Climatic Significance and Environmental Impact,* J. W. Hurrell, Y. Kushnir, G. Ottersen M. Visbeck, American Geophysical Union, 113-146.

James, I. 1994: *Introduction to Circulating Atmospheres*. Cambridge University Press, 422 pp.

Kalnay, E., M. Kanamitsu, R. Kistler, W. Collins, D. Deaven, L. Gandin, M. Iredell, S. Saha, G. White, G. Woollen, Y. Zhu, M. Chelliah, W. Ebisuzaki, W. Higgins, J. Janowiak, K. C. Mo, C. Ropelewski, J. Wang, A. Leetmaa, R. Reynolds, R. Jenne, and D. Joseph, 1996: The NCEP/NCAR 40-year reanalysis project. *BAMS*, **77**, 437-471.

Kaplan, A., M. Cane, Y. Kushnir, A. Clement, B. Blumenthal, B Rajagopalan, 1998: Analyses of global sea surface temperature 1856-1991, *J. Geophys. Res.,* **103**, 18567-18589.

Kaplan, A., Y. Kushnir, M. Cane, and M. B. Blumenthal, 1997: Reduced space optimal analysis for historical data sets: 136 years of Atlantic sea surface temperatures. *J. Geophys. Res.,* **102**, 27835-27860.

Kistler, R., E. Kalnay, W. Collins, S. Saha, G. White, J Woollen, M. Chelliah, W. Ebisuzaki, M Kanamitsu, V. Kousky, J. van den Doo, R. Jenne, and M. Fiorino, 2001: The NCEP-NCAR 50-year reanalysis: Monthly means CD-ROM and documentation. *Bull. Amer. Meteor. Soc.*, **82**, 247-268.

Kushnir, Y. and N. C. Lau, 1992: The General Circulation Model response to a North Pacific SST anomaly- Dependence on time scale and pattern polarity. *J. Climate*, **5**, 271-283.

Kushnir, Y., 1994: Interdecadal variations in North Atlantic sea surface temperature and associated atmospheric conditions. *J. Climate*, **7**, 141-157.

Kushnir, Y., and I. M. Held, 1996: Equilibrium atmospheric response to North Atlantic SST anomalies. *J. Climate*, **9**, 1208-1220.

Kushnir, Y., W. A. Robinson, I. Blade, N. M. J. Hall, S. Peng, and R. Sutton, 2002: Atmospheric GCM response to extratropical SST anomalies: Synthesis and evaluation. *J. Climate*, **15**, 2233-2256.

Kutzbach, J. E., 1970: Large-scale features of monthly mean Northern Hemisphere anomaly maps of sea-level pressure. *Mon. Wea. Rev.*, **98**, 708-716.

Latif, M. and T. P. Barnett, 1994: Cayses if decadak climate variability in the North Pacific/North Atlantic sector. *Science*, **266**, 634-637.

Latif, M. and T. P. Barnett, 1996: Decadal climate variability over the North Pacific and North America: Dynamics and predictability. *J. Climate*, **9**, 2407-2423.

Lau, N. C. and M. J. Nath, 1994: A modeling study of the relative roles of tropical and extratropical SST anomalies in the variability of the global atmosphere-ocean system. *J. Climate*, **7**, 1184-1207.

Lorenz, J. L. and D. L. Hartmann, 2001: Eddy-zonal flow feedback in the Southern Hemisphere. *J. Atmos. Sci.*, **58**, 3315-3327.

Lorenz, J. L. and D. L. Hartmann, 2003: Eddy-zonal flow feedback in the Northern Hemisphere winter. *J. Climate*, **16**, 1212-1227.

Marshall, J., Y. Kushnir, D. Battisti, P. Chang, A. Czaja, R. Dickson, J. Hurrell, M. McCartney, R. Saravan, and M. Visbeck, 2001a: North Atlantic Climate Variability: Phenomena, Impacts and Mechanisms. *International Journal of Climatology*, **21**, 1863-1898.

Marshall, J., H. Johnson, and J. Goodman, 2000b: A study of the interaction of the North Atlantic Oscillation with ocean circulation. *J. Climate,* **14**, 1399-1421.

Mehta, V. M., M. J. Suarez, J. Manganello, and T. L. Delworth, 2000: Predictability of multiyear to decadal variations in the North Atlantic Oscillation and associated Northern Hemisphere climate variations: 1959-1993. *Geophys. Res. Lett.*, **27**, 121-124.

Namias, J., 1963: Large-scale air-sea interactions over the North Pacific from summer 1962 through the subsequent winter. *J. Geophys. Res.*, **68**, 6171-6186.

Namias, J., 1965: Short period climate fluctuations. *Science*, **147**, 696-706.

Namias, J. and A. M. Born, 1970: Temporal coherence in North Pacific sea surface temperature pattern. *J. Geophys. Res.*, **75**, 5952-5955.

Namias, J., and D. R. Cayan, 1981: Large-scale air-sea interactions and short period climate fluctuations. *Science*, **214**, 869-876.

Nonaka, M. and S. P. Xie, 2003: Covariations of Sea surface temperature and wind over the Kuroshio and its extension: evidence for ocean-to-atmosphere feedback. *J. Climate*, **16**, 1404-1413.

North, G. R., T. L. Bell, R. F. Cahalan and F. J. Moeng, 1982: Sampling errors in the estimation of empirical orthogonal functions. *Mon. Wea. Rev.*, **110**, 699-706.

O'Neill, L. W., D. B. Chelton, and S. K. Esbensen, 2003: Observations of SST-induced perturbations of the wind stress field over the Southern Ocean on seasonal timescales. *J. Climate*, **16**, 2340-2354.

Palmer, T. N., and Z. Sun, 1985: A modelling and observational study of the relationship between sea surface temperatures in the north-west Atlantic and the atmosphere general circulation. *Quart. J. Roy. Met. Soc.*, **111**, 947-975.

Peng, S. L, L. A. Mysak, H. Ritchie, J. Derome, and B. Dugas, 1995: On the difference between early and middle winter atmospheric response to sea surface temperature anomalies in the northwest Atlantic. *J. Climate*, **8**, 137-157.

Peng, S. L., and J. S. Whitaker, 1999: Mechanisms determining the atmospheric response to midlatitude SST anomalies. *J. Climate*, **12**, 1393-1408.

Peng, S. L., W. A. Robsinson and S. Li, 2002: North Atlantic SST forcing of the NAO and relationships with intrinsic hemispheric variability, Geophys. Res. Lett., 29, doi: 1029/2001GL01043.

Philander, S. G., 1990: *El Niñ o, La Niñ a, and the Southern Oscillation*. San Diego: Academic Press, 293 pp.

Pitcher, E.J., M. L. Blackmon, G. T. Bates, and S. Munoz, 1988: The effect of North Pacific sea surface temperature anomalies on the January climate of a general circulation model. *J. Atmos. Sci.,* **45**, 172-188.

Reynolds, R. W., 1993: Impact of Mount Pinatubo aerosols on satellite derived sea surface temperatures. *J. Climate*, **6**, 768-774.

Reynolds, R. W., and T. M. Smith, 1994: Improved global sea surface temperature analyses using optimum interpolation. *J. Climate*, **7**, 929-948.

Reynolds, R.W., C. K. Folland, and D. E. Parker, 1989: Biases in satellite derived sea surface temperature data. *Nature*, **341**, 728-731.

Reynolds, R. W., N. A. Rayner, T. M. Smith, D. C. Stokes, and W. Wang, 2002: An improved in situ and satellite SST analysis for climate. *J. Climate*, **15**, 1609–1625.

Rodwell, M. J., D. P. Rowell, and C. K. Folland, 1999: Ocean forcing of the wintertime North Atlantic oscillation and European climate. *Nature*, **398**, 320-323.

Seager, R., M. Visbeck, N. Naik, J. Miller, G. Krahmann, and H. Cullen, 2000: Causes of Atlantic Ocean climate variablity between 1958 and 1998. *J. Climate*, **13**, 2845-2862.

Thompson, D. W. J. and J. M. Wallace, 1998: The Arctic Oscillation signature in wintertime geopotential height and temperature fields. *Geophys. Res. Lett.*, **25**, 1297-1300.

Thompson, D. W. J. and J. M. Wallace, 2000: Annular modes in the extratropical circulation. Part I: Month-to-moth variability. *J. Climate*, **13**, 1000-1016.

Thompson, D. W. J., J. M. Wallace and C. Hergerl, 2000: Annular modes in the extratropical circulation. Part II: Trends. *J. Climate*, **13**, 1018-1036.

Thompson, D. W. J and J. M. Wallace, 2001: Regional impacts of the Northern Hemisphere Annular Mode. *Science*, **293**, 85-89.

Ting M. and S. Peng, 1995: Dynamics of early and middle winter atmospheric responses to northwest SST anomalies. *J. Climate*, **8**, 2239-2254.

van Loon, H., J. C. Rogers, 1978: Seesaw in winter temperatures between Greenland and Norther Europe. 1. General description. *Mon. Wea. Rev.*, **106**, 296-310.

Visbeck, M., E. P. Chassignet, R. G. Curry, T. L. Delworth, R. R. Dickson, and G. Krahmann, 2003: The Ocean s Response to North Atlantic Oscillation Variability. *The North Atlantic Oscillation: Climatic Significance and Environmental Impact,* J. W. Hurrell, Y. Kushnir, G. Ottersen M. Visbeck, American Geophysical Union, 113-146.

Walker, G. T. and E. W. Bliss, 1932: World Weather V. *Mem. R. Meteorol.* Soc., **4**, 53-83.

Wallace, J. M. and P. V. Hobbs, 1977: *Atmospheric Science: An Introductory Survey.* Academic Press, 467 pp.

Wallace, J. M., 2000: North Atlantic Oscillation/annular mode: Two paradigms---one phenomenon. *Quart. J. Roy. Met. Soc.*, **126**, 791-805.

Wallace, J. M. and D. S. Gutzler, 1981: Teleconnections in the geopotential height field during the Northern Hemisphere winter. *Mon. Wea. Rev.*, **109**, 784-812.

Wallace, J. M, and Q. R. Jiang, 1987: On the observed structure of interannual variability of the atmosphere/ocean climate system. *Atmospheric and Oceanic Variability*, J. Cattle, Ed., Royal Meteorological Society, 17-43.

Wallace, J. M., T. P. Mitchell and C. Deser, 1989: The influence of sea-surface temperature on surface wind in the eastern equatorial Pacific: seasonal and interannual variability. *J. Climate*, **2**, 1492-1499.

Wallace, J. M., C. Smith and Q. Jiang, 1990: Spatial patterns of atmosphere-ocean interaction in the northern winter. *J. Climate*, **3**, 990-998.

Wallace, J. M. and D. W. J. Thompson, 2002: The Pacific center of action of the Northern Hemisphere Annular Mode: Real or artifact? *J. Climate*, **15**, 1987-1991.

Woodruff, S. D., R. J. Slutz, R. L. Jenne, and P. M. Steurer, 1987: A Comprehensive Ocean-Atmosphere Data Set. *Bull. Amer. Meteor. Soc.*, **68**, 521-527.

Xie, S. P., J. Hafner, Y. Tanimoto, W. T. Liu, H. Tokinaga and H. Xu 2002: Bathymetric effect on the winter sea surface temperature and climate of the Yellow and East China Seas. *Geophys. Res. Lett.*, **29**, 2228 doi:10.1029/2002GL015884.